5-2016

Discharge-Suspended Sediment Relations: Near-channel Environment Controls Shape and Steepness, Land Use Controls Median and Low Flow Conditions

Angus A. Vaughan
Utah State University

DISCHARGE-SUSPENDED SEDIMENT RELATIONS: NEAR-CHANNEL ENVIRONMENT CONTROLS SHAPE AND STEEPNESS, LAND USE CONTROLS MEDIAN AND LOW FLOW CONDITIONS

by

Angus A. Vaughan

A thesis submitted in partial fulfillment
of the requirements for the degree

of

MASTER OF SCIENCE

in

Watershed Science

Approved:

_____	_____
Patrick Belmont, Ph.D. Major Professor	Peter Wilcock, Ph.D. Committee Member
_____	_____
Charles Hawkins, Ph.D. Committee Member	Mark R. McLellan, Ph.D. Vice President for Research and Dean of the School of Graduate Studies

UTAH STATE UNIVERSITY
Logan, UT

2016

ABSTRACT

Discharge-Suspended Sediment Relations: Near-channel Environment Controls Shape and Steepness, Land Use Controls Median and Low Flow Conditions

by

Angus A. Vaughan, Master of Science

Utah State University, 2016

Major Professor: Patrick Belmont, Ph.D.
Department: Watershed Science

We analyzed recent total suspended solids (TSS) data from 45 gages on 36 rivers throughout the state of Minnesota. Watersheds range from 32 to 14,600 km^2 and represent a variety of distinct settings in terms of topography, land cover, and geologic history. Our study rivers exhibited three distinct patterns in the relationship between discharge and TSS: simple power functions, threshold power functions, and peaked or negative power functions. Differentiating rising and falling limb samples, we generated sediment rating curves (SRC) of form $TSS = aQ^b$, Q being normalized discharge. Rating parameters *a* and *b* describe the vertical offset and steepness of the relationships. We also used the fitted SRCs to estimate TSS values at low flows and to quantify event-scale hysteresis.

In addition to quantifying the watershed-average topographic, climatic/hydrologic, geologic, soil and land cover conditions, we used high-resolution lidar topography data to characterize the near-channel environment upstream of gages. We used Random Forest statistical models to analyze the relationship between basin and channel features and the rating parameters. The models enabled us to identify morphometric variables that provided the greatest explanatory

power and examine the direction, form, and strength of the partial dependence of the response variables on individual predictor variables. The models explained between 43% and 60% of the variance in the rating curve parameters and determined that Q-TSS relation steepness (exponent) was most related to near-channel morphological characteristics including near-channel local relief, channel gradient, and proportion of lakes along the channel network. Land use within the watershed explained most variation in the vertical offset (coefficient) of the SRCs and in TSS concentrations at low flows.

(120 pages)

PUBLIC ABSTRACT

Discharge-Suspended Sediment Relations: Near-channel Environment Controls Shape and Steepness, Land Use Controls Median and Low Flow Conditions

Angus A. Vaughan

Erosion, transport and deposition of fine sediment (clay, silt and fine sand) influence the form and function of river systems. Excess suspended sediment degrades stream ecosystems and is implicated as a leading cause of water quality and aquatic life impairment. Therefore, understanding the factors that control fine sediment transport patterns is an interesting topic for basic science and one that has important management and policy implications.

In this study, we sought to understand how attributes of the landscape and channel network might control the shape, steepness and vertical offset of the relationship between river discharge and suspended sediment. Watershed and channel attributes included in our analysis were high-resolution topography, geology, soil erodibility, climate, and land use. Our results indicated that land use within the watershed most controlled sediment concentrations at low and moderate flows, with higher percentages of agriculture and lower forest cover associated with higher sediment concentrations. Conversely, the steepness, or rate-of-change, of the discharge-suspended solids relationships was dominantly affected by the topography and landforms near the channel. Rivers with high sediment concentrations at high water discharge were those with steep channel gradients and with bluffs and tall banks near the channel, which are likely important sediment sources. These results support previous findings that sediment load reduction at high flows may be best achieved by management approaches aimed at reducing the magnitude and frequency of high flows and controlling erosion from near-channel sediment sources, rather than additional regulations on land use aimed at reducing erosion from upland soils.

ACKNOWLEDGMENTS

This work was funded through a National Science Foundation grant (NSF ENG 1209445) for the REACH (Resilience under Accelerated Change) project. The study would not have been possible without the prodigious amount of water and sediment data collected by the Minnesota Pollution Control Agency and Department of Natural Resources, the U.S. Geological Survey, and the Metropolitan Council Environmental Services division. I gratefully acknowledge the help I received with data requests and other inquiries from multiple staff members at those agencies.

I would especially like to thank my advisor, Patrick Belmont, for his tremendous amount of help and support throughout the entire research process. In addition to the insight he provided on this project, Patrick helped me develop into a better and more rigorous thinker and scientist and set an inspiring example of how to use good science to inform policy and management. I also thank my other committee members, Peter Wilcock and Chuck Hawkins. Peter's insight and ideas led me to think more deeply and critically about ways to analyze my data and about what the results might mean from a geomorphic and management perspective. Chuck's statistical expertise was invaluable for conceiving and carrying out the analysis for this project, and his writing suggestions made this thesis more readable. I also received advice on statistical analysis from Richard Cutler. John Olson was generous with his time, helping me implement his method for quantifying geologic setting and offering other advice. Dan Bone aided with data preparation.

I thank my friends in the Belmont Lab, who listened to me talk about my research as it slowly unfolded from an unsure idea to a finished thesis. They provided excellent ideas and feedback along the way. Along with the rest of the Watershed Sciences and Natural Resources community, they provided a supportive and fun atmosphere in which to live, work, and play for two years. Finally, I thank my family for their love and support throughout this process, and for instilling in me a love of the natural world and of learning.

Angus A. Vaughan

CONTENTS

Page

ABSTRACT iii

PUBLIC ABSTRACT v

ACKNOWLEDGMENTS vi

LIST OF TABLES viii

LIST OF FIGURES ix

INTRODUCTION 1

BACKGROUND 6

Sediment Rating Curves and Relation with Basin Characteristics 6
Overview of Regulation of Fine Sediment in Minnesota and Description of Study Area 8

DATA AND METHODS 14

Q-TSS Data and Relationships 14
Landscape and Environmental Data and Methods 19
Random Forest Modeling 31

RESULTS 36

DISCUSSION 49

CONCLUSIONS 57

REFERENCES 58

APPENDICES 72

Appendix A. Tables of Values for All Response and Predictor Variables Used in RF Models 73
Appendix B. Daily Discharge versus Instantaneous Discharge Analysis 97
Appendix C. Q-TSS Relations for All Study Gages 100

LIST OF TABLES

Table		Page
1	Predictions for each SRC class from Random Forest model	40
A.1	Watershed Morphometry Metrics	73
A.2	Watershed Land Use/Land Cover Metrics	76
A.3	Watershed Soil and Geology Characteristics	79
A.4	Watershed Climate and Hydrology Metrics	82
A.5	Cumulative, Distance-Weighted Near-channel Metrics, 10 km Upstream of Gage	85
A.6	Cumulative, Distance-Weighted Near-channel Metrics, 50 km Upstream of Gage	88
A.7	Rating Curve Parameters	91
A.8	Rating Curve Parameters	94

LIST OF FIGURES

Figure		Page
1	Location of study gages within MN	5
2	Nutrient regions defining TSS TMDL standards in MN	9
3	Representative Q-TSS relationships and explanation of computation of hysteresis metric	18
4	Summary of GIS datasets used to describe the geomorphic and environmental setting of the watersheds and channel networks upstream of study gages	20
5	Explanation of near-channel analysis	27
6	Map of combined SRC exponent values	38
7	Map of SRC shapes throughout Minnesota	39
8	Results from Random Forest classification model for SRC shape	44
9	Results from Random Forest regression model for SRC rising limb exponent	45
10	Results from Random Forest regression model for SRC rising limb coefficient	46
11	Results from Random Forest regression model for SRC combined exponent	47
12	Results from Random Forest regression model for SRC hysteresis	48
B.1	Absolute difference in rating curve exponents for SRCs created using mean daily and instantaneous flow data	98
B.2	Percent difference in exponents for SRCs created using mean daily and instantaneous flow data	99

INTRODUCTION

Predicting the flux of suspended sediment from a watershed is a fundamental problem in geomorphology, with important implications for water quality, land and water resource management and policy, and aquatic ecosystem health. Fine sediment (clay, silt and fine sand) is generally the dominant component of a river's sediment load [*Syvitski et al.*, 2000; *Turowski et al.*, 2010], globally comprising about 90% of total sediment and a large fraction of the phosphorus and carbon flux to the ocean [*Milliman and Meade*, 1983; *Owens and Walling*, 2002; *Regnier et al.*, 2013]. Suspended sediment concentrations measured at a given location integrate influences from all sediment sources and sinks above that point, and are therefore expected to depend on watershed characteristics such as geology, climate, vegetative cover, level of glaciation, rainfall intensity, slope, topographic relief, and human impacts [*Langbein and Schumm*, 1958; *Ahnert*, 1970; *Wischmeier and Smith*, 1978; *Summerfield and Hulton*, 1994; *Syvitski et al.*, 2000, 2014; *Mueller and Pitlick*, 2013]. However, long-term denudation rates do not depend strongly on climate (precipitation or mean annual temperature) or topographic relief, but instead on changes in base level [*Hack*, 1975; *Riebe et al.*, 2001; *von Blanckenburg*, 2005]. Recent studies have demonstrated that the near-channel environment may be a dominant factor contributing sediment, even in agricultural watersheds [*Walter and Merritts*, 2008; *Belmont et al.*, 2011b; *Stout et al.*, 2014; *Donovan et al.*, 2015], which raises the question, 'do metrics characterizing watershed-average or near-channel conditions provide better predictability for riverine sediment fluxes?'

Erosion, transport and deposition of fine sediment influence the form and function of river systems. Concentrations of suspended sediment, especially at overbank discharges, have implications for rates of vertical accretion and sediment storage on floodplains [*Wolman and Leopold*, 1957; *Knox*, 1977b; *Lauer and Parker*, 2008; *Viparelli et al.*, 2013]. Fine sediment in excess of a channel's transport capacity can lead to channel narrowing by accretion on channel

bars and inset floodplains [*Grams and Schmidt*, 2005; *Dean et al.*, 2011]. Systematic increases in river flows can likewise widen and deepen channels and exacerbate near-channel erosion [*Belmont et al.*, 2011b; *Lenhart et al.*, 2011; *Schottler et al.*, 2014]. Understanding how and at what discharges fine sediment is transported through a river network is, therefore, a geomorphically important problem.

Although suspended sediment is a natural component of aquatic ecosystems, excess sediment degrades stream ecosystems and is implicated as a leading cause of water quality and aquatic life impairment. For example, excessive SSC can cause significant reduction in algal biomass and primary productivity by reducing light penetration and photosynthesis, with cascading effects to higher trophic levels [*Bilotta and Brazier*, 2008; *Finlay*, 2011]. Elevated SSC can also cause a reduction of population size and species richness among invertebrates through abrasion or clogging of exposed respiratory or feeding structures, forcing of increased invertebrate drift, and loss of habitat through clogging of interstitial spaces in coarse streambed sediments [*Richards and Bacon*, 1994; *Wood and Armitage*, 1997; *Bilotta and Brazier*, 2008]. Prolonged exposure to elevated SSC can cause mortality, reduced growth, reproduction and recruitment among fish, as well as shift aquatic predator-prey relationships and prompt fish migration out of affected reaches [*Schwartz et al.*, 2008, 2011]. Suspended sediment transport is also strongly associated with nutrient and contaminant transport. Phosphorus is commonly adsorbed to fine sediment particles and sediment-associated transport often dominates the total phosphorus load exported from a catchment, which can cause eutrophication problems in water bodies downstream [*Walling et al.*, 1997; *Verstraeten and Poesen*, 2002]. Additionally, pesticides, organic contaminants, heavy metals, and other pollutants are stored and transported along with fine sediments [*Pereira et al.*, 1996; *Symader et al.*, 1997; *Peck et al.*, 2004; *Jones et al.*, 2006; *Kolok et al.*, 2014]. Understanding the controls on the suspended sediment fluxes,

therefore, is not only an intriguing topic for basic science, but also one that has important management and policy implications.

An important metric for characterizing the suspended sediment regime in river systems is the empirical sediment rating curve (SRC) [*Asselman*, 2000; *Hu et al.*, 2011; *Warrick*, 2014]. SRCs describe the average relation between river discharge (Q) and suspended sediment concentration (SSC) or total suspended solids (TSS)[1]. Q-TSS relationships are distinguishing characteristics of a river's sediment regime that represent the combined effects of erosion, transport and deposition occurring across the range of flows upstream from that point in the watershed. Therefore, regional variation in Q-TSS relationships may offer insight into geomorphic processes and dominant sediment sources and sinks within watersheds and thereby provide a basis for identifying regions that require different management, restoration and rehabilitation practices.

In this study, we sought to improve understanding of landscape and environmental controls on Q-TSS relationships. We used Q and TSS data to construct SRCs for 45 gages on 36 separate rivers throughout the state of Minnesota, USA (Figure 1). We observed a wide range of forms for Q-TSS relationships and sought to understand spatial and geomorphic patterns in those relationships by asking the following questions: Which landscape or channel characteristics most

[1] SSC and TSS are related but distinct terms, often used interchangeably in the literature to refer to the solid-phase material suspended in the water column [*Gray et al.*, 2000]. SSC and TSS refer to distinct laboratory analytical methods for measuring sediment concentrations. SSC is based on the dry weight of all sediment from a known volume of water-sediment mixture. TSS is based on the dry weight of sediment from a subsample of the original sample. SSC samples are collected using a width- and depth-integrated sampling technique, whereas TSS are collected as grab samples [*Ellison et al.*, 2014]. For samples containing substantial proportions of sand-size material, TSS values tend to be lower than the corresponding SSC values, and SSC measurements are thus considered more reliable for natural-water samples [*Gray et al.*, 2000; *Ellison et al.*, 2014]. Sediment concentration values are reported as TSS for our study gages and we refer to the data accordingly. Hereafter we also use TSS to refer to suspended sediment concentrations more generally.

influence the shape of Q-TSS relationships? Why are some river systems more sensitive to increases in discharge than others? Can analysis of Q-TSS relationships offer insight into dominant sediment sources and geomorphic processes within a watershed and channel-floodplain system? Can we develop a better predictive understanding of Q-TSS relations to support decisions related to water quality regulations, water and land management, and restoration practices?

To answer these questions, we generated a large dataset describing the geologic, climatic, hydrologic, soil, land use, and topographic setting upstream of study gages. We utilized high-resolution topography that adequately characterizes many of the key features that may control the movement of water and sediment through the landscape [*Passalacqua et al.,* 2015]. We characterized these features at the watershed scale and also characterized features specific to the channel-floodplain corridor. We used Random Forest (RF) statistical models to explore the association between these factors and the shape of Q-TSS relations, taking advantage of RF models' ability to handle complex, non-linear interactions among variables while making no assumptions about the form of those relationships [*Cutler et al.*, 2007; *Olson and Hawkins*, 2012]. We used variable importance measures to identify morphometric variables that provided the greatest explanatory power and partial dependence plots to examine the direction, form, and strength of the partial dependence of response variables on individual predictor variables.

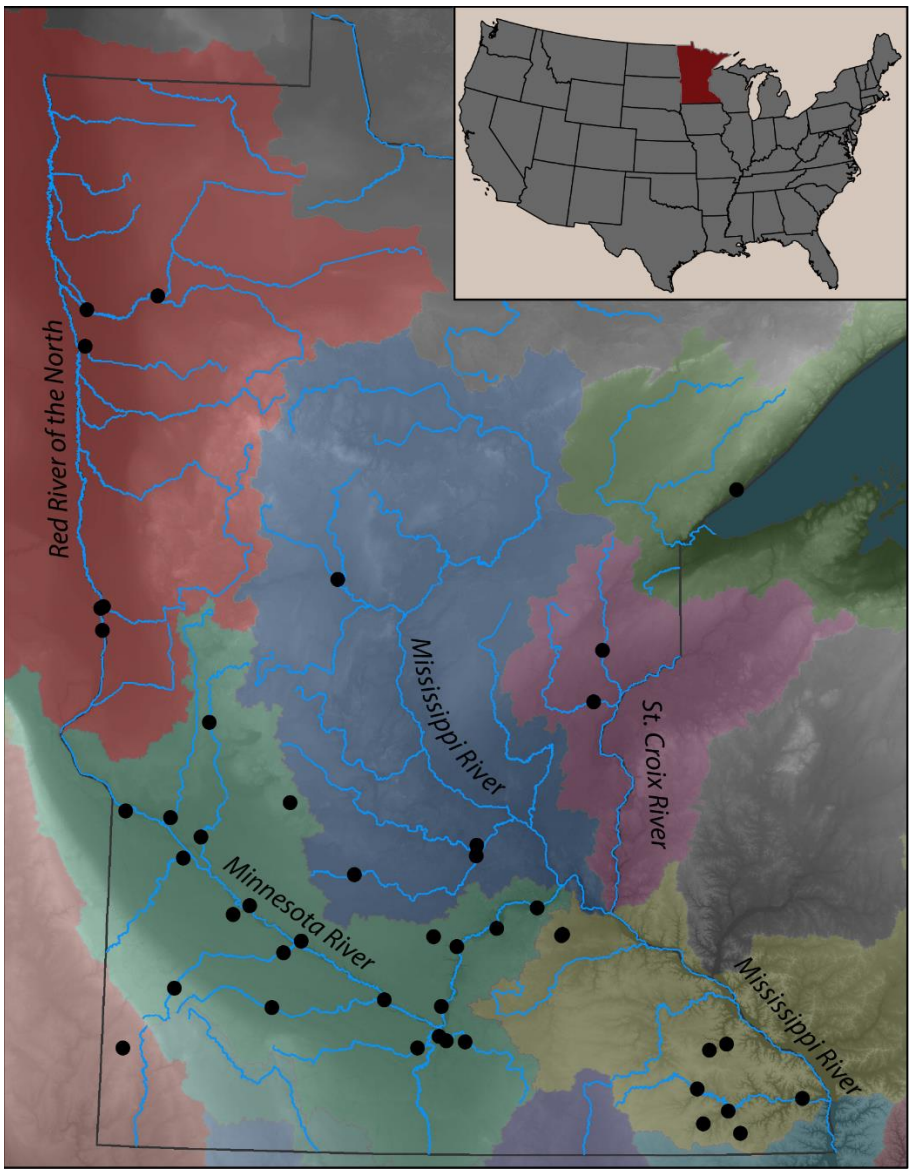

Figure 1. Location of study gages within MN, shown over map of HUC-4 major watersheds. Base map data from the National Hydrography Dataset (watershed boundaries and streamlines) and U.S. Geological Survey (DEM). Projection: NAD 1983, UTM Zone 15 N. **Inset:** location of MN within the USA.

BACKGROUND

Sediment Rating Curves and Relation with Basin Characteristics

The concentration of sediment in suspension depends not only on the capacity of the flow to transport sediment but also on the rate at which fine sediment is supplied. This can result in different sediment concentrations at the same water discharge, depending on the rate of sediment supply. Therefore, suspended sediment transport cannot be predicted as a function of the hydraulics alone and empirical relations are used instead. [*Asselman*, 2000; *Fan et al.*, 2012]. Such relations are typically derived from statistical regression on the Q and SSC data [*Warrick*, 2014] and most commonly take the form of a power relation:

$$TSS = aQ^b \qquad (1)$$

Equation 1 can be linearized using a log-transform of the SSC and Q data:

$$\log(TSS) = b \log(Q) + \log(a) \qquad (2)$$

where *a* and *b* are the sediment rating coefficient and exponent, respectively [*Mimikou*, 1982; *Asselman*, 2000; *Syvitski et al.*, 2000; *Yang et al.*, 2007; *Sadeghi et al.*, 2008; *Hu et al.*, 2011; *Fan et al.*, 2012; *Warrick*, 2014]. The empirical relations model the combined effect of increased transport capacity at higher discharges and the degree to which new sediment sources are accessed or depleted during conditions that cause high discharge [*Asselman*, 2000].

Because suspended sediment transport is a function of sediment supply as well as transport capacity, studies have sought to understand the shape of rating curves in terms of environmental and basin properties that may influence sediment production and supply to rivers. Generally, researchers have focused on basin-scale parameters describing average topography/relief, climate, geology, soil properties and land use history [*Syvitski et al.*, 2000; *Ali*

and de Boer, 2008]. Topographic measures that have been related to SRC shape include basin area, length and width; watershed mean elevation and slope; basin relief and hypsometric integral; average streambed slope and watershed mean and extreme values for various climate variables such as temperature and precipitation [*Bogárdi*, 1961; *Mimikou*, 1982; *Lu and Higgitt*, 1999; *Syvitski et al.*, 2000; *Yang et al.*, 2007]. These studies have used single or multiple regression to study correlation between the rating curve parameters and the various basin metrics. Additionally, studies have analyzed the influence of similar basin-scale characteristics on suspended sediment yield [*Lu and Higgitt*, 1999; *Restrepo et al.*, 2006; *Ali and de Boer*, 2008; *de Vente et al.*, 2011].

Watershed-average characteristics may produce adequate predictions of sediment dynamics if sediment is being supplied from throughout the watershed. However, studies of multiple streams in Minnesota and elsewhere have demonstrated that sediment supply may be dominated by near-channel sources. For example, Belmont et al. [2011b] used geochemical fingerprinting as well as aerial and terrestrial lidar analyses, aerial photography, and water and sediment gaging data to create a sediment budget for the Le Sueur River, a tributary and major sediment contributor to the Minnesota River (itself a tributary of the Mississippi River) in southern Minnesota. The sediment budget showed that over the period of 2000-2010, 70 percent of the fine sediment supplied to the Le Sueur River was derived from the near-channel environment, originating from erosion of bluffs, banks, ravines, and from channel incision, even though the channel network comprises only 1 percent of the landscape. In the same study, analysis of radiogenic nuclides in cores from Lake Pepin, a naturally dammed lake on the Mississippi River below the confluence with the Minnesota River, showed that the dominant source of sediment carried by the river has shifted. In the mid-1900s, the sediment load was predominantly derived from upland agricultural soil erosion, but since then the sediment has shifted to being primarily derived from near-channel sources such bluffs and ravines.

Radionuclide sediment fingerprinting data from the Root River in southeastern Minnesota suggest that the majority of suspended sediment there, too, is derived from near-channel sources [*Stout et al.*, 2014]. The ^{10}Be fingerprinting signature from Root River sediment suggests that the original source for the sediment was erosion from agricultural fields, but depleted levels of the short-lived tracer ^{210}Pb suggest that much of that sediment has been stored in the floodplain and terraces for at least 70 years. The sediment is now being re-worked from the channel-adjacent floodplain and terraces and entering the river system as suspended sediment.

Because the near-channel environment comprises such a small fraction of any given watershed (circa 1%), processes causing erosion from near-channel sources are not likely to be well represented by the basin-scale morphometrics commonly used to investigate and explain suspended sediment dynamics in rivers. Analysis to determine the dominant factors controlling sediment dynamics in rivers will likely be improved by the development of metrics that specifically quantify aspects of the near-channel environment that directly control sediment generation and transport. Accurate quantification of the near-channel environment has only become feasible recently, with availability of high resolution topography data and imagery [*Passalacqua et al.*, 2012, 2015; *Tarolli et al.*, 2012].

Overview of Regulation of Fine Sediment in Minnesota and Description of Study Area

The United States Environmental Protection Agency [2000] has listed elevated sediment loads (siltation) and turbidity as a leading cause of impairment in U.S. streams. The federal Clean Water Act mandates that states monitor streams in order to determine impairment and, if necessary, develop Total Maximum Daily Load (TMDL) criteria to address those impairments [*Minnesota Pollution Control Agency*, 2011]. The State of Minnesota established suspended sediment criteria by grouping watersheds into four regions, namely the northern, central, and southern regions and a distinct region for the mainstem Red River of the North (Figure 2). Total

Suspended Solids (TSS) concentrations are required to not exceed 15, 30, 65 or 100 mg/L, respectively, more than 10 percent of the time over a multiyear window.

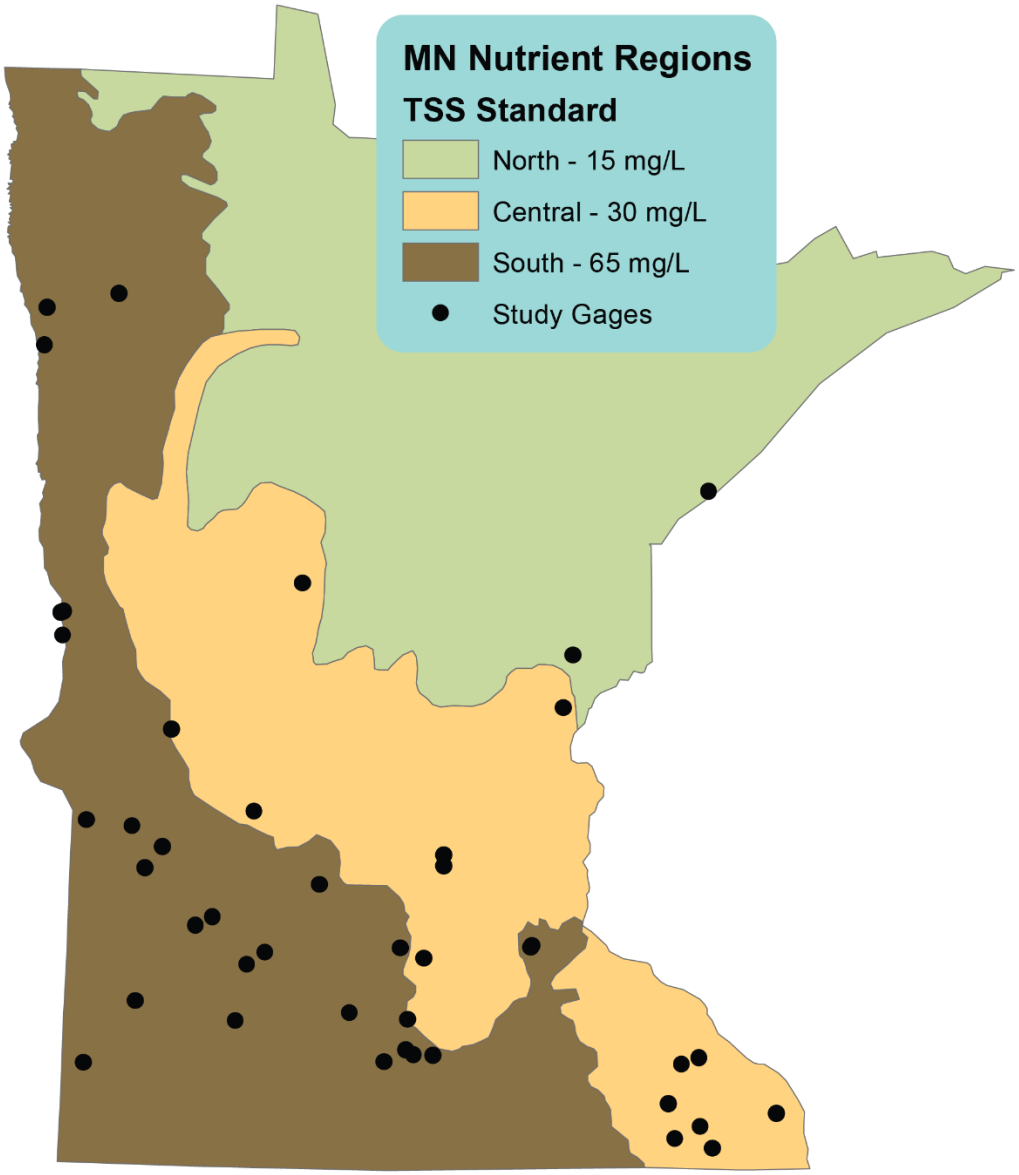

Figure 2. Nutrient regions defining TSS TMDL standards in MN. Not shown is the distinct zone for the Red River mainstem, with a TMDL criterion of 100 mg/L.

The regional delineations are broadly based on USEPA Level III ecoregions. Regional criteria are based on two lines of evidence: 1.) Statistical analyses of paired biological and water quality (i.e. TSS) data to determine ecologically damaging threshold TSS concentrations and 2.) Analysis of TSS data from "least impacted" and reference streams [*Minnesota Pollution Control Agency*, 2011]. The different standards reflect coarse-scale variation in suspended sediment regimes and ecological settings across the state, produced by diverse geologic, geomorphic, climatic and land use settings and histories. However, localized variation in geomorphic conditions may cause significant variation in sediment transport regimes, and thus background loads, within these zones. An understanding of the environmental and geomorphic factors that set the natural background and sensitivity of sediment loads throughout Minnesota is a primary focus of this study.

Coarse-scale variation in watershed settings throughout Minnesota is briefly outlined in the section below and a summary of environmental characteristics of each study watershed is presented in the Tables A.1-A.6 in Appendix A.

Streams in the Minnesota River Basin (MRB) are naturally primed to deliver high sediment loads, a result of that basin's geologic history and more recent human alterations to the system. The current geomorphic setting of tributaries in the MRB is strongly influenced by the incision of the mainstem Minnesota River that occurred during glacial outburst floods from Lake Agassiz starting 13,400 years ago [*Upham*, 1890, 1895; *Shay*, 1967; *Clayton and Moran*, 1982; *Matsch*, 1983; *Thorleifson*, 1996; *Fisher*, 2003]. The mainstem incised as much as 70 m, resulting in a lowered base level for the tributary streams, which have responded with subsequent incision and knickpoint migration 35-40 km upstream. This incision has created high relief and more steeply sloped "knick zones" below the knick points [*Belmont*, 2011; *Gran et al.*, 2011, 2013]. Within the knick zones, tall bluffs composed primarily of glacial till are common along the valley and channel margins. Bluffs erode through fluvial toe erosion, groundwater sapping,

and freeze-thaw processes and supply large amounts of fine and coarse sediment to the channel [*Sekely et al.*, 2002; *Belmont et al.*, 2011b; *Gran et al.*, 2011, 2013, *Day et al.*, 2013a, 2013b; *Schaffrath et al.*, 2015]. Above the knick zones, the landscape has relatively little relief and streams have low gradients with wide alluvial floodplains [*Belmont*, 2011]. Modern human-caused alterations have also promoted high sediment yields and geomorphically active systems. Stream flows and water yields have increased in the MRB since the mid-20th century, largely due to a combination of enhanced artificial drainage from agricultural fields and increase in precipitation [*Lenhart et al.*, 2011; *Schottler et al.*, 2014, Kelly et al., in review], with a concomitant large increase in sediment loading [*Kelley and Nater*, 2000; *Engstrom et al.*, 2009; *Belmont et al.*, 2011b]. Soils in the MRB are primarily fine-grained Mollisols, and row crop (corn and soy) agriculture dominates, comprising 92% of the basin's land use [*Kelley and Nater*, 2000]. Average annual precipitation ranges from 560 mm in the northwestern portion of the basin to 800 mm in the southeast, while annual runoff ranges from 50 mm to 150 mm along the same gradient [*Anthony et al.*, 2010].

Stream flows in the Mississippi River Basin have also shown a slightly increasing trend over the 20th and early 21st centuries [*Novotny and Stefan*, 2007]. Surface geology of the Upper Mississippi River Basin (defined here as above the confluence with the Minnesota River) is similar to that of the MRB, comprising primarily Pleistocene till [*Hobbs and Goebel*, 1982]. However, streams in the Upper Mississippi River Basin did not experience the downcutting event associated with glacial lake outburst flooding, as did the MRB streams. Therefore, Mississippi River tributaries lack the incised, bluff-dominated, and steep bedslope characteristics of MRB tributary knick zones, and are therefore likely to have different sediment transport regimes characterized by lower transport rates and sediment concentrations. The Upper Mississippi Basin contains primarily Alfisol soils, whose sandy texture and poor fertility have historically limited agricultural land use to 44% of the basin's area [*Kelley and Nater*, 2000]. However, the

southwestern part of this basin (including the North and South Forks of the Crow River included in this study) is dominated by more fertile Mollisols and is heavily farmed.

The Lower Mississippi River Basin (defined here as below the confluence with the Minnesota River down to the southern border of Minnesota) flows through the driftless area of southeastern Minnesota. That region remained mostly unglaciated during the last glacial cycle and is characterized by topography consisting of rolling uplands dissected by deeply incised bedrock valleys with wide, flat alluvial valley bottoms [*Knox*, 1977a, 2001, 2006; *Beach*, 1994; *Stout et al.*, 2014]. Poor agricultural land use practices in the late 1800s to the early 1900s resulted in a pulse of erosion from agricultural uplands. Much of the eroded sediment was stored in the floodplains and continues to be remobilized by erosion of banks and alluvial terraces, maintaining elevated sediment yields despite improved land management practices [*Trimble*, 1999, 2009, 2012; *Stout et al.*, 2014; *Belmont et al.*, 2016]. This region is the wettest in the state, with average annual precipitation values ranging between approximately 800-900 mm.

The Lake Superior Basin, located in northeastern Minnesota, is underlain by bedrock of the Canadian Shield and is characterized by thin soil cover over volcanic and metamorphic rocks [*Anthony et al.*, 2010]. The basin is primarily forested, with little agriculture. The St. Croix River Watershed is also primarily forested and characterized by poor soil for agriculture (predominantly Alfisols, with some isolated Inceptisols and Spodosols in the headwaters area) [*Kelley and Nater*, 2000; *Engstrom et al.*, 2009]. Average annual precipitation is relatively high in these basins, between about 750 and 800 mm.

The mainstem Red River of the North flows through highly erodible silt and clay lacustrine deposits from Glacial Lake Agassiz [*Hobbs and Goebel*, 1982]. The fine clay and silt lake plain sediments are easily suspended and tend to stay in suspension even during low-flow conditions, resulting in high TSS concentrations across the range of flows [*Minnesota Pollution Control Agency*, 2011]. The Red River mainstem, therefore, has the highest TSS threshold

criterion in the state, at 100 mg/L. Many Red River tributaries extend beyond the glacial Lake Agassiz basin and the surficial geology in those basins is dominantly till and glacio-lacustrine sediments [*Hobbs and Goebel*, 1982]. The topography of the Red River Basin is exceptionally flat, and the land use is predominately agriculture (66%) [*Melesse*, 2004; *Anthony et al.*, 2010]. This basin is in the driest part of the state, with average annual precipitation values around 500 mm.

DATA AND METHODS

Q-TSS Data and Relationships

We obtained TSS and Q data from the Minnesota Department of Natural Resources (MDNR) and Pollution Control Agency (MPCA) Cooperative Stream Gaging program. The TSS data were collected as grab samples from the middle of the stream cross-section less than 1m below the water surface [*Ellison et al.*, 2014]. To minimize the impact of nonstationary hydrologic and geomorphic conditions, while still including enough data to produce stable relations and meaningful results, we examined data from all gages that have TSS data spanning 10 years after the year 2000. Additionally, we obtained data for two gages, Sand Creek and the Credit River, from the Metropolitan Council Environmental Services (MCES) stream monitoring program. We relaxed the 10-year criterion to include gages from several watersheds that have been the focus of a substantial amount of related research. These exceptions included three gages on the Le Sueur River in the Minnesota River Basin (with 5, 6, and 9 years of data) and five gages in the Root River watershed in the Lower Mississippi River Basin (each with 3-5 years of data). Including these basins greatly expanded the contrasts in Q-TSS relationships and landscape characteristics in our dataset. The Q-TSS relationships for these gages are constrained by an average of 155 points of paired Q and TSS data.

Due to data availability limitations, we used daily mean discharge values rather than instantaneous discharge at the time of the TSS measurement. However, we compared results using instantaneous and daily average data for time periods and gages where both were available (partial records at 44 gages, see Appendix B, Figure B.1 and B.2). We determined that the two approaches yielded similar rating curves and that using daily mean Q, available over the entire time period, was preferable to using instantaneous Q data over the shorter time period for which those data were available.

In total, we analyzed paired Q and TSS data from 45 gages: 22 from the Minnesota River Basin, 4 from the Upper Mississippi River Basin, 9 from the Lower Mississippi Basin, 6 from the Red River of the North Basin, 2 from the St. Croix River Basin, and one each from the Missouri River and the Lake Superior Basins (Figure 1). Watersheds draining to the gages range in size from roughly 32 km^2 to 15,000 km^2 with a median of 1175 km^2. The average number of data points (paired Q and TSS values) across all gages was 210 (standard deviation 90), for a total of 9650 paired Q and TSS points across all gages. For all sites, the average number of years with data was 9.3 (standard deviation 3.1). The average number of years per site with 20 or more points was 5.2 (standard deviation 2.7).

We normalized discharge by the geometric mean of the sample discharges for each gage, as suggested by Warrick [2014]. The normalization facilitates comparison between basins of different size. Normalizing by the geometric mean, specifically, is optimal because the geometric mean is the center of mass of the log-transformed discharge data. When a least-squares regression is fitted to the log-transformed, geometric mean-normalized discharge and the log-transformed TSS data, the center of mass of the data is at the y-intercept, and the intercept term of the regression (termed â) describes the vertical offset of the center of mass of the TSS data [*Warrick*, 2014]. In other words, the SRC coefficient quantifies the TSS value corresponding to the geometric mean of discharge values (i.e., the y-intercept, when $\log(Q/Q_m) = 0$). This procedure also eliminates the potentially problematic correlation between the y-intercept parameter (â) and the slope parameter (b). The parameters *a* and *b* derived from traditional rating curve analysis are strongly negatively correlated, whereas the parameter â provides a more independent and robust measure of vertical offset in the sediment rating curve [*Warrick*, 2014].

We fit linear least-squares regressions to the normalized and log-transformed Q and TSS data, generating â (intercept) and b (slope) values for each rating curve. However, many gages have Q-TSS relations that are not well represented by a single log-log linear regression. Some

relations have flat slopes at low discharges and then pass a threshold beyond which TSS values increase with increasing Q (which we call threshold relations). Other relations start out flat or with positive slope, and then reach a threshold beyond which the TSS concentrations decrease as Q increases (we call these "peaked" relations). Examples of each of these forms of Q-TSS relation are shown in Figure 3A-C. Q-TSS relations for all gages are included in Appendix C. A single regression line through all of the data for these gages would misrepresent the relations and result in biased regression parameters. Several studies have experimented with fitting rating curves with more complex functions than log-linear (i.e. power) functions. These techniques include regression with modified power functions that include correction factors or additive error terms [*Asselman*, 2000; *Sadeghi et al.*, 2008], regression with second or third order polynomials [*Sadeghi et al.*, 2008; *Fan et al.*, 2012], and fitting of various other functions [*Sadeghi et al.*, 2008]. Warrick [2014] suggests using locally weighted scatter smoothing (lowess) fitting techniques and analyzing residuals about those functions for Q/SSC data that don't follow the power function form. However, none of these approaches readily allow for quantifiable and easily interpretable comparison between relations at different gages.

To more accurately characterize relations that did not follow a simple power function, we split the data at breakpoints located at the transitions in slope on rating curves and fit separate log-linear relations to the data on each side of the breakpoint. These breakpoints are a distinguishing and important characteristic of many of our study gages and may represent critical transitions in geomorphic process or sediment availability. To find the location of the breakpoints, we used the Python programming language function *scipy.interpolate.splrep*, which implements the spline interpolation method outlined by Dierckx [1975]. The algorithm fits a linear spline to the data, automatically detecting the ideal location of breakpoints in the data. The number of knots found by the function depends on a user-specified smoothing parameter, whose value must be tuned depending on the number of data points and the scatter in the data. For each

gage, we computed the spline interpolation over a broad range of smoothing parameter values. For the final fit, we kept only those breakpoints that were stable over a broad range of smoothing values and persisted as the smoothing parameter approached higher values that eventually produced a single spline with no breakpoints. The necessity of specifying a smoothing parameter adds some subjectivity to the process of locating breakpoints. Final spline fits had either no breakpoint (i.e., a simple log-linear relation with no breakpoints) or one breakpoint (for threshold and peaked SRC).

To characterize TSS concentrations at low flow conditions, we used the fitted SRC relations to compute the estimated TSS value at the 90% exceedance Q, a low flow condition. We computed the 90% exceedance Q using the sampled flows rather than the entire flow record, in order to measure a more consistent location on each Q-TSS relation.

Suspended sediment rating curves commonly display hysteresis, defined here as different TSS values for the same discharge on the rising limb and falling limb of a flood [*Walling*, 1974; *Loughran*, 1976; *Walling and Webb*, 1982; *Klein*, 1984; *Soler et al.*, 2008; *Fan et al.*, 2012]. Multiple studies have shown that improved rating curves with reduced scatter around the regression line are obtained by fitting separate rating curves to the rising and falling limb data [*Walling*, 1974; *Loughran*, 1976; *Klein*, 1984; *Asselman*, 2000; *Sadeghi et al.*, 2008]. Inspection of rating curves for our study gages revealed that hysteresis is common, especially at higher flows, with rising limb TSS values generally higher than falling limb TSS values. Accordingly, we divided the Q-TSS data by flow stage. For any relations exhibiting breakpoints, we classified points to the left of the breakpoint as “low flow”, and points to the right as “high-flow”. We focused most of our analysis on the high-flow data, because high flows tend to be more geomorphically important. We classified points as rising limb or falling limb by whether the mean daily discharge for the data point was larger or smaller, respectively, than the previous day’s discharge. We fit separate regressions to the rising and falling limb data in addition to a

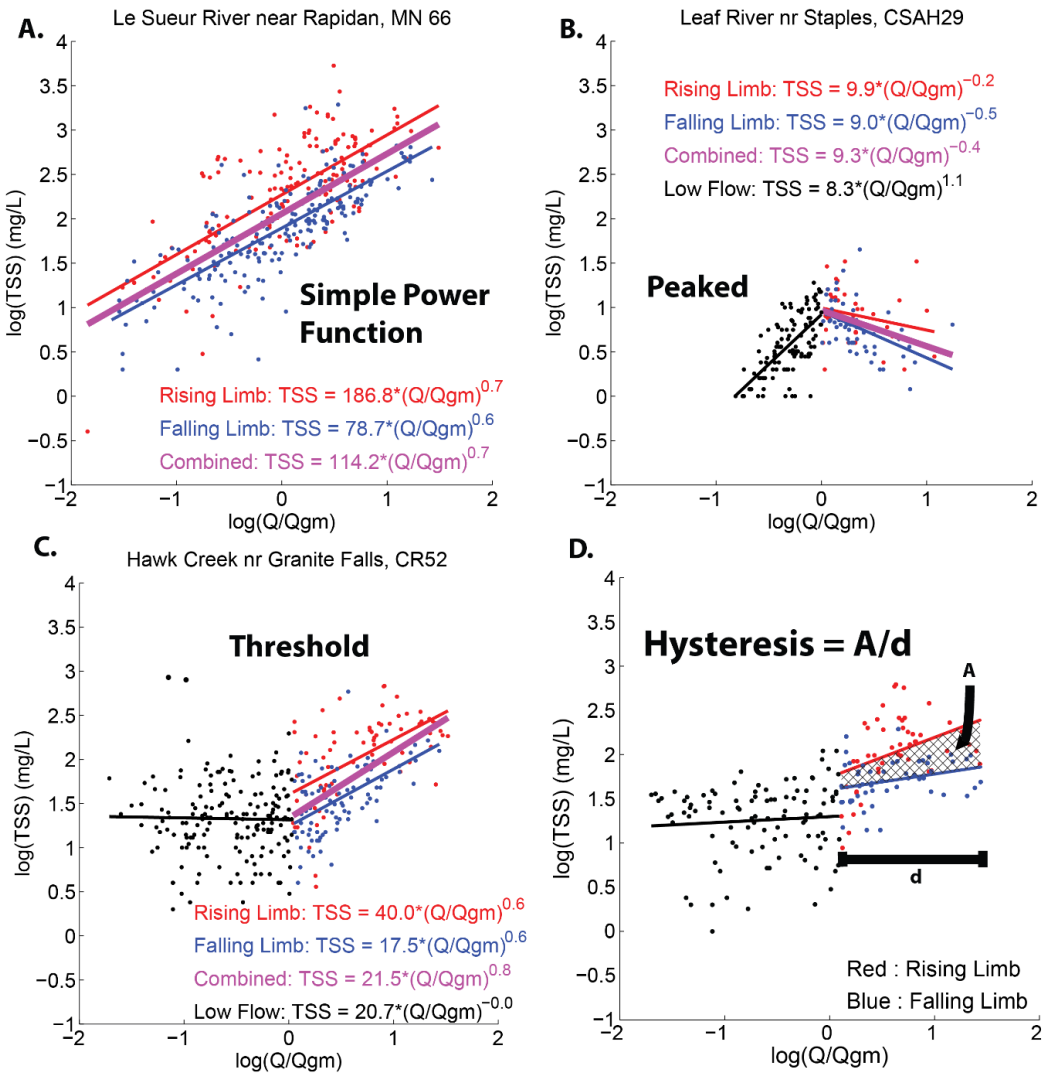

Figure 3. A – C. Representative Q-TSS relationships, showing the three broad categories of relationships observed. **D.** Explanation of computation of hysteresis metric.

regression fit to all above-breakpoint data (i.e., the combined rising and falling limb data).

Hysteresis is an interesting and geomorphically meaningful component of the Q-TSS response, possibly indicating sediment depletion over the course of storm events. In order to include the magnitude of hysteresis in our analysis, we quantified hysteresis for use as a response

variable in an RF model as the average distance between the rising and falling limb regression lines. We computed this value by first calculating the area between the two regression lines (A in Figure 3d), subtracting the integral of the falling limb regression line from the integral of the rising limb regression line. Each integral was calculated over the interval from the smallest to the largest discharge value in the above-breakpoint (i.e. the combined rising and falling limb) dataset, or over the entire dataset if no breakpoint was present. We then normalized this area by dividing by the horizontal distance encompassed by the same interval used for integration (d in Figure 3d). This procedure yielded the average distance between the rising and falling limb regression lines. Values for all SRC parameters for each gage are in Table A.7 and A.8.

Landscape and Environmental Data and Methods

Basin-Scale Analysis

We quantified the land cover/land use, soil erodibility, climatic/hydrologic, geologic, and topographic setting of study watersheds for use as predictor variables in our RF models. Datasets used and metrics extracted are summarized in Figure 4, and are described in further detail below. Values of each metric, for each watershed, are contained in Tables A.1 – A.4.

Land Cover/Land Use

We obtained the 2011 edition of the 2006 land cover layer from the National Land Cover Dataset (NLCD) and simplified it into six broad groups: water/perennial ice/snow (NLCD types 11,12), developed (NLCD 21,22,23,24), barren (NLCD 31), forest/shrub land/herbaceous (NLCD 41,42,43, 51,52, 71,72,73,74), agriculture (NLCD 81,82), and wetlands (NLCD 90,95). We calculated the percentage of land in each land cover class within all study watersheds and included percent forestland, agriculture and wetlands in the statistical models.

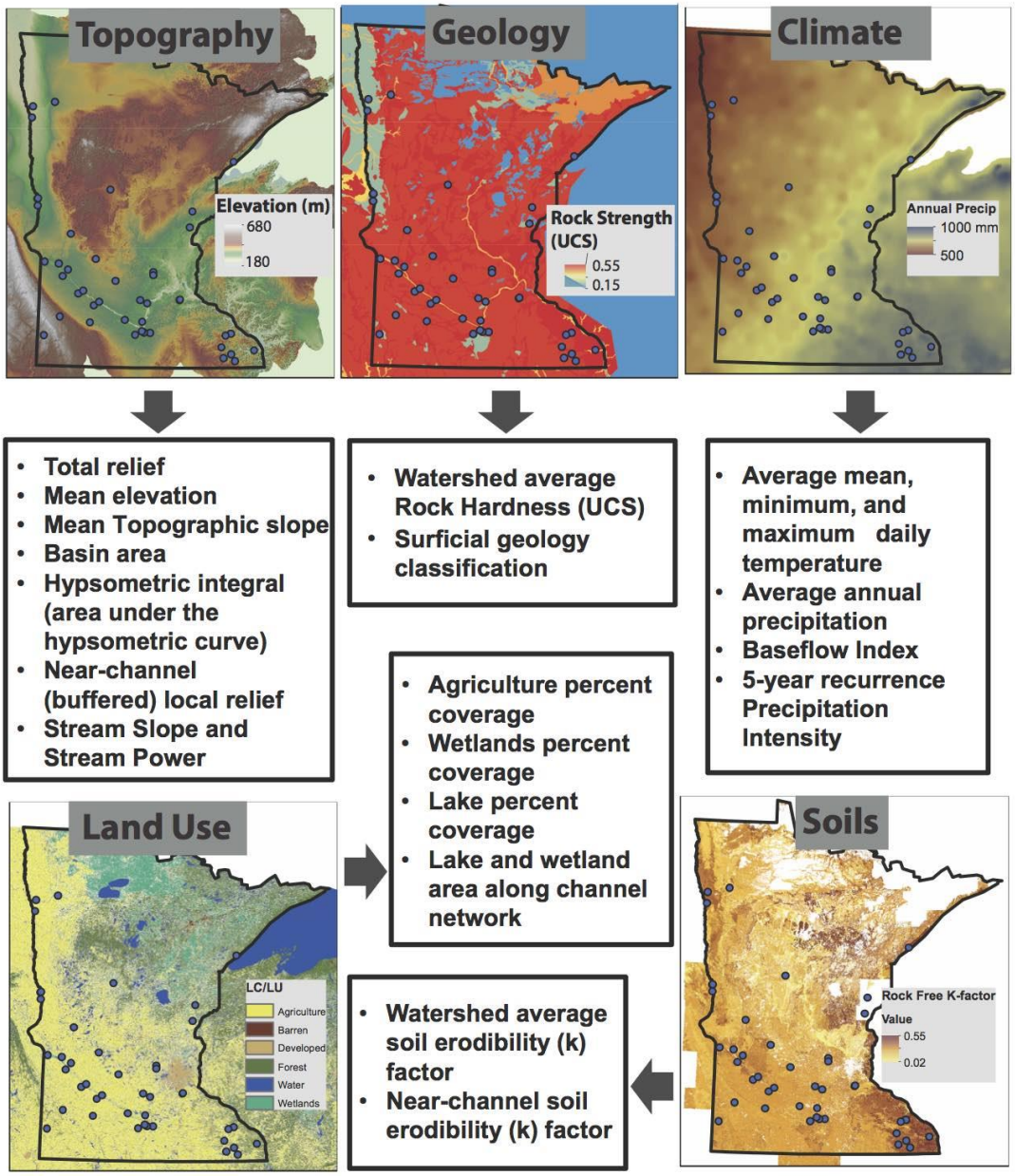

Figure 4. Summary of GIS datasets used to describe the geomorphic and environmental setting of the watersheds and channel networks upstream of study gages. Also shown are the metrics derived from these datasets to quantify them.

Climate

We used PRISM (Parameter-elevation Relationships on Independent Slopes Model) data to characterize the long-term average climatic setting of the study watersheds. PRISM is a

gridded dataset produced by interpolation of climate station (point) data. Temperature and precipitation are calculated for each cell of a DEM based on a climate-elevation regression incorporating station data weighted by physiographic similarity of the station to the grid cell. Physiographic variables taken into account are location, elevation, coastal proximity, topographic facet orientation, vertical atmospheric layer, topographic position, and orographic effectiveness of the terrain [*Daly et al.*, 1994, 2008]. We used the 30-year normals to represent long-term climate averages, computed at a spatial resolution of 800 m. We obtained average annual precipitation and annual minimum, maximum, and mean temperature data and calculated watershed averages of those metrics using the Zonal Statistics as Table tool in ArcGIS.

We obtained precipitation intensity estimates from the NOAA Precipitation Frequency Data Server (http://hdsc.nws.noaa.gov/hdsc/pfds/). We obtained gridded data for the 10 minute, 60 minute, and 24 hour intensities for precipitation events with a 5-year recurrence interval (i.e., powerful, but not catastrophic storms) and used Zonal Statistics as Table in ArcGIS to compute average precipitation intensity values for each watershed.

Baseflow Index

Baseflow index (BFI) is the ratio of base flow to total flow in a stream and is a measure of the flashiness of a stream. Flashy streams that receive a relatively high proportion of their water as stormflow will have a low BFI, whereas streams with more stable hydrographs generally receive most of their water as baseflow and will have a high BFI. We obtained a 1-km resolution gridded BFI dataset produced by the U.S. Geological Survey [*Wolock*, 2003]. The gridded data were generated by interpolating point BFI values estimated for 8,249 streamgages across the US. The streamgages each had a streamflow record at least 10 years long and drainage area less than 1000 km^2. Point estimates of annual BFI at the streamgages were computed using an automated hydrograph flow separation program employing a local minima approach with a recession slope

test [*Wolock*, 2003]. We computed the average BFI value for each watershed using the Zonal Statistics as Table tool in ArcGIS.

Soils

We used data from the Soil Survey Geographic Database (SSURGO) to characterize soil types within the study watersheds. Specifically, we evaluated soil erodibility K factor data, which quantify the susceptibility of soil particles to detachment by water (i.e., by rill or sheet erosion). The K factor represents the average, long-term potential soil response to the erosive power of rainstorms. It is a lumped parameter incorporating the integrated erosive effects of multiple processes including raindrop impact, surface flow, localized topography-driven deposition, and rainwater infiltration. It represents the inherent erodibility of the soil based on its physical properties, and is measured to be independent of antecedent soil-moisture and soil-surface conditions and rainstorm regimes [*Renard et al.,* 1997].

K factor values are reported as both "whole soil" and "rock free" estimates. Rock free K estimates exclude rock fragments larger than 2 mm and indicate the erodibility of only the fine-earth fraction of the soil layer. These estimates are obtained from regression equations developed from rainfall simulation plot experiments. The equations incorporate the percentage of silt, sand, and organic matter as well as soil structure and saturated hydraulic conductivity [*Renard et al.*, 1997]. K values range from 0.02 to 0.69, with higher K values representing soils that are more susceptible to erosion by water. Whole soil K estimates incorporate the effects of rock fragments, which can alter erodibility of a soil. Rock fragments on the soil surface decrease soil detachment by rainfall, while rock fragments present in coarse textured (sandy and loamy) soil can decrease infiltration, thereby increasing runoff and soil erosion. Whole soil K factor estimates are adjusted from the rock free estimates accordingly to account for these effects [*Renard et al.,* 1997].

As it is not inherently obvious which value is more appropriate, we extracted and analyzed both whole soil and rock free K factor values. To quantify soil erodibility across the watershed with a single number, we calculated the mean surface layer K factor within the watershed, weighted by area. K factor data are reported for each soil horizon, but we only analyzed the surface layer, as that is the soil directly available to be eroded. We used the dominant condition aggregation method to obtain the K factor value for each SSURGO map unit polygon. We then converted SSURGO soil unit polygons to rasters with 10 m resolution as that sufficiently reproduced the detail of the original polygons. We used the Zonal Statistics as Table tool in ArcGIS to compute the watershed average value.

SSURGO data are obtained at the county scale, and some discontinuity in the K factor data exists across county lines. However, we determined that the discrepancies were not enough to cause significant, systematic errors when comparing different parts of the state. Nevertheless, we also obtained STATSGO soil data, which are coarser, regional data scaled up from the SSURGO dataset. Due to the method used to rescale the data, the data are more continuous and lack the discrepancy at county boundaries seen in SSURGO data. We computed watershed-average K factor values from the STATSGO data in addition to the watershed-average values computed from the SSURGO datasets, and tested both in our RF models.

Geology

Geologic setting and lithology have been shown to exert strong controls on sediment transport regimes in many cases [*Hicks et al.*, 1996; *Tamene et al.*, 2006; *Belmont et al.*, 2007; *Ali and de Boer*, 2008; *Mueller and Pitlick*, 2013]. Strength of the bedrock and its susceptibility to erosion should influence sediment generation and thus transport regime. We attempted to capture this effect by computing the average rock strength of the surficial lithology within the study watersheds. We used the national 1:5,000,000-scale surface geology map by Soller and Reheis

[2009] and followed the methods of Olson and Hawkins [2012] to compute average rock strength values, measured as uniaxial compressive strength (UCS), for each map unit lithology. Olson and Hawkins [2012] characterized physical and chemical properties, including UCS, of lithologic types using data from the OZCHEM National Whole Rock Geochemistry Database, the Earthchem Geochemical Database, the National Geochemical Database, and literature searches.

We used map unit descriptions from Soller and Reheis [2009] to derive lithology subclasses for the surface geology map units. For example, one unit mapped as a predominantly loamy/silty till, is described as: "Glacial till sediments – unsorted material ranging in size from clay to boulders, deposited by glacial ice. Includes minor areas of ice-contact and lake sediment. Predominantly loamy (silty) till." In the database constructed by Olson and Hawkins [2012], separate physical and chemical attributes are specified for individual grain size/texture classes of till (i.e., the boulder subclass of till has different properties than the gravel till subclass). Because the unit described above has grains ranging from clay to boulders, we included a subclass for clay, silt, sand, gravel and boulders. The computation method of Olson and Hawkins [2012] allows different subclasses to be weighted differently according to their relative proportion in the unit. Possible weighting descriptions are, in order of descending importance, "major", "minor", and "incidental". Because the above unit was described as predominantly silty, the silt subclass was weighted as "major", while clay and sand were classified as "minor", and gravel and boulders were classified as "incidental".

Once a weighted-average rock UCS was computed for each map lithology, we converted the data to a raster format with 100 m resolution, which sufficiently preserved the mapped features. We used the Zonal Statistics as Table tool to derive a basin-average UCS value for each study watershed. In addition to this quantitative characterization, we also implemented a simpler characterization by classifying each watershed and gage location by the dominant surface lithology, using the following classes determined from the map of Hobbs and Goebel [1982]:

unconsolidated, calcareous till, non-calcareous till, and colluvium. Our methods for characterizing the geology are relatively coarse, as the geologic maps themselves were of coarse scale. We cannot capture, for example, specific locations where the river channel interacts with bedrock, alluvial deposits or terraces. These finer-scale features may be important to sediment transport regimes, but are not available at the large scale of our analysis. Nevertheless, our methods capture the broad-scale variations in geology across the state and the corresponding variation in rock strength.

Topography

We extracted several common basin-scale morphometrics describing the topographic setting of the watersheds. These metrics included the total relief, mean and maximum elevations and mean topographic slope within the watershed. We also used the Hypsometric Tools ArcGIS toolbox [*Davis*, 2010] to compute the hypsometric integral, which measures the area under the hypsometric (area-elevation) curve.

Near-Channel Analysis

To characterize the potential of the channel-floodplain corridor to contribute to suspended sediment, we computed metrics describing channel gradient, near-channel local relief, stream power and other characteristics. Local relief is intended to capture the degree to which the channel is able to access potential large sediment sources in the form of tall banks, bluffs, and terraces. Those features have been shown to be important sediment sources in watersheds in the Midwest and elsewhere [*Nolan and Hill*, 1991; *Simon*, 2006; *Juracek and Ziegler*, 2009; *Trimble*, 2009; *Belmont et al.*, 2011b; *Stout and Belmont*, 2014; *Stout et al.*, 2014; *Donovan et al.*, 2015]. To calculate local relief, we used the ArcGIS Focal Statistics tool, computing relief within a moving square window of 75m by 75m on the 3m lidar DEMs. From visual inspection of the DEMs for multiple study watersheds, that window size is adequately large to encompass most

geomorphically important features such as bluffs and terraces. We split the NHDplus stream line dataset into 500 m-long segments, and created a 100 m buffer for each segment. We computed the average local relief value within each of those buffers (Figure 5A).

Stream power is a measure of the rate of potential energy expenditure per unit length of channel, or alternatively, the measure of a stream's ability to perform geomorphic work and transport sediment [*Knighton*, 1998]. It is defined as:

$$\Omega = \gamma QS \qquad (3)$$

where Ω is stream power, γ is the specific weight of water, Q is discharge, and S is channel slope. We calculated stream power at 3 km increments along the entire NHDplus stream network for study basins. Streamlines were snapped to the network used by the StreamStats application (http://water.usgs.gov/osw/ streamstats/) to enable calculation of a representative discharge, which we chose to be the 2 year recurrence interval flood. StreamStats computes estimates of peak flow statistics for ungaged sites by implementing regional regression equations that relate peak flow statistics calculated from log-Pearson Type III analysis at gaged sites to corresponding basin and climatic characteristics. Basin characteristics used in the regression equations are drainage area, main-channel slope, percent lake area, storage area, percent soil hydrologic group A, percent soil hydrologic group D, and mean annual runoff [*Lorenz et al.*, 2009]. We used StreamStats to compute the magnitude of the 2-year recurrence interval flood at the midpoint of each 3 km stream segment, and used that discharge as the input to the stream power calculation. We calculated channel slope along each NHDplus segment from a 30 m resolution DEM "burned" to coincide with the NHD plus stream lines. We used the ArcGIS Add Surface Information tool to calculate an average slope along each segment. Channel slope was calculated at 50 m increments along the stream lines, and those local measurements were averaged to compute a single value for each 3 km segment.

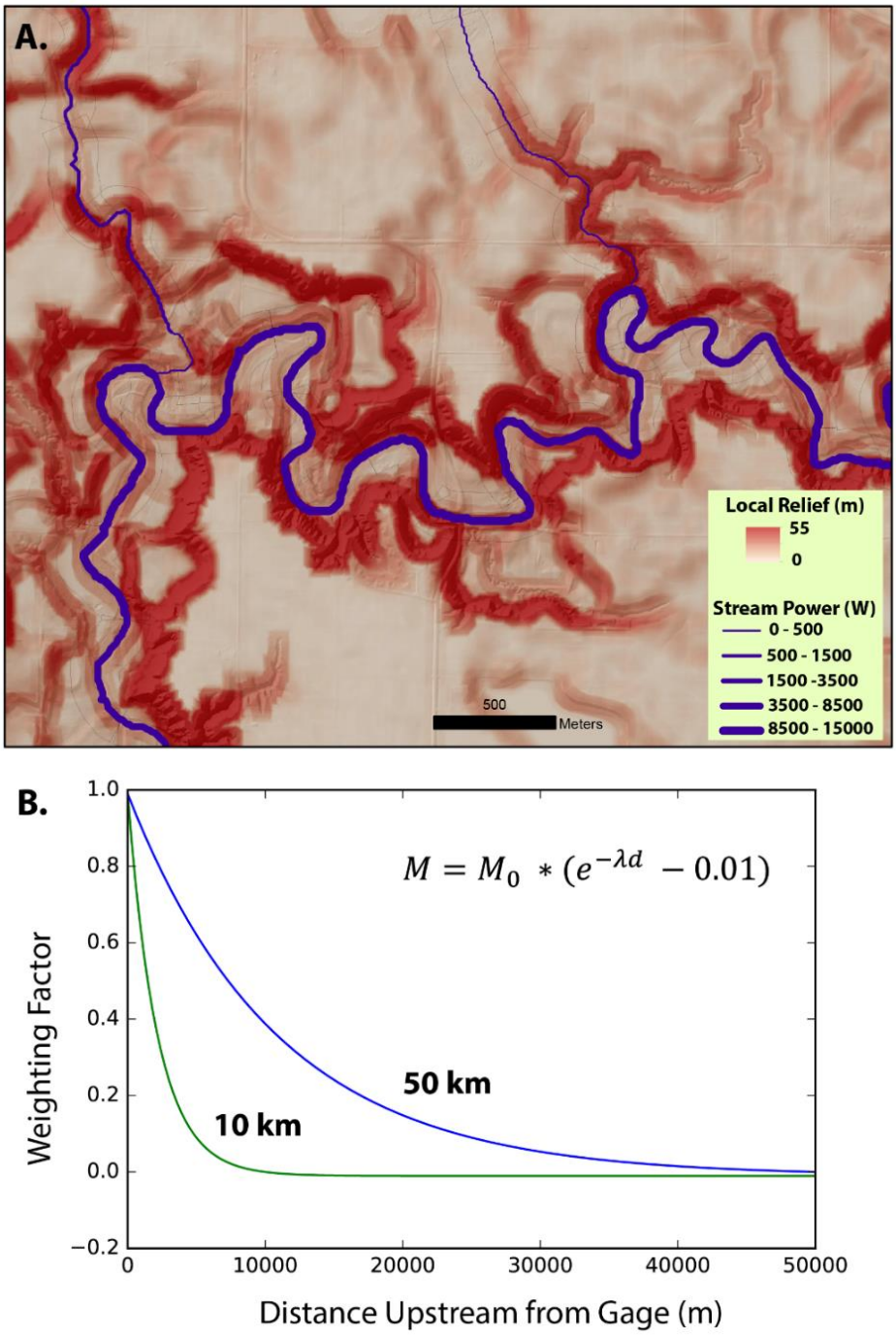

Figure 5. Explanation of near-channel analysis. **A.** Example of near-channel local relief and stream power datasets. Average values for all near-channel metrics were computed within the 50 m stream buffer (shown in gray). **B.** Decay functions used to weight near-channel metric values computed for each stream segment by their distance upstream from the gage. Aggregate values for each metric were computed by summing distance-weighted values for each stream segment. Functions decaying to 0 weight at both 10 and 50 km were used.

Unit stream power (stream power normalized by channel width) may be more appropriate than total stream power for comparing streams of different sizes. Width normalization produces a metric with units of power per unit area of streambed, rather than power per unit length, which allows for a more meaningful comparison of values between rivers of different size. We estimated unit stream power using simple downstream hydraulic geometry relations (after Leopold and Maddock [1953]) relating stream width to the 2-year recurrence flood:

$$W = aQ^b \qquad (4)$$

where Q is the 2-year recurrence flood computed with StreamStats. Hand-digitized stream bank data were available for the Le Sueur River, which we used to compute average width along the stream network. We used those data in conjunction with the discharge data to compute a value of b = 0.7. Using that value, we divide equation 3 (ignoring the coefficient) by equation 4, to obtain:

$$\omega = \frac{\gamma QS}{Q^{0.7}} = \gamma Q^{0.3} S \qquad (5)$$

The assumption that the hydraulic geometry relation for stream width computed from one stream applies to all study streams (justifying omitting the coefficient parameter and using the exponent of 0.7 universally) admittedly makes our unit stream power estimates coarse. However, several recent studies have suggested similar scaling of channel width among rivers in vastly different environments [*Parker et al.*, 2007; *Jerolmack*, 2015]. Nevertheless, the computation addresses the issue of different spatial scales in our different study basins, and we tested whether it may be more predictive for Q-TSS relations than total stream power.

In addition to average local near-channel relief and stream power, we also computed average near-channel soil erodibility factor values within the same buffers used for local relief. Additionally, we computed the area within the stream network buffer comprising lakes, marshes

and reservoirs from the NHDplus Waterbodies dataset. Such waterbodies along the stream network are likely to act as significant sediment sinks, and thus impact the sediment transport regime.

Sediment entrained far upstream of a stream gage may be redeposited before being transported past the gage. Therefore, near-channel geomorphic conditions far upstream from the gage are less likely to directly influence the sediment regime than conditions closer to the gage. The area of the stream network that exerts the strongest control on the sediment regime at the gage is likely to be limited to the distance that fine sediment particles typically move during storm events. However, predicting and measuring typical travel distances for suspended sediment is difficult and travel distances are highly variable from system to system and from storm to storm. Thus, the travel distance behavior of suspended sediment is generally poorly understood [*Walling*, 1983; *Bonniwell et al.*, 1999; *De Vente et al.*, 2007; *Pizzuto et al.*, 2014]. There have been several attempts to resolve this problem. Verhoff et al. [1979] observed phosphorus transport as a proxy for fine sediment transport, as the two are often closely related. Working under the assumption that water moves as a kinematic wave with celerity faster than the movement of the individual water and sediment (phosphorus) particles, they analyzed the relative timing of discharge hydrographs and total phosphorus concentration chemographs at gaging sites to estimate average particle travel distances. For the Sandusky River watershed in Ohio, they found that median travel distances varied from about 30 km in a tributary high in the watershed to 80-200 km on the mainstem river lower in the watershed. They noted that average travel distances were apparently influenced by channel slope and that travel distances were generally lower in upper reaches of tributaries than in the mainstem. For a given point in the watershed, travel distances increased with increasing discharge and with increasing storm duration [*Verhoff et al.*, 1979].

More recently, efforts have been undertaken to use radionuclides to trace suspended sediment plumes and determine average transport distances. Using similar methods and assumptions as Verhoff et al. [1979], but using ^{7}Be, ^{137}Cs, and ^{210}Pb as tracers, Matisoff et al. [2002] estimated fine sediment transport distances over a 48-hour storm event. In two small, agricultural watersheds (69.5 km^2 and 90.5 km^2) draining to Lake Erie, they calculated transport distances ranging from 6.3 to 26.1 km over the course of the event. Using similar methods, Bonniwell et al. [1999] estimated fine sediment transport distances over the course of a snowmelt hydrograph in a mountain stream. They calculated transport distances ranging from 60 km at the peak of the hydrograph to 12 km during baseflow conditions. Clearly, fine sediment transport distances are highly variable between different watershed settings, and even within individual watersheds depending on local conditions and flow. However, these studies shed light on the order of magnitude of transport distance one might expect for fine sediment, in the tens of kilometers.

To represent upstream distance weighting of near-channel morphometrics in a simple, yet reasonable way, we created two sets of near-channel data, corresponding to two length scales upstream from the gage, 10 km and 50 km. The shorter length roughly corresponds with the shorter particle travel distances measured in the aforementioned studies, and represents channel-floodplain conditions a short distance (in terms of typical fine sediment transport distances) upstream from the gage. The longer distance incorporates conditions farther upstream, and approaches some of the larger transport distances reported above. Especially in some of the larger watersheds in this study, 50 km may underestimate the average event-scale transport distances. However, we did not use a larger number because a number of watersheds in this study have maximum distances upstream from the gage in the 20-30 km range. Extending the near-channel study zone to distances much more than that would bias comparisons between watersheds of substantially different size.

To achieve the upstream distance weighting, we applied exponential decay functions to the raw near-channel metric values for each stream segment (Figure 5B):

$$M = M_0 * (e^{-\lambda d} - 0.01) \qquad (6)$$

where M is the distance-weighted metric, M_0 is the original value of the metric, d is the distance of the stream segment upstream from the gage, and λ is a constant. We specifically selected λ values to force the exponential decay to <0.01 at either 10 km or 50 km, such that stream segments farther upstream than the maximum distance value are effectively eliminated from the analysis. We summed all positive distance-weighted values to get, for each metric, a single value representing the aggregate condition for that metric within the specified distance upstream.

Random Forest Modeling

We used Random Forest (RF) models to analyze the complex relationships between the basin and channel metrics (predictor variables) and the rating curve shapes (response variables). RF models are an ensemble tree-based statistical tool, based on Classification and Regression Tree (CART) methods, that have been developed relatively recently and are being applied extensively to classification and regression problems in ecology, bioinformatics, and other fields [*Liaw and Wiener*, 2002; *Cutler et al.*, 2007; *Strobl et al.*, 2007, 2008; *Olson and Hawkins*, 2012]. RF models have been shown to perform as well as or better than the best available classification and regression methods [*Cutler et al.*, 2007; *Olson and Hawkins*, 2012] and have several advantageous characteristics compared with more classical statistical techniques such as single or multiple linear regression. RF models can handle complex, non-linear interactions among predictor variables, and make no assumptions about the form of the relations between predictor and response variables [*Cutler et al.*, 2007; *Olson and Hawkins*, 2012]. This feature offers a clear advantage over linear models. Many processes in geomorphology are threshold-

based or otherwise non-linear, so the assumption of a linear relationship between predictor and response variables is often suspect. Additionally, RF models are fully non-parametric, so they require no distributional assumptions for variables as do many traditional statistical inference methods such as ANOVA or statistical hypothesis testing. Unlike classical regression models, RF models can be used for datasets for which the number of predictor variables greatly exceeds the number of observations. Further, RF models do not assume independence of predictor variables [*Cutler et al.*, 2007]. Finally, RF methods not only produce an accurate classifier or regression model but, importantly, can also be used to interpret the structure of a multivariate dataset through the use of variable importance measures and partial dependence plots.

RF models are an extension of Classification and Regression Tree (CART) methods, which must be understood first to understand RF models. The CART algorithm produces a tree with nodes representing groups of data points that are most similar with respect to values of the response variable of interest (either class membership in a classification model or numerical values in a regression model) within the groups compared to the dataset as a whole [*Breiman et al.*, 1984; *Jones and Linder*, 2015]. Starting with the original node containing all the data, the dataset is split into two new "daughter" nodes based on each data point's value for one particular predictor variable. Data points with predictor variable values smaller than the split value are placed in one node, whereas points with predictor variable values greater than the split value are placed in another node. (Note that this process works only for continuous predictor variables. Categorical variables for which "smaller" and "larger" have no meaning, are treated slightly differently.) The algorithm considers every unique value for each predictor variable in the dataset, choosing the optimal predictor variable and value of that predictor variable that results in the maximum increase in homogeneity of the response variable in each daughter node compared to the unpartitioned data. For regression RF models, mean squared error is used to measure the homogeneity of the response variable within nodes. Homogeneity is maximized when the mean

squared error is minimized. This occurs when individual response variable values are each close to the mean of all values within the node, or in other words, when each individual value is close to all others within the node. For classification models, homogeneity is measured with the "Gini" index, which measures the proportion of observations in the node whose class is different than the most common class in the node. Each resulting daughter node is recursively partitioned until further partitioning no longer increases homogeneity in potential daughter nodes. At this point the tree is said to be fully grown. To summarize in simple terms, at each partitioning step the algorithm chooses the predictor variable that best differentiates the observations of the response variable in the node being partitioned, putting observations that are most similar to each other in the same daughter node. The predictions of the model for observations falling in each node are computed as the average of all observations in that node (for regression models) or by majority vote of classes within the node (for classification models).

The RF procedure improves on the CART method, being more accurate as well as much more stable to small perturbations in the data [*Breiman*, 2001; *Cutler et al.*, 2007]. The RF algorithm grows a large ensemble of classification or regression trees (typically 500), with each tree trained on a different bootstrapped sample of the dataset. The trees are grown in the same manner as described above for the CART procedure, with an important exception: The predictor variables available to be considered by the model at each partition are limited to a randomly selected subsample of the entire set of predictor variables. Once each tree is fully grown in this manner, predictions are made onto the samples not included in each bootstrap sample (termed "out-of-bag" samples), and then the predictions are averaged across the entire ensemble of trees. Because predictions are made onto the out-of-bag samples not used to train the models, the accuracy rates for out-of-bag predictions are essentially cross-validated accuracy estimates [*Cutler et al.*, 2007]. The randomness induced by training on different bootstrapped samples (in which approximately 63% of the original observations occur at least once) and limiting the

potential predictor variables insures that individual trees are independent of one another. This process results in a better classification or regression when predictions across all the trees are averaged [*Breiman*, 2001; *Cutler et al*., 2007].

We constructed separate RF models for each of the following response variables: 1.) The general classified shape of the rating curve (simple power function, threshold power function, peaked SRC), 2.) The slope of the rising limb rating curve, 3.) the intercept of the rising limb rating curve, 4.) the slope of the combined (rising and falling limb) rating curve, 5.) the intercept of the combined rating curves, 6.) the predicted TSS value at the 90% exceedance flow (i.e. low flow), and 7.) hysteresis. The first model is a classification RF model. The rest of the models are regression RF models. The default of 500 trees were generated to construct each model, as a sensitivity analysis showed model performance did not improve with a larger number of trees. We used the default values for the size of the set of predictor variables available at each partition: $p^{1/2}$ for the classification model and p/3 for the regression model, where p is the total number of predictor variables in the model. We used the randomForest package in the R statistical computing software to carry out these analyses.

Variable importance plots generated for RF models constructed using the entire set of predictor variables showed that many predictor variables were unimportant. Additionally, pairwise comparisons between variables showed that several predictor variables were correlated, which can confound interpretation of RF variable importance measures [*Strobl et al.*, 2008; *Olson and Hawkins*, 2012]. To eliminate highly correlated predictor variables and to create the most parsimonious model excluding "noisy" variables with no real signal, we adopted an iterative modeling approach as suggested by Olson et al. [2012]. Using variable importance plots we sequentially eliminated the least important variables from each model, proceeding with variable exclusion until model performance declined. To measure model performance, we used out-of-bag prediction accuracy for the classification RF model and out-of-bag mean-square error for the

regression RF models. We generated partial dependence plots for each predictor variable remaining in the final models to graphically assess the dependence of the response variables on these important predictor variables.

To test our hypothesis that near-channel geomorphic conditions significantly affect sediment dynamics and that predictive models would perform worse if using only watershed-average metrics, we constructed RF models as above, but restricted the predictor variables to only the watershed-average variables. The process for variable selection was the same, but all near-channel metrics were excluded from the beginning.

RESULTS

The Q-TSS relationships broadly fell into three categories (Figure 3). The most common shape (26 gages) was a simple power (log-log linear) relation (Figure 3A). Six gages had peaked relations with a breakpoint above which TSS values decreased as log-log linear relations for the rising and falling limb. Three of the simple power function relations had negative slopes over their entire range of Q values, and we classified these along with the peaked SRC, for a total of 9 peaked/negative SRC (Figure 3B). Thirteen gages exhibited threshold relations, with Q-TSS shape essentially flat up to a given Q value and then increasing as a log-log linear relation above that threshold (Figure 3C). The presence of breaks in slope in the peaked and threshold relations suggests that geomorphic thresholds may be crossed at these discharges, at which particular sediment sources or sinks are accessed or depleted. Interestingly, many of the thresholds were located near the geometric mean of the sample discharges (i.e., at zero on the Q-TSS plots). It seems unlikely that this phenomenon is simply coincidence and the underlying physical basis for this observation merits further investigation, but is beyond the scope of this paper.

Fitted regression parameters quantified the substantial variation in SRC shape. Rising limb SRC exponents ranged from -2.32 to 1.62, with a mean of 0.46 and median of 0.55. Rising limb coefficients ranged from 4.9 to 202 mg/L, with a mean of 58.5 mg/L and a median of 50.3 mg/L. Combined (rising limb and falling limb) SRC exponents ranged from -2.36 to 1.69, with a mean of 0.43 and median of 0.49. Combined SRC coefficients ranged from 4.1 to 138 mg/L, with a mean of 43.5 mg/L and a median of 37.7 mg/L. Values of hysteresis ranged from -0.05 mg/L to 0.60 mg/L, with a mean of 0.24 mg/L and median 0.25 mg/L. Full results of the Q-TSS analysis, along with results of the morphologic and environmental analyses for each gage/watershed, are shown in Appendix B**.**

Several interesting geographic trends were apparent in the data. The steepest (highest exponent) relations, characterizing rivers that are most sensitive to changes in flow, were dominantly clustered in the driftless area of southeastern Minnesota and near the mouths (i.e., within the knickzones) of Minnesota River tributaries (Figure 6). Those rivers are generally characterized by high near-channel relief and steep stream gradients. Gages with smallest exponents or that have negative or peaked SRC were clustered in the central part of the state within the Upper Mississippi and St. Croix Watersheds, and near the headwaters of Minnesota River tributaries (Figures 6, 7). These rivers are low-gradient and tend to lack the near-channel topography that characterizes rivers with steep power function relations. Notably, Minnesota River tributaries with paired gages exhibited markedly different Q-TSS responses at the gages above and within the incised knickzone. Gages above the knickzone tended to have shallow or negatively sloped Q-TSS relations, even though they generally have the same land use, surface geology, climate, and soil conditions as the gages within the knickzone that had steep Q-TSS relations. This observation qualitatively highlights the strong control that near-channel geomorphic conditions and geologic history exert on the steepness of Q-TSS relations. Unlike the power function and peaked SRCs, clear geographic trends were not immediately obvious in the threshold relations (Figure 7).

The RF model performed well at classifying the simple power function and peaked/negative SRC forms, correctly classifying 87% and 80% of the relations, respectively (Table 1). The model performed worse for threshold relations, correctly predicting 58% of the relations and misclassifying the rest as simple power functions. Overall, the model correctly classified 78% of the relation forms. Although we initiated the model using all (39) watershed-average and near-channel predictor variables, we progressively winnowed the pool of predictor

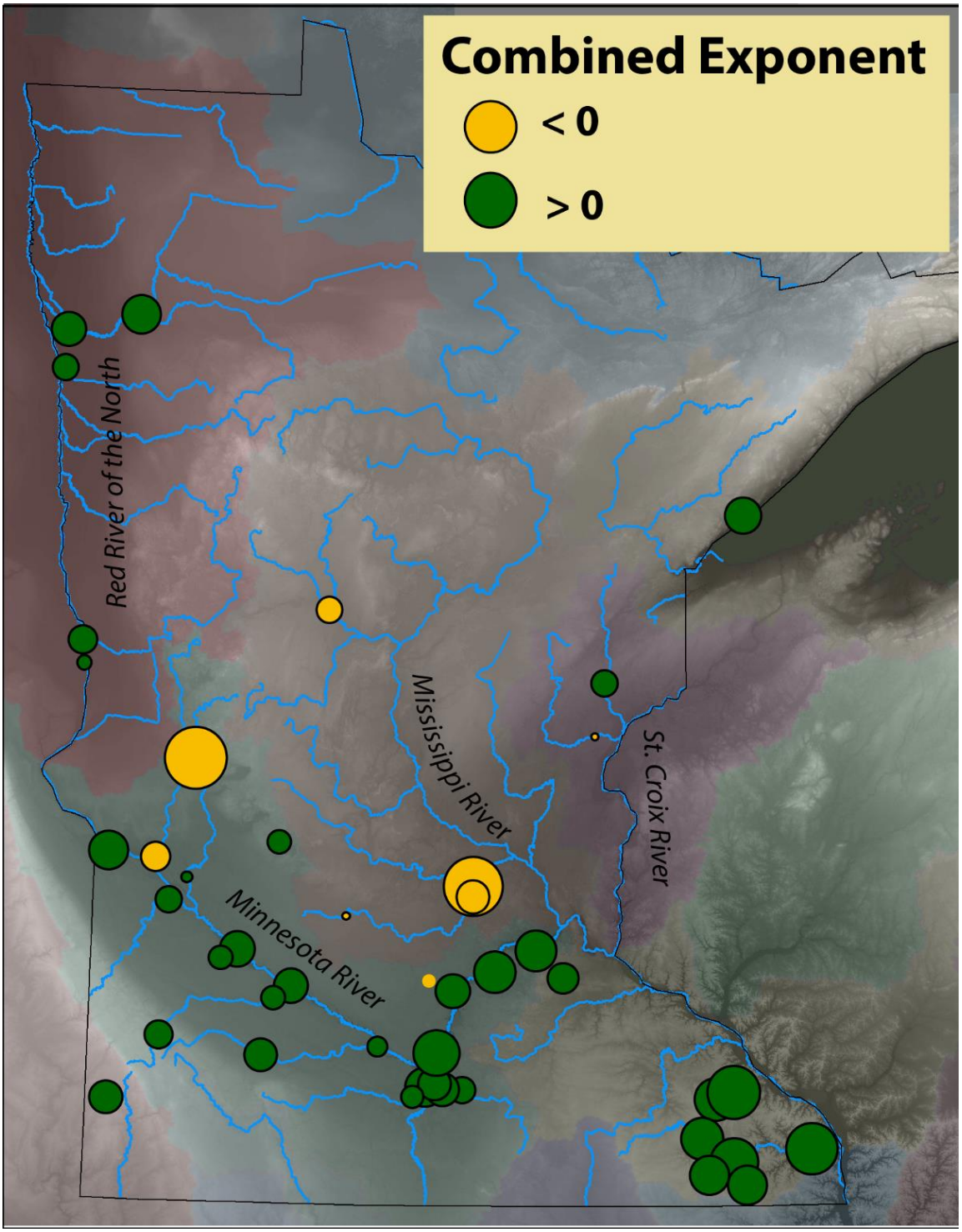

Figure 6. Map of combined SRC exponent values. Points are sized relative to the value of the exponent or coefficient. Positive values are shown in green, negative values in yellow. HUC 4 watersheds are outlined in color.

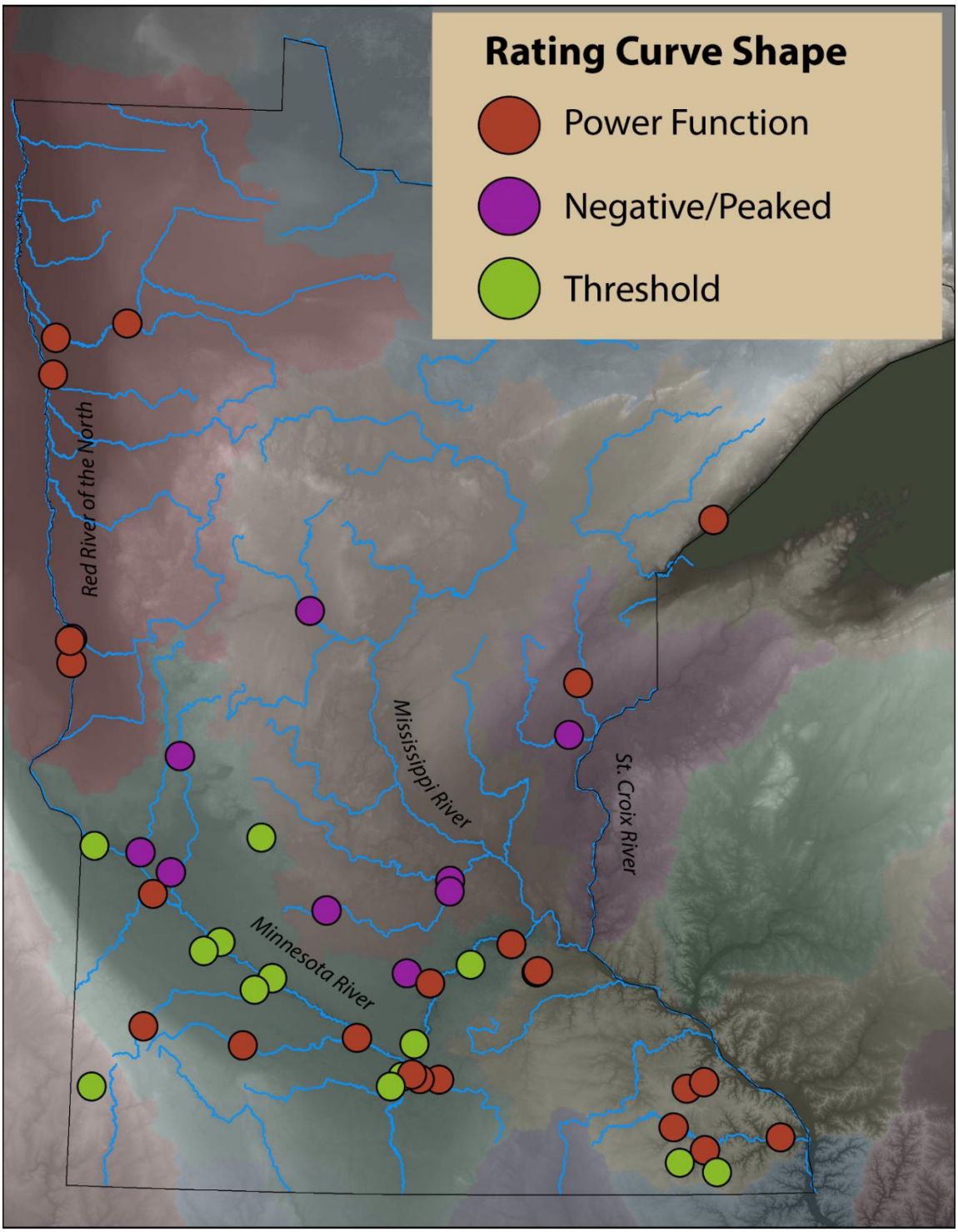

Figure 7. Map of SRC shapes throughout Minnesota. HUC 4 watersheds are outlined in color.

variables to optimize predictive power, iteratively eliminating predictor variables that were unimportant. The important variables for this model were, in decreasing order of importance: near-channel topographic slope within 10 km upstream of the gage, channel gradient within 50 km upstream, the near-channel waterbody area within 50 km upstream, channel gradient within 10 km upstream, and the watershed average mean annual temperature (Figure 8A). Partial dependence plots (Figure 8B-F**)** show that increasing near-channel topographic slope was associated with decreased probability of belonging to the peaked/negative class, whereas increasing near-channel waterbody area increased the probability of belonging to this class. The remaining relationships were complex. For both stream gradient metrics, increasing gradient was associated with decreasing probability of belonging to the peaked/negative class at low stream gradient values. Slightly above the median gradient value, increasing gradient was associated with increasing probability of belonging to the peaked/negative class.

The RF model for predicting SRC rising limb exponents explained approximately 50% of the variance in the exponent values and contained mostly near-channel morphologic predictor metrics. Variables selected by the model as important were stream slope within 10 km upstream of the gage, near-channel local relief within 10 km upstream of the gage, the near-channel waterbody area within 50 km upstream, the mean watershed slope, and the watershed average

Table 1. Predictions for each SRC class from Random Forest model.

		Predicted Class			
		Simple Power	Peaked/negative	Threshold	% Correctly Classified
Actual Class	Simple Power	20	1	2	87%
	Peaked/negative	1	8	1	80%
	Threshold	5	0	7	58%

rock-free K-factor (Figure 9A**)**. Partial dependence plots showed largely non-linear relationships between predictor variables and the response variable (Figure 9B-F**)**. The direction of the correlations generally conformed with expectations. Stream slope was positively correlated with the SRC rising limb exponent, with most of the dependence occurring over the bottom quarter of stream slope values. Near-channel local relief was also positively correlated with the SRC exponent, with the dependence occurring over almost the entire range of relief values. Near-channel waterbody (lake and wetland) area was negatively correlated with the SRC exponent. The SRC exponents showed almost no dependence on mean watershed slope at low to moderate slope values (approximately the bottom 75% of the data), but SRC exponents then increased with increasing slope. The relationship between SRC exponent values and soil erodibility was slightly negative at low K-factor values (bottom 25% of the K-factor data), but then positive at higher values.

Variables selected as important in the RF model for SRC rising limb coefficient (i.e., TSS value at the median flow value) were percent coverage of agriculture, 10-minute (5-year recurrence) precipitation intensity, percent coverage of forest, local relief within 10 km upstream of the gage, and unit stream power within 50 km upstream of the gage (Figure 10A**)**. The model explained 43% of the variance in rising limb coefficient values. Partial dependence plots showed relationships were non-linear and mostly consistent with expectations (Figure 10B-F). Percent agriculture had a positive correlation with SRC rising limb coefficient, whereas percent forest cover had a corresponding negative correlation. Percent forest and agricultural coverage were negatively correlated, but removing either from the RF model significantly worsened model performance. For that reason, both predictor variables were retained. SRC rising limb coefficient values did not depend on precipitation intensity over most of the range of that variable, but were strongly positively correlated over the upper 25% of the range. This metric varied within fairly limited range within our study watersheds, from about 110 mm/hr to 130 mm/hr, so the strong

dependence occurred over only about 6-7 mm/hr. The gages driving this relationship (i.e. that have high rising limb coefficients and high precipitation intensity) were grouped geographically, all located within the lower Minnesota River Basin. Unit stream power had a consistently increasing relationship with SRC coefficient, although the relationship flattened out at the highest stream power values. Local relief had a complex relationship with the SRC coefficient, negative over the first half of the data range, and then positive over the upper half of the range.

Results from the RF models for the combined above-breakpoint (rising and falling limb dataset) SRC exponents and coefficients were similar to those for the rising limb exponents and coefficients in terms of variables selected as important. The combined SRC coefficient model found most of the same important variables as the rising limb model. Unit stream power within 50 km upstream was removed, whereas near-channel topographic slope within 10 km and watershed area were added. The combined SRC coefficient model performed slightly worse than the rising limb coefficient model (~37% variance explained compared with ~43%). The combined SRC exponent model also found most of the same important variables as the rising limb exponent model (Figure 11). The only exception was that mean watershed slope was replaced with mean annual precipitation. The combined SRC exponent model performed much better than the rising limb model, explaining approximately 60% of the variance.

The RF model for TSS concentrations at the 90% exceedance (i.e., low) flow behaved similarly to the SRC coefficient models. The model explained 45% of the variance and found percent forest, percent agriculture, watershed area, and near-channel topographic slope within 10 km as the important predictor variables. Percent agriculture and basin area were positively correlated with low-flow TSS concentrations, whereas percent forest and topographic slope were negatively correlated.

The RF model for hysteresis was winnowed to three key predictor variables – local relief within 10 km upstream, mean annual precipitation, and percent wetland – and explained ~ 43% of

the variance (Figure 12A). Hysteresis was strongly positively dependent on near-channel local relief and mean annual precipitation at the low end of the ranges of those variables, and then the relationships flattened out. Hysteresis was negatively dependent on percent coverage of wetlands (Figure 12B-D).

The performance of models constructed using only watershed-average variables was, in all cases, worse than the models containing both watershed and near-channel metrics. The watershed-only rising limb exponent model explained approximately 42% of the variance, compared with 50% for the model containing both watershed-average and near-channel metrics. For the rising limb coefficient, the watershed-only model explained 31% of the variance, compared with 43% for the model containing both watershed-average and near-channel metrics. For the combined rising and falling limb exponent models, the comparison was 45% (watershed-only) to 60% (watershed and near-channel), and for the combined high flow coefficient models, 30% (watershed-only) to 37% (watershed and near-channel).

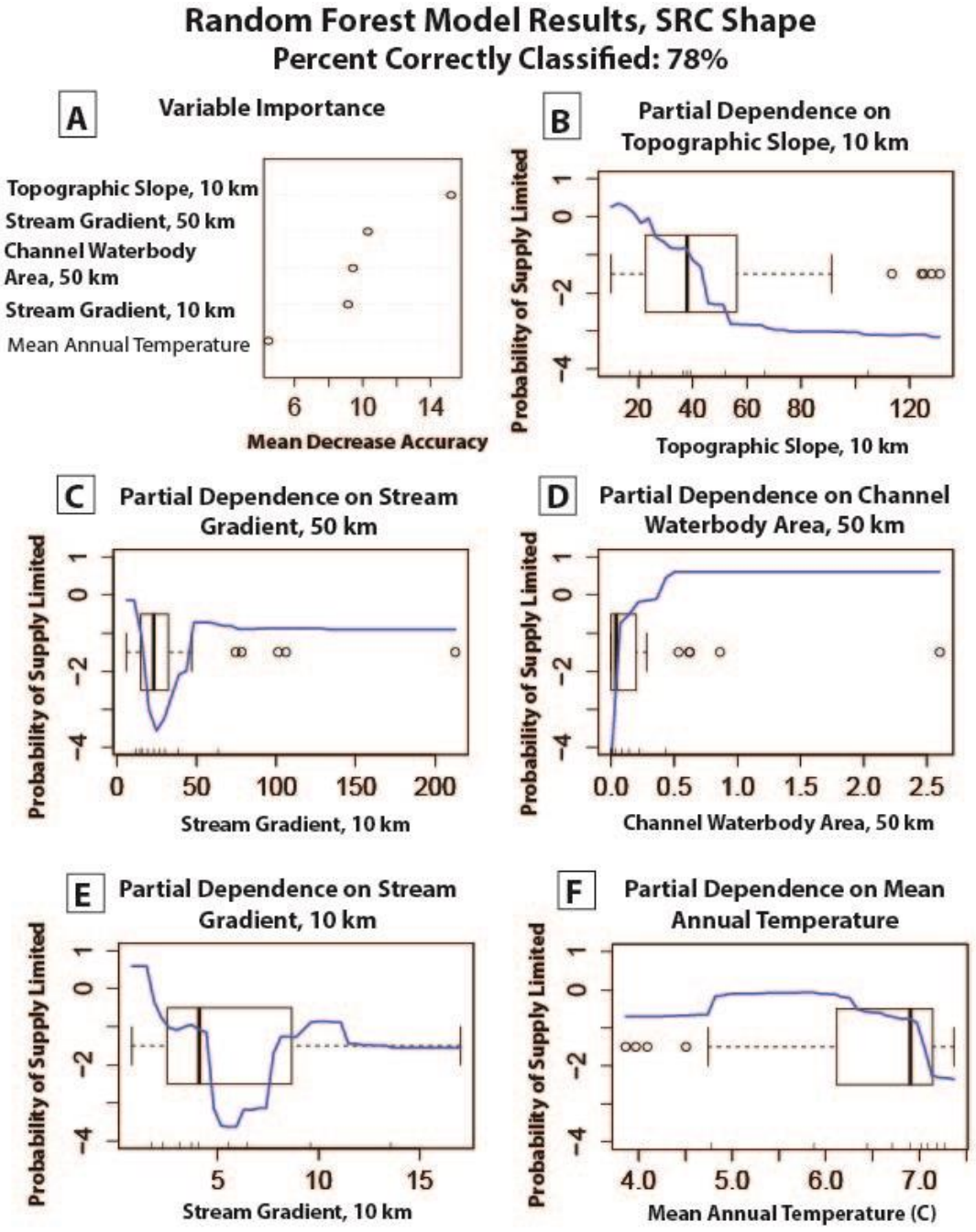

Figure 8. Results from Random Forest classification model for SRC shape. **A.** Variable importance plot. X-axis shows the mean decrease in model predictive accuracy when values for the variable in question are permuted. Variables are ranked in terms of importance, with most important variable at the top. Near-channel metrics are shown in bold, watershed-average metrics are shown in regular font. **B – F.** Partial dependence plots showing relative probability (represented by a logit expression of the probability) of belonging to the Peaked/Negative class given variations in the selected predictor variable. Also shown on graphs are box-and-whisker plots showing distribution of values for each predictor variable.

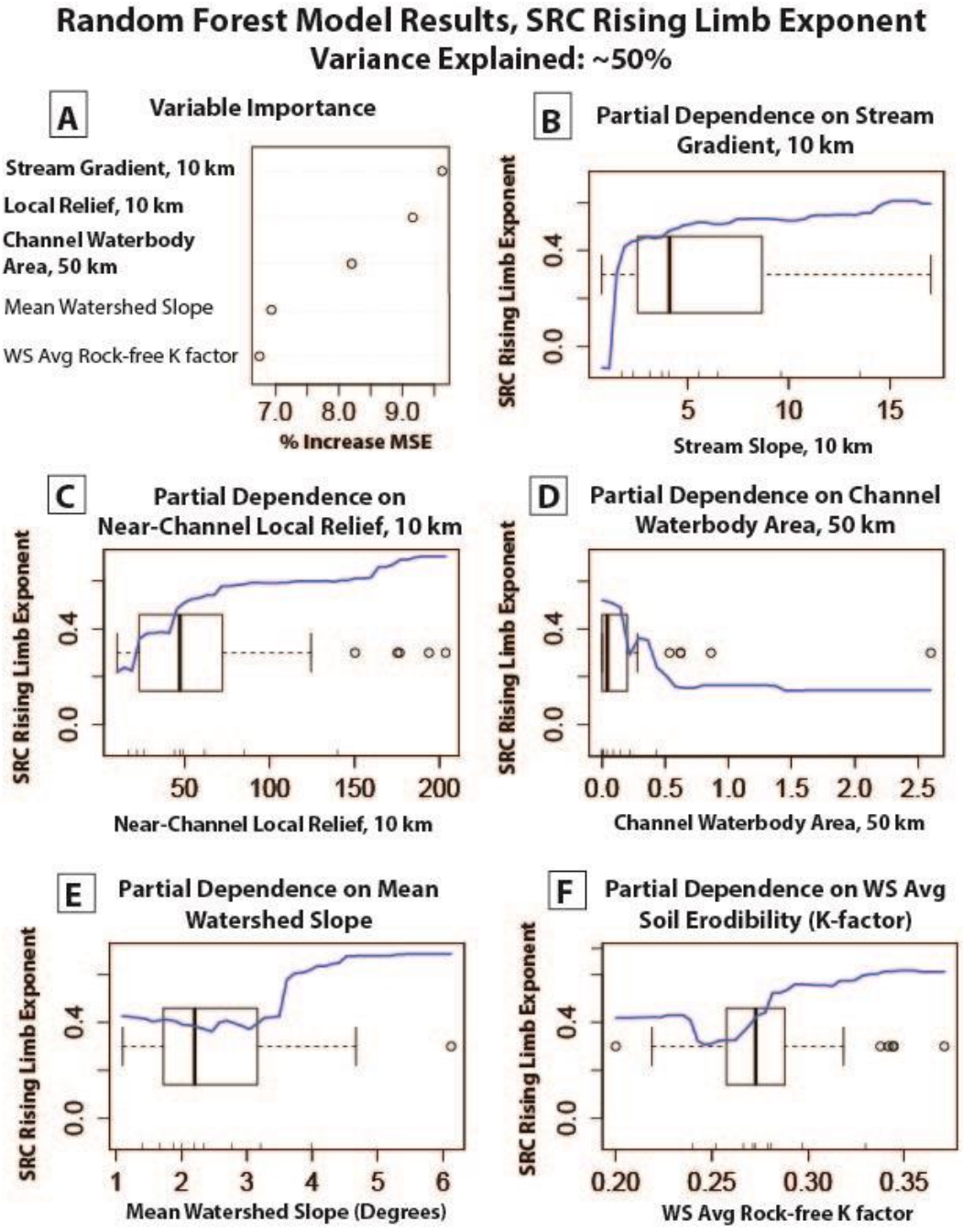

Figure 9. Results from Random Forest regression model for SRC rising limb exponent. **A.** Variable importance plot. X-axis shows the percent increase in model mean-square-error when values for the variable in question are permuted. Variables are ranked in terms of importance, with most important variable at the top. Near-channel metrics shown in bold, watershed-average metrics shown in regular font. **B – F.** Partial dependence plots showing estimated value of the SRC rising limb exponent given variations over the range of the selected predictor variable. Also shown on graphs are box-and-whisker plots showing distribution of values for each predictor variable.

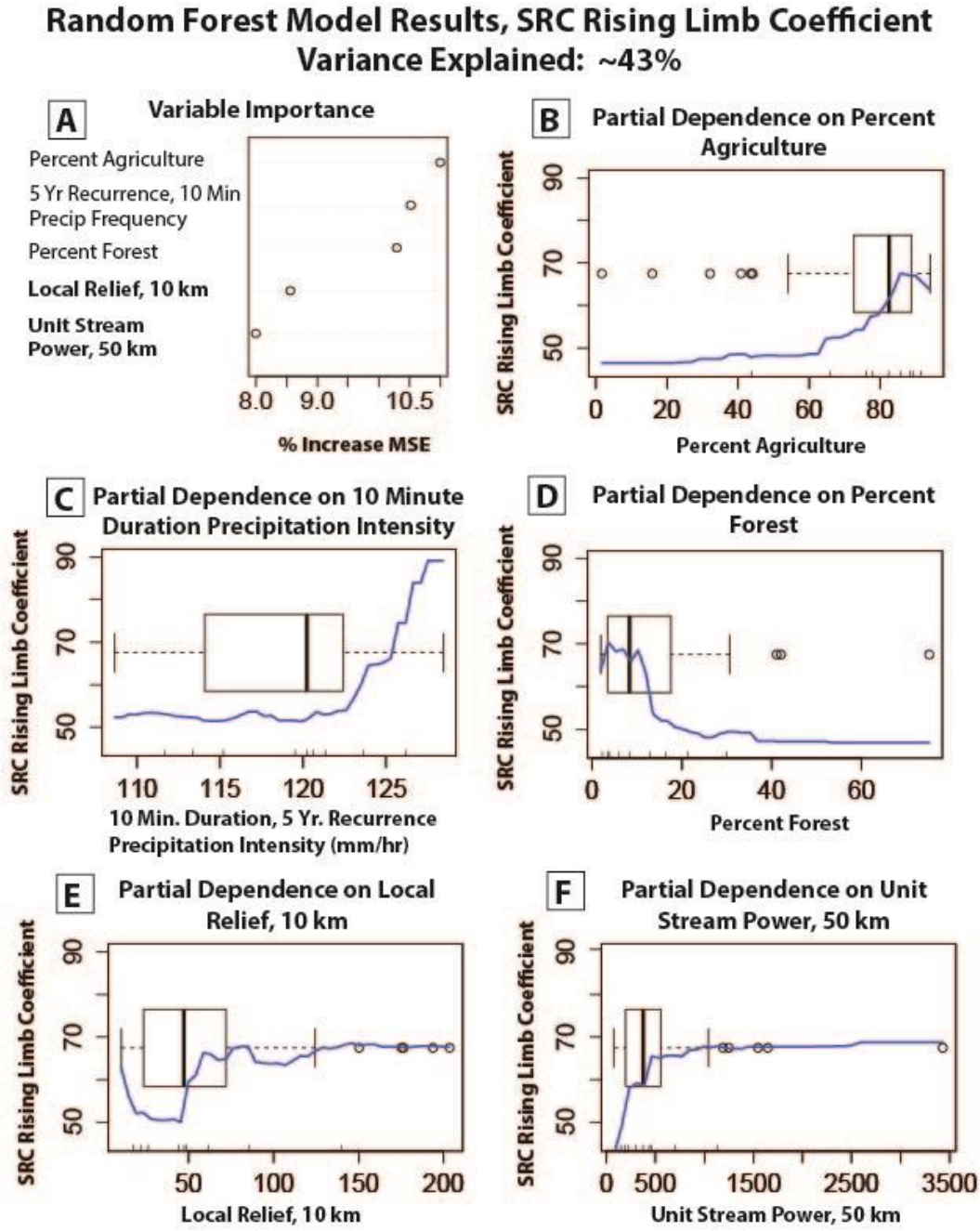

Figure 10. Results from Random Forest regression model for SRC rising limb coefficient. **A.** Variable importance plot. X-axis shows the percent increase in model mean-square-error when values for the variable in question are permuted. Variables are ranked in terms of importance, with most important variable at the top. Near-channel metrics shown in bold, watershed-average metrics shown in regular font. **B – F.** Partial dependence plots showing estimated value of the SRC rising limb coefficient given variations over the range of the selected predictor variable. Also shown on graphs are box-and-whisker plots showing distribution of values for each predictor variable.

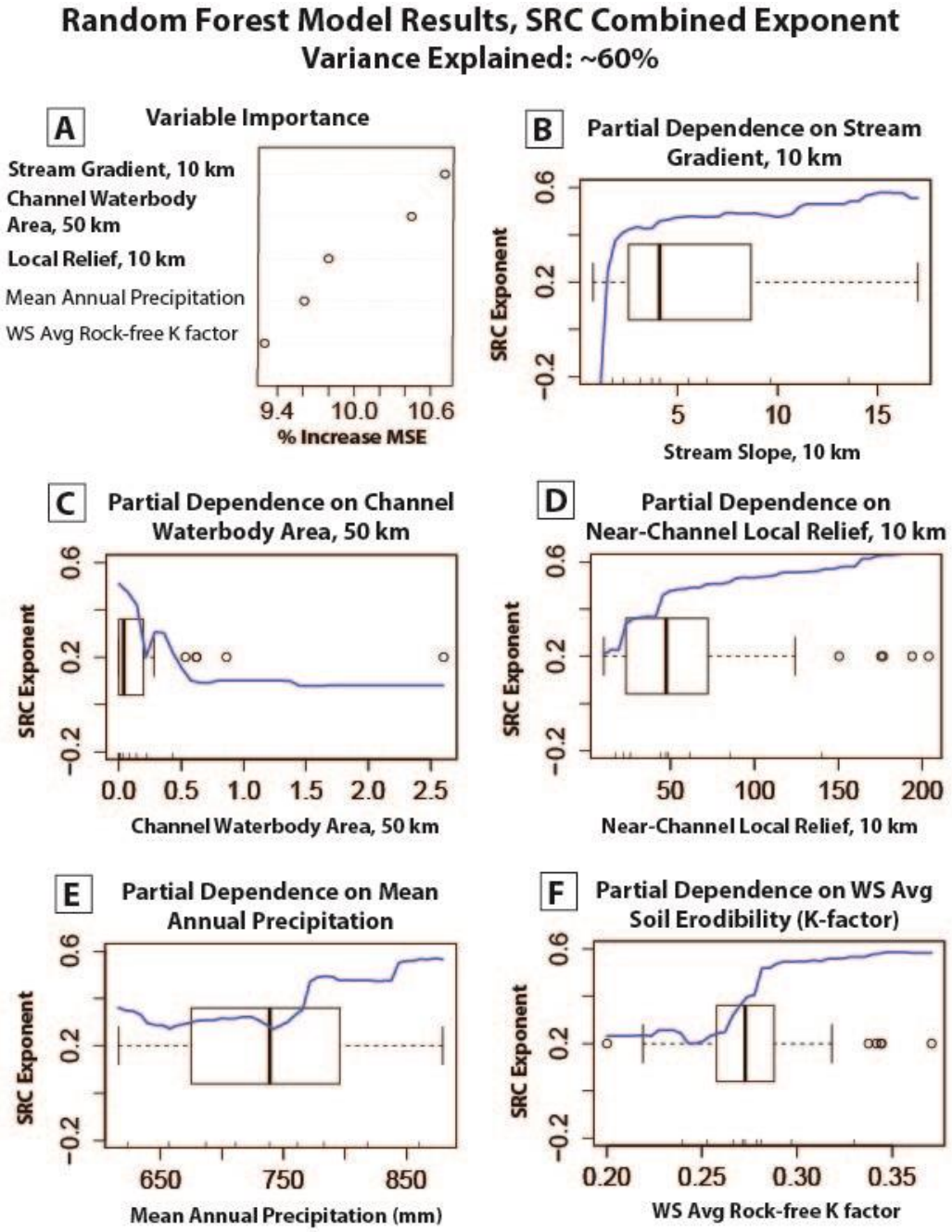

Figure 11. Results from Random Forest regression model for SRC combined (rising and falling limb data) exponent. **A.** Variable importance plot. X-axis shows the percent increase in model mean-square-error when values for the variable in question are permuted. Variables are ranked in terms of importance, with most important variable at the top. Near-channel metrics shown in bold, watershed-average metrics shown in regular font. **B – F.** Partial dependence plots showing estimated value of the SRC exponent given variations over the range of the selected predictor variable. Also shown on graphs are box-and-whisker plots showing distribution of values for each predictor variable.

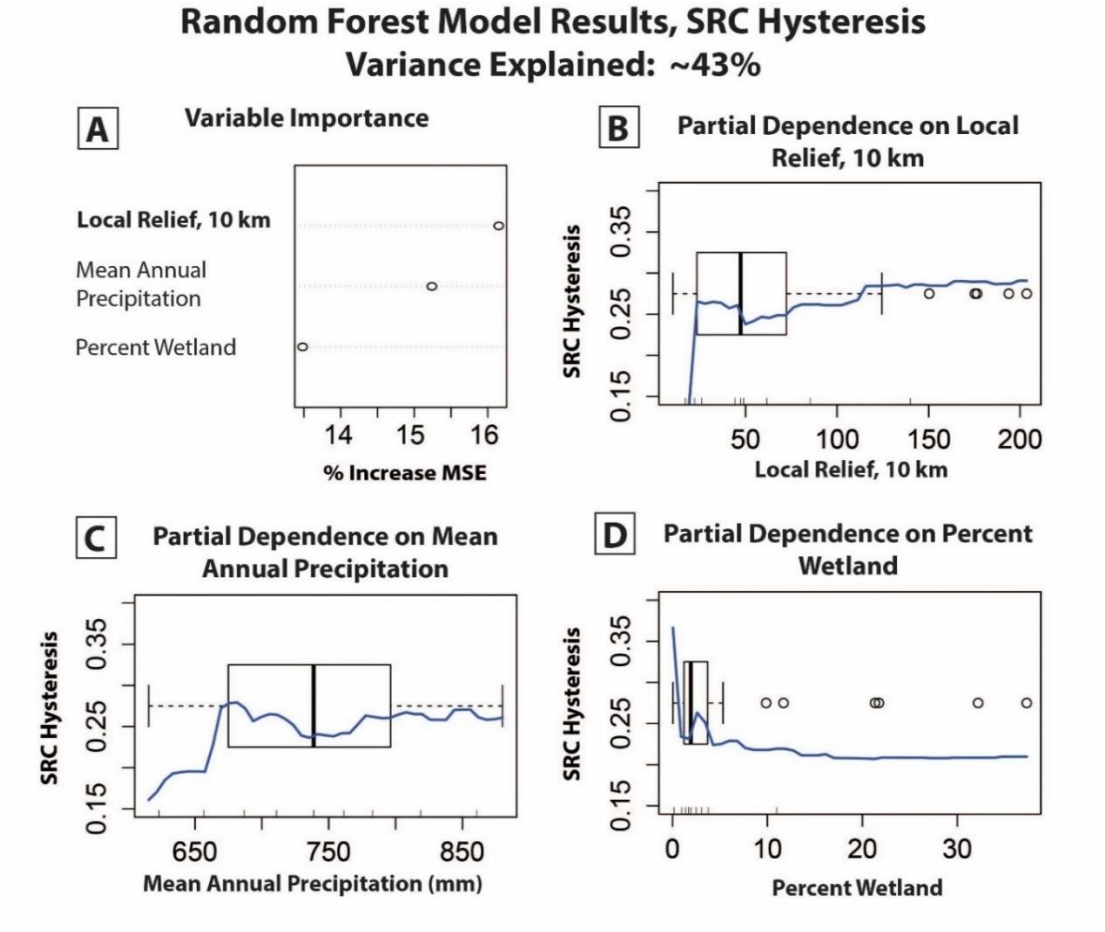

Figure 12. Results from Random Forest regression model for SRC hysteresis. **A.** Variable importance plot. X-axis shows the percent increase in model mean-square-error when values for the variable in question are permuted. Variables are ranked in terms of importance, with most important variable at the top. Near-channel metrics shown in bold, watershed-average metrics shown in regular font. **B – D.** Partial dependence plots showing estimated value of SRC hysteresis given variations over the range of the selected predictor variable. Also shown on graphs are box-and-whisker plots showing distribution of values for each predictor variable.

DISCUSSION

We sought to understand how topographic and other attributes of the landscape and channel network may control the shape, steepness and vertical offset of the relationship between river discharge and suspended sediment. Our results indicated that sediment dynamics throughout Minnesota could be reasonably well predicted by near-channel characteristics and a few watershed-scale average characteristics. Several interesting insights emerged from our analyses, which shed light on dominant geomorphic processes and sediment sources and sinks within these watershed and channel-floodplain systems.

Perhaps the most interesting result was that Q-TSS relation steepness (exponent) was most related to near-channel morphological characteristics, whereas the vertical offset (coefficient) of the SRCs, as well as TSS concentrations at low flows, were most affected by land use within the watershed. The finding that SRC exponents were strongly positively associated with near-channel local relief and stream gradient provides further evidence that tall channel banks, bluffs and fluvial terraces, where present, are important sediment sources at high discharges, especially in streams with high gradient (and thus erosive and transport power). That hysteresis was also positively associated with higher near-channel local relief suggests that these sources may become depleted over the course of storm events. This hypothesis is consistent with the observation that sediment accumulates via mass failure at the toe of bluffs and banks in the intervening period between storm events, and then is mobilized at higher discharges and depleted before the peak of a flood hydrograph [*Belmont et al.*, 2011a; *Day et al.*, 2013a, 2013b]. The negative correlations between SRC exponents and near-channel waterbody area indicates that lakes and marshes upstream of gages serve as sediment sinks, especially at high discharges, and can exert strong control on transport dynamics. Interestingly, the percent coverage of waterbody areas within the watershed was not selected in any of our models. Only lakes and wetlands

directly connected to the channel network appear to exert sufficient control on the transport regime so as to show up in our models. The apparent lack of importance of these features is consistent with the notion that sediment delivery ratios are low in this relatively flat landscape [*Gran et al.*, 2011; *Maalim et al.*, 2013; *Belmont et al.*, 2014].

We showed, however, that other aspects of the upland environment can exert a strong control on fine sediment transport regimes. The finding that SRC coefficients and low-flow (90% exceedance) TSS concentrations were most strongly associated with watershed land use, exhibiting a positive correlation with agricultural land and negative correlation with forest cover, suggests that land use may set the average, or baseline sediment supply conditions for these rivers. Sediment from upland sources such as agricultural fields appears to be available for transport by streams not only during events that cause high discharge but during more moderate flow conditions as well. However, the absence of these variables in the shape and exponent models suggest that modern land use may exert little control on the shape or steepness of the Q-TSS relations.

These findings have important implications for water quality criteria and watershed management. Because land use appears to have most influence on TSS concentrations at low and moderate flows, regulations on land use aimed at reducing erosion from upland soils may be most effective at reducing TSS during those flow conditions. However, if the near-channel geomorphic environment determines the shape and steepness of the relations, then TSS reduction at high flows may be best achieved by management approaches aimed at reducing the magnitude and frequency of high flows and controlling erosion from near-channel sources, rather than additional regulations on land use aimed at reducing erosion from upland soils. These findings further call into question whether a strict percentage exceedance water quality criterion, as is applied in Minnesota and many other states (e.g., a river is considered impaired if the water

quality criterion is exceeded more than 10% of the time) adequately accommodates for landscape settings that are naturally prone to produce large volumes of sediment.

That our models explain only 40 to 60 percent of the variance in the various response variables suggests that some key conditions may be missing or imperfectly characterized by our metrics. Conditions that are likely important but were not included due to lack of available data are grain size distributions in sediment source and sink areas, bank and soil cohesion properties, and vegetation type and density along the channel.

The lack of full explanation of the response variables within the models could also be due to error or incompleteness in the characterization of the response variables, such as might be caused by seasonal or year-to-year shifting of Q-TSS relations. We have accounted for within-event variation in SRCs by splitting the data by rising and falling limb. However, SRCs have also been shown to shift at a seasonal timescale due to differing hydrologic conditions or variation in sediment availability associated with early season flushing and late season depletion [*Mimikou*, 1982; *Fenn et al.*, 1985; *Syvitski et al.*, 2000; *Lana-Renault and Regüés*, 2009]. SRCs can also experience annual or persistent shifts due to large hydrologic events or changes in land use or water management [*Syvitski et al.*, 2000; *Hu et al.*, 2011; *Warrick*, 2014]. If SRCs for different seasonal or temporal periods encompassed in our data were systematically different, grouping all those data together to create one SRC could result in incomplete or erroneous characterization of a TSS regime that would more accurately be represented (and predicted) using several SRCs describing different seasonal or temporal states of the system. We examined our Q and TSS data for evidence of shifting rating curves at both a yearly and seasonal timescale. We found some evidence of seasonal, counterclockwise hysteresis (with higher TSS concentrations in the summer than in the spring) in a number of the peaked relations. However, we found little evidence of persistent, systematic annual changes in SRCs that would warrant splitting the data further and predicting separate periods or system states differently. Our data do not cover a

sufficient period of time to test whether longer-term land use and hydrologic changes may have altered the Q-TSS relations we observed.

Previous modeling efforts carried out across larger spatial scales than ours have found that watershed-average predictor variables successfully explain significant amounts of variation in SRC parameter values. Syvitski et al. [2000] used multiple linear regression to evaluate correlations between SRC parameters and watershed properties from catchments throughout the world. Their models for predicting the SRC coefficient from watershed-scale predictor variables (including basin relief, mean annual discharge, long-term sediment yield, latitude, and mean annual temperature) had R^2 values ranging from 0.70 to 0.75, significantly higher than our models. They used combinations of the same predictor variables to generate multiple linear regression models predicting the exponent parameter, which had R^2 values ranging from 0.51 to 0.58. Our RF models for SRC exponents performed comparably or slightly better. Our combined high flow exponent model, which is most similar methodologically to Syvitski's [2000] SRC exponents model, has an R^2 value of 0.60. In this case, our approach using RF models and including near-channel predictors appeared to offer an advantage over the methods used in the previous study, especially considering the much narrower range of climate, topography and land use evaluated in our analysis. Mimikou [1982] constructed multiple linear regression models to predict the rating parameters for rivers in Greece, using the following predictor variables: mean annual precipitation, watershed area, basin relief, main channel length, and average channel slope. Because Greece has pronounced dry and wet seasons, Mimikou [1982] divided the data by those seasons and created separate models. For the rating curve exponent, her models explained 88% and 61% of the variance in the wet and dry seasons, respectively. For the rating curve coefficient, the models explained 67% and 45% of the variance in the wet and dry seasons, respectively. Nearly all of the explanatory variables used in that study were also included in our

study, but most of them were removed from the final models because they were determined to be unimportant.

While no previous studies have characterized the near-channel environment in the level of detail that we have here, a few previous studies found that near-channel geomorphic conditions explain most variation in SRC form. Fan et al. [2012] found that SRC coefficients were related to bed material and channel cross section shape (width to depth ratio) in the upper Yellow River in China, whereas the exponent parameters were related to stream power. They found that flat SRCs (with large coefficient values and small exponent values) corresponded to reaches with low stream power and large width-depth ratios. Reaches with flat SRCs also flowed through intensively weathered materials or loose sedimentary deposits that can be transported at most discharges. Steeper rating curves (small coefficient, large exponent) corresponded to reaches with higher stream power, coarser bed material, and smaller width-depth ratios. Hu et al. [2011] found similar patterns in the Yangtze River, although they also found that human activities including damming of the river had significantly altered the sediment transport regimes there.

These comparisons between our results and results from similar studies raise a paradox, in that the studies reach somewhat conflicting conclusions regarding the geomorphic and environmental conditions that exert most influence over SRC shape. Syvitski [2000] and Mimikou [1982] found that watershed-scale morphometrics and hydrologic/climatic variables successfully explained variation in SRC exponent and coefficient values. Our study, as well as those of Fan et al. [2012] and Hu et al. [2011] found that channel-floodplain morphology was consistently important for explaining variation in SRC shape. Our RF models developed with only watershed-scale predictor metrics consistently performed worse than models developed with both watershed and near-channel metrics. Moreover, our study found that many of the basin-scale variables important in the models of Syvitski [2000] and Mimikou [1982] did not adequately explain the variation in SRC shape for rivers throughout Minnesota and were removed

from our RF models. This inconsistency may be due to the differing spatial scales at which the analyses were conducted. Syvitski's [2000] study, for example, encompassed rivers throughout the world, including rivers across a wide range of climatic and topographic settings. With such wide ranges, watershed morphometrics appear to adequately represent the different processes and erosion rates that result in variations in SRC shape. At the scale of our study, however, which encompassed smaller watersheds spread over a more homogenous landscape (in terms of large-scale topography, geology, and climate), these metrics may not have varied over a wide enough range to show any effect. An alternative interpretation is that at the regional scale of our study, the assumption that watershed-scale morphometrics can capture processes important to fine sediment generation and transport within the watershed breaks down. That interpretation would further suggest, then, that that assumption may not be valid at the larger scale of analysis either, but that those watershed-scale morphometrics are simply correlated with other variables (e.g., near-channel relief) that are in reality fundamentally controlling the sediment response.

The variability in shape and steepness of the Q-TSS relationships we analyzed has important implications for water quality regulations. Because near-channel geomorphic conditions and geologic history vary at local as well as regional scales, strong variation in Q-TSS relations occurs within the boundaries delineating nutrient regions currently used for TMDL regulation of TSS levels in Minnesota. For example, paired gages on several streams in the Minnesota River Basin exhibit distinct shapes, even though they are within the same TSS TMDL zone. The lower gage on High Island Creek (Henderson) had an exponent of 0.69 and coefficient of 103 mg/L, whereas the upper gage (Arlington) had an exponent of -0.12 and coefficient of 29 mg/L. The catchments above the two gages have similar land use, surface geology, climate, and soil properties, and are managed for TSS standards under the same criterion, and yet have vastly different background Q-TSS relationships. Thus, it appears that the current regulatory framework does not account for important local variability in TSS dynamics and that an approach to

delineating regions for TSS standards that incorporated more detailed local geomorphic and environmental conditions could provide a more rigorous basis for regulation.

While we acknowledge that long-term and short-term rates are not always equal [*Kirchner et al.*, 2001] it is useful to consider how landscape and river network attributes may influence sediment regimes over multiple timescales. Our findings that sediment dynamics (as described by SRC parameters) in Minnesota are not strongly associated with variation in watershed-scale topographic relief, mean annual precipitation, or mean annual temperature agree with the findings presented by von Blanckenburg [2005] that long-term denudation rates do not vary systematically with those variables. Results from our study also support the observations of Riebe et al. [2001] and von Blanckenburg [2005] that long term denudation rates are high in areas of rapid uplift or base level fall, with the latter strongly influencing near-channel morphology in Minnesota. We observed the largest SRC exponents at gages within the knick zones of Minnesota River tributaries and in the driftless area of southeastern Minnesota, characterized by tall alluvial terrace streambanks and wide valleys. Base level changes and associated channel incision have established the large values of near-channel local relief and steep stream gradients within the Minnesota River Basin knick zones. Similarly, rivers in the driftless area (the Whitewater and Root Rivers) also experienced base level fall in the late Pleistocene as glacial outwash events scoured the channel, and have experienced base level rise over the Holocene after a glacial outwash event on the Chippewa River dammed up the Mississippi River downstream. Further, they experienced largescale disturbance in the form of rapid hillslope denudation from agricultural uplands in the late 1800s and early 1900s and associated deposition of large alluvial terraces in confined and partly confined river valleys [*Trimble*, 2009; *Stout et al.*, 2014]. Significantly out of equilibrium, and similarly characterized by high near-channel relief, these rivers also have large sediment loads and steep SRCs. Thus, even though our models used

current geomorphic conditions to predict Q-TSS dynamics, it is important to consider the geologic and base level history that may be driving those dynamics over longer timescales.

Our results confirmed that near-channel geomorphic conditions were important to watershed sediment dynamics across the wide range of landscape settings investigated here. When high-resolution topography data are available to characterize those near-channel conditions, such information may significantly improve predictions. Future research should focus on developing increasingly targeted and meaningful near-channel morphometrics. With increasing availability of high resolution topography data for accurately characterizing the near-channel environment, we expect that future models for predicting the shape, steepness and vertical offset of Q-TSS relations will benefit from evaluating a combination of watershed-average and near-channel metrics.

CONCLUSIONS

Our analysis of Q-TSS relationships throughout the state of Minnesota revealed that the steepness of the curves is mainly explained by near-channel geomorphic conditions and base level controls, whereas TSS concentrations at average and low flows are controlled by land use within the basin. Near-channel characteristics, particularly local relief and stream gradient, were consistently among the most important predictor variables in our models, supporting the notion that the near-channel environment contains useful information with regard to sediment sources and dynamics in rivers. We obtained much better predictive models by being able to quantify the near-channel environment than by using watershed-average descriptive metrics alone. Land use within the watersheds, particularly agricultural and forest land cover, was important in determining the vertical offset (or TSS at average flow conditions) of Q-TSS relations. However, most of the basin-scale metrics used to explore controls on SRC parameters and sediment loads in previous studies were excluded from our models because they were determined by the RF algorithm to be unimportant and unable to explain variation in SRC parameters for our study gages.

It is important to note that our statistical modeling does not establish causation in the relationships we observe. Nevertheless, it does provide insight into which factors are likely important in determining suspended sediment regimes. The technique of examining variation in Q-TSS relationships and the geomorphic and environmental settings associated with those relationships appears to provide an indirect but useful way of identifying important sediment sources within a watershed. Moreover, by better understanding geomorphic and environmental conditions associated with certain suspended sediment response patterns, this type of analysis could help inform the process of delineating regulatory zones for sediment.

REFERENCES

Ahnert, F. (1970), Functional Relationships Between Denudation, Relief, and Uplift in Large Mid-Latitude Drainage Basins, *Am. J. Sci.*, *268*, 243–263.

Ali, K. F., and D. H. de Boer (2008), Factors Controlling Specific Sediment Yield in the Upper Indus River Basin, Northern Pakistan, *Hydrol. Process.*, *22*(October 2007), 3102–3114, doi:10.1002/hyp.

Anthony, S. T., T. R. Vandegrift, and H. G. Stefan (2010), *Annual Stream Runoff and Climate in Minnesota ' s River Basins*, Minneapolis.

Asselman, N. E. M. (2000), Fitting and interpretation of sediment rating curves, *J. Hydrol.*, *234*, 228–248, doi:10.1016/S0022-1694(00)00253-5.

Beach, T. (1994), The Fate of Eroded Soil: Sediment Sinks and Sediment Budgets of Agrarian Landscapes in Southern Minnesota, 1851-1988, *Ann. Assoc. Am. Geogr.*, *84*(1), 5–28, doi:10.1111/j.1467-8306.1994.tb01726.x.

Belmont, P. (2011), Floodplain width adjustments in response to rapid base level fall and knickpoint migration, *Geomorphology*, *128*, 92–101, doi:10.1016/j.geomorph.2010.12.026.

Belmont, P., F. J. Pazzaglia, and J. C. Gosse (2007), Cosmogenic 10Be as a tracer for hillslope and channel sediment dynamics in the Clearwater River, western Washington State, *Earth Planet. Sci. Lett.*, *264*(1–2), 123–135, doi:10.1016/j.epsl.2007.09.013.

Belmont, P., K. Gran, C. E. Jennings, C. Wittkop, and S. S. Day (2011a), Holocene landscape evolution and erosional processes in the Le Sueur River, central Minnesota, *F. Guid.*, *24*, 439–455, doi:10.1130/2011.0024(21).

Belmont, P. et al. (2011b), Large shift in source of fine sediment in the upper Mississippi river., *Environ. Sci. Technol.*, *45*(20), 8804–10, doi:10.1021/es2019109.

Belmont, P., J. K. Willenbring, S. P. Schottler, J. Marquard, K. Kumarasamy, and J. M. Hemmis

(2014), Toward generalizable sediment fingerprinting with tracers that are conservative and nonconservative over sediment routing timescales, *J. Soils Sediments*, *14*(8), 1479–1492, doi:10.1007/s11368-014-0913-5.

Belmont, P., T. Dogwiler, and K. Kumarasamy (2016), *An integrated sediment budget for the Root River watershed , southeastern Minnesota*.

Bilotta, G. S., and R. E. Brazier (2008), Understanding the influence of suspended solids on water quality and aquatic biota, *Water Res.*, *42*, 2849–2861, doi:10.1016/j.watres.2008.03.018.

von Blanckenburg, F. (2005), The control mechanisms of erosion and weathering at basin scale from cosmogenic nuclides in river sediment, *Earth Planet. Sci. Lett.*, *237*(3–4), 462–479, doi:10.1016/j.epsl.2005.06.030.

Bogárdi, J. (1961), Some Aspects of the Application of Sediment Transportation to Engineering Problems, *J. Geophys. Res.*, *66*(10), 3337–3346.

Bonniwell, E. C., G. Matisoff, and P. J. Whiting (1999), Determining the times and distances of particle transit in a mountain stream using fallout radionuclides, *Geomorphology*, *27*(1–2), 75–92, doi:10.1016/S0169-555X(98)00091-9.

Breiman, L. (2001), Random forests, *Mach. Learn.*, *45*(1), 5–32, doi:10.1023/A:1010933404324.

Breiman, L., J. H. Friedman, R. A. Olshen, and C. J. Stone (1984), *Classification and regression trees*, Wadsworth and Brooks/Cole, Monterey, California, USA.

Clayton, L., and S. R. Moran (1982), Chronology of late wisconsinan glaciation in middle North America, *Quat. Sci. Rev.*, *1*(1), 55–82, doi:10.1016/0277-3791(82)90019-1.

Cutler, D. R., T. C. Edwards, K. H. Beard, A. Cutler, K. T. Hess, J. C. Gibson, and J. J. Lawler (2007), Random Forests for Classification in Ecology, *Ecology*, *88*(11), 2783–2792, doi:10.1890/07-0539.1.

Daly, C., R. P. Neilson, and D. L. Phillips (1994), A Statistical-Topographic Model for Mapping Climatological Precipitation over Mountainous Terrain, *J. Appl. Meteorol.*, *33*, 140–158.

Daly, C., M. Halbleib, J. I. Smith, W. P. Gibson, M. K. Doggett, G. H. Taylor, J. Curtis, and P. P. Pasteris (2008), Physiographically Sensitive Mapping of Climatological Temperature and Precipitation Across the Conterminous United States, *Int. J. Climatol.*, 1549–1555., doi:10.1002/joc.

Davis, J. (2010), Hypsometry Toolbox,

Day, S. S., K. B. Gran, P. Belmont, and T. Wawrzyniec (2013a), Measuring bluff erosion part 1: Terrestrial laser scanning methods for change detection, *Earth Surf. Process. Landforms*, *38*(10), 1055–1067, doi:10.1002/esp.3353.

Day, S. S., K. B. Gran, P. Belmont, and T. Wawrzyniec (2013b), Measuring bluff erosion part 2: Pairing aerial photographs and terrestrial laser scanning to create a watershed scale sediment budget, *Earth Surf. Process. Landforms*, *38*(January), 1068–1082, doi:10.1002/esp.3359.

Dean, D. J., M. L. Scott, P. B. Shafroth, and J. C. Schmidt (2011), Stratigraphic, sedimentologic, and dendrogeomorphic analyses of rapid floodplain formation along the Rio Grande in Big Bend National Park, Texas, *Bull. Geol. Soc. Am.*, *123*(9–10), 1908–1925, doi:10.1130/B30379.1.

Dierckx, P. (1975), An algorithm for smoothing, differentiation and integration of experimental data using spline functions, *J. Comput. Appl. Math.*, *1*(3), 165–184, doi:10.1016/0771-050X(75)90034-0.

Donovan, M., A. Miller, M. Baker, and A. Gellis (2015), Sediment contributions from floodplains and legacy sediments to Piedmont streams of Baltimore County, Maryland, *Geomorphology*, *235*(February), 88–105, doi:10.1016/j.geomorph.2015.01.025.

Ellison, C. A., B. E. Savage, and G. D. Johnson (2014), Suspended-sediment concentrations, loads, total suspended solids, turbidity, and particle-size fractions for selected rivers in Minnesota, 2007 through 2011, *U.S. Geol. Surv. Sci. Investig. Rep.*, *5205*, 43.

Engstrom, D. R., J. E. Almendinger, and J. A. Wolin (2009), Historical changes in sediment and

phosphorus loading to the upper Mississippi River: Mass-balance reconstructions from the sediments of Lake Pepin, *J. Paleolimnol.*, *41*(4), 563–588, doi:10.1007/s10933-008-9292-5.

Fan, X., C. Shi, Y. Zhou, and W. Shao (2012), Sediment rating curves in the Ningxia-Inner Mongolia reaches of the upper Yellow River and their implications, *Quat. Int.*, *282*, 152–162, doi:10.1016/j.quaint.2012.04.044.

Fenn, C. R., a. M. Gurnell, and I. R. Beecroft (1985), An evaluation of the use of suspended sediment rating curves for the prediction of suspended sediment concentration in a proglacial stream, *Geogr. Ann.*, *67*(1), 71–82, doi:10.2307/520467.

Finlay, J. C. (2011), Stream size and human influences on ecosystem production in river networks, *Ecosphere*, *2*(8), art87, doi:10.1890/ES11-00071.1.

Fisher, T. G. (2003), Chronology of glacial Lake Agassiz meltwater routed to the Gulf of Mexico, *Quat. Res.*, *59*(2), 271–276, doi:10.1016/S0033-5894(03)00011-5.

Grams, P. E., and J. C. Schmidt (2005), Equilibrium or indeterminate? Where sediment budgets fail: Sediment mass balance and adjustment of channel form, Green River downstream from Flaming Gorge Dam, Utah and Colorado, *Geomorphology*, *71*(1–2), 156–181, doi:10.1016/j.geomorph.2004.10.012.

Gran, K., P. Belmont, S. Day, C. Jennings, J. W. Lauer, E. Viparelli, P. Wilcock, and G. Parker (2011), An Integrated Sediment Budget for the Le Sueur River Basin. MPCA Report wq-iw7-29o., , (June), 1–128.

Gran, K. B., N. Finnegan, A. L. Johnson, P. Belmont, C. Wittkop, and T. Rittenour (2013), Landscape evolution, valley excavation, and terrace development following abrupt postglacial base-level fall, *Bull. Geol. Soc. Am.*, *125*(11), 1851–1864, doi:10.1130/B30772.1.

Gray, J. R., G. D. Glysson, L. M. Turcios, and G. E. Schwarz (2000), Comparability of Suspended-Sediment Concentration and Total Suspended Solids Data, *Water-Resources*

Investig. Rep. 00-4191, (August), 20 pp, doi:Report 00-4191.

Hack, J. T. (1975), *Dynamic equilibrium and landscape evolution*.

Hicks, D., J. Hill, and U. Shankar (1996), Variation of suspended sediment yields around New Zealand : the relative importance of rainfall and geology, *Iahs Publ.*, (236), 149–156.

Hobbs, H. C., and J. E. Goebel (1982), S-01 Geologic Map of Minnesota, Quaternary Geology,

Hu, B., H. Wang, Z. Yang, and X. Sun (2011), Temporal and spatial variations of sediment rating curves in the Changjiang (Yangtze River) basin and their implications, *Quat. Int.*, *230*(1–2), 34–43, doi:10.1016/j.quaint.2009.08.018.

Jerolmack, D. (2015), Climate and Tectonics: Why Self-organized River Channels Just Don't Care (that much), in *2015 AGU Fall Meeting*, AGU.

Jones, O. A. H., N. Voulvoulis, and J. N. Lester (2006), Partitioning behavior of five pharmaceutical compounds to activated sludge and river sediment, *Arch. Environ. Contam. Toxicol.*, *50*(3), 297–305, doi:10.1007/s00244-005-1095-3.

Jones, Z., and F. Linder (2015), Exploratory Data Analysis using Random Forests, *73rd Annu. MPSA Conf.*

Juracek, K. E., and A. C. Ziegler (2009), Estimation of Sediment Sources Using Selected Chemical Tracers in the Perry Lake Basin, Kansas, USA, *Int. J. Sediment Reserach*, *24*(1), 108–125.

Kelley, D. W., and E. a. Nater (2000), *Historical Sediment Flux from Three Watersheds into Lake Pepin, Minnesota, USA*.

Kirchner, J. W., R. C. Finkel, C. S. Riebe, D. E. Granger, J. L. Clayton, J. G. King, W. F. Megahan, and F. Sites (2001), Mountain erosion over 10 yr , 10 k . y ., and 10 m . y . time scales, , (7), 591–594.

Klein, M. (1984), Anti clockwise hysteresis in suspended sediment concentration during individual storms, *Catena*, *11*(1), 251–257, doi:10.1016/S0341-8162(84)80024-7.

Knighton, D. (1998), *Fluvial Forms and Processes*, John Wiley and Sons, New York.

Knox, J. (1977a), Human Impacts on Wisconsin Stream Channels, *Ann. Assoc. Am. Geogr.*, *67*(3).

Knox, J. C. (1977b), Human Impacts on Wisconsin Stream Channels, *Ann. Assoc. Am. Geogr.*, *67*(4), 323–342.

Knox, J. C. (2001), Agricultural influence on landscape sensitivity in the Upper Mississippi River Valley, *Catena*, *42*(2–4), 193–224, doi:10.1016/S0341-8162(00)00138-7.

Knox, J. C. (2006), Floodplain sedimentation in the Upper Mississippi Valley: Natural versus human accelerated, *Geomorphology*, *79*(3–4), 286–310, doi:10.1016/j.geomorph.2006.06.031.

Kolok, A. S., M. K. Sellin Jeffries, L. Knight, D. D. Snow, and S. L. Bartelt-Hunt (2014), The hourglass: A conceptual framework for the transport of biologically active compounds from agricultural landscapes, *J. Am. Water Resour. Assoc.*, *50*(2), 266–274, doi:10.1111/jawr.12158.

Lana-Renault, N., and D. Regüés (2009), Seasonal patterns of suspended sediment transport in an abandoned farmland catchment in the Central Spanish Pyrenees, *Earth Surf. Process. …*, *1301*(June), 1291–1301, doi:10.1002/esp.

Langbein, W., and S. Schumm (1958), Yield of sediment in relation to mean annual precipitation, *… , Am. Geophys. Union*.

Lauer, J. W., and G. Parker (2008), Modeling framework for sediment deposition, storage, and evacuation in the floodplain of a meandering river: Theory, *Water Resour. Res.*, *44*(8), 1–16, doi:10.1029/2006WR005529.

Lenhart, C. F., E. S. Verry, and J. A. Brooks, K. N. Magner (2011), Adjustment of Prairie Pothole Streams to Land-use, Drainage and Climate Changes and Consequences for Turbidity Impairment, *River Res. Appl.*

Leopold, L. B., and T. Maddock Jnr (1953), The Hydraulic Geometry of Stream Channels and Some Physiographic Implications, *Geol. Surv. Prof. Pap. 252*, 57.

Liaw, a, and M. Wiener (2002), Classification and Regression by randomForest, *R news*, *2*(December), 18–22, doi:10.1177/154405910408300516.

Lorenz, D. L., C. A. Sanocki, and M. J. Kocian (2009), Techniques for Estimating Peak Flow on Small Streams Techniques for Estimating Peak Flow on Small Streams, *USGS Sci. Investig. Rep.*

Loughran, R. J. (1976), The calculation of suspended-sediment transport from concentration v. discharge curves: Chandler river, N.S.W., *Catena*, *3*(1), 45–61, doi:10.1016/S0341-8162(76)80017-3.

Lu, X., and D. L. Higgitt (1999), Sediment yield variability in the Upper Yangtze, China, *Earth Surf. Process. Landforms*, *24*(12), 1077–1093, doi:10.1002/(SICI)1096-9837(199911)24:12<1077::AID-ESP36>3.0.CO;2-M.

Maalim, F. K., A. M. Melesse, P. Belmont, and K. B. Gran (2013), Modeling the impact of land use changes on runoff and sediment yield in the le sueur watershed, minnesota using GeoWEPP, *Catena*, *107*(August), 35–45, doi:10.1016/j.catena.2013.03.004.

Matisoff, G., E. C. Bonniwell, and P. J. Whiting (2002), Radionuclides as indicators of sediment transport in agricultural watersheds that drain to Lake Erie., *J. Environ. Qual.*, *31*(1), 62–72, doi:10.2134/jeq2002.0062.

Matsch, C. L. (1983), River Warren, the southern outlet of Lake Agassiz, in *Glacial Lake Agassiz: Geological Association of Canada Special Paper 26*, edited by J. T. Teller and L. Clayton, pp. 232–244.

Melesse, A. M. (2004), Spatiotemporal dynamics of land surface parameters in the Red River of the North Basin, *Phys. Chem. Earth, Parts A/B/C*, *29*(11–12), 795–810, doi:10.1016/j.pce.2004.05.007.

Milliman, J. D., and R. H. Meade (1983), World-Wide Delivery of River Sediment to the Oceans, *J. Geol.*, *91*(1), 1–21, doi:10.2307/30060512.

Mimikou, M. (1982), An investigation of suspended sediment rating curves in western and northern Greece, *Hydrol. Sci. J.*, *27*, 369–383, doi:10.1080/02626668209491116.

Minnesota Pollution Control Agency (2011), Aquatic Life Water Quality Standards Draft Technical Support Document for Total Suspended Solids (Turbidity), , (May), 50.

Mueller, E. R., and J. Pitlick (2013), Sediment supply and channel morphology in mountain river systems: 1. Relative importance of lithology, topography, and climate, *J. Geophys. Res. Earth Surf.*, *118*(4), 2325–2342, doi:10.1002/2013JF002843.

Nolan, B. K. M., and B. R. Hill (1991), Suspended-sediment budgets for four drainage basins tributary to Lake Tahoe, California and Nevada, 1984-87, , 45.

Novotny, E. V., and H. G. Stefan (2007), Stream flow in Minnesota: Indicator of climate change, *J. Hydrol.*, *334*(3–4), 319–333, doi:10.1016/j.jhydrol.2006.10.011.

Olson, J. R., and C. P. Hawkins (2012), Predicting natural base-flow stream water chemistry in the western United States, *Water Resour. Res.*, *48*(2), 1–19, doi:10.1029/2011WR011088.

Owens, P. N., and D. E. Walling (2002), The phosphorus content of fluvial sediment in rural and industrialized river basins, *Water Res.*, *36*, 685–701, doi:10.1016/S0043-1354(01)00247-0.

Parker, G., P. R. Wilcock, C. Paola, W. E. Dietrich, and J. Pitlick (2007), Physical basis for quasi-universal relations describing bankfull hydraulic geometry of single-thread gravel bed rivers, *J. Geophys. Res. Earth Surf.*, *112*(4), 1–21, doi:10.1029/2006JF000549.

Passalacqua, P., P. Belmont, and E. Foufoula-Georgiou (2012), Automatic geomorphic feature extraction from lidar in flat and engineered landscapes, *Water Resour. Res.*, *48*(3), 1–18, doi:10.1029/2011WR010958.

Passalacqua, P. et al. (2015), Analyzing high resolution topography for advancing the understanding of mass and energy transfer through landscapes: A review, *Earth-Science*

Rev., *148*, 174–193, doi:10.1016/j.earscirev.2015.05.012.

Peck, M., R. W. Gibson, A. Kortenkamp, and E. M. Hill (2004), Sediments Are Major Sinks of Steroidal Estrogens in Two United Kingdom Rivers, *Environ. Toxicol. Chem.*, *23*(4), 945, doi:10.1897/03-41.

Pereira, W. E., J. L. Domagalski, F. D. Hostettler, L. R. Brown, and J. B. Rapp (1996), Occurrence and accumulation of pesticides and organic contaminants in river sediment, water and clam tissues from the San Joaquin River and tributaries, California., *Environ. Toxicol. Chem.*, *15*(2), 172–180, doi:10.1897/1551-5028(1996)015<0172:OAAOPA>2.3.CO;2.

Pizzuto, J. et al. (2014), Characteristic Length Scales and Time-Averaged Transport Velocities of Suspended Sediment in the Mid-Atlantic Region, USA, *Water Resour. Res.*, *50*, 790–805, doi:10.1002/2013WR014664.Received.

Regnier, P. et al. (2013), Anthropogenic perturbation of the carbon fluxes from land to ocean, *Nat. Geosci.*, *6*(8), 597–607, doi:10.1038/ngeo1830.

Renard, K. G., G. R. Foster, G. a Weesies, D. K. Mccool, and D. C. Yoder (1997), *Predicting Soil Erosion By Water : a Guide To Conservation Planning With the Revised Universal Soil Loss Equation (Rusle)*.

Restrepo, J. D., B. Kjerfve, M. Hermelin, and J. C. Restrepo (2006), Factors controlling sediment yield in a major South American drainage basin: The Magdalena River, Colombia, *J. Hydrol.*, *316*, 213–232, doi:10.1016/j.jhydrol.2005.05.002.

Richards, C., and K. L. Bacon (1994), Influence of Fine Sediment on Macroinvertebrate Colonization of Surface and Hyporheic Stream Substrates, *Gt. Basin Nat.*, *54*(2), 106–113.

Riebe, C. S., J. W. Kirchner, D. E. Granger, and R. C. Finkel (2001), Strong tectonic and weak climatic control of long term chemical weathering rates, *GSA Bull.*, *29*(6), 511–514, doi:10.1130/0091-7613(2001)029<0511:STAWCC>2.0.CO;2.

Sadeghi, S. H. R., T. Mizuyama, S. Miyata, T. Gomi, K. Kosugi, T. Fukushima, S. Mizugaki, and Y. Onda (2008), Development, evaluation and interpretation of sediment rating curves for a Japanese small mountainous reforested watershed, *Geoderma*, *144*, 198–211, doi:10.1016/j.geoderma.2007.11.008.

Schaffrath, K. R., P. Belmont, and J. M. Wheaton (2015), Landscape-scale geomorphic change detection: Quantifying spatially variable uncertainty and circumventing legacy data issues, *Geomorphology*, *250*, 334–348, doi:10.1016/j.geomorph.2015.09.020.

Schottler, S. P., J. Ulrich, P. Belmont, R. Moore, J. W. Lauer, and J. E. Engstrom, Daniel R. Almendinger (2014), Twentieth century agricultural drainage creates more erosive rivers, *Hydrol. Process.*, *28*(4), 1951–1961, doi:10.1002/hyp.

Schwartz, J. S., M. Dahle, and R. Bruce Robinson (2008), Concentration-Duration-Frequency Curves for Stream Turbidity: Possibilities for Assessing Biological Impairment 1, *JAWRA J. Am. Water Resour. Assoc.*, *44*(4), 879–886, doi:10.1111/j.1752-1688.2008.00186.x.

Schwartz, J. S., A. Simon, and L. Klimetz (2011), Use of fish functional traits to associate in-stream suspended sediment transport metrics with biological impairment., *Environ. Monit. Assess.*, *179*(1–4), 347–69, doi:10.1007/s10661-010-1741-8.

Sekely, A. C., D. J. Mulla, and D. W. Bauer (2002), Streambank slumping and its contribution to the phosphorus and suspended sediment loads of the Blue Earth River, Minnesota, *J. Soil Water Conserv.*, *57*(5), 243–250.

Shay, C. T. (1967), Vegetation history of the southern Lake Agassiz basin during the past 12,000 years, in *Life, Land, and Water: Proceedings of the 1960 Conference on Environmental Studies of the Glacial Lake Agassiz Basin*, edited by W. J. Mayer-Oakes, pp. 231–252, University of Manitoba Press, Winnipeg, Canada.

Simon, A. (2006), Evaluation of the Importance of Channel Processes in CEAP-Watershed Suspended-Sediment Yields, *Eighth Fed. Interag. Sediment. Conf. (8thFISC)*,, 815–822.

Soler, M., J. Latron, and F. Gallart (2008), Relationships between suspended sediment concentrations and discharge in two small research basins in a mountainous Mediterranean area (Vallcebre, Eastern Pyrenees), *Geomorphology*, *98*(1–2), 143–152, doi:10.1016/j.geomorph.2007.02.032.

Soller, D. R., M. C. Reheis, C. P. Garrity, and D. R. Van Sistine (2009), *Map Database for Surficial Materials in the Conterminous United States. Data Series 425, scale 1:5,000,000.*

Stout, J. C., and P. Belmont (2014), TerEx Toolbox for semi-automated selection of fluvial terrace and floodplain features from lidar, *Earth Surf. Process. Landforms*, *39*(5), 569–580, doi:10.1002/esp.3464.

Stout, J. C., P. Belmont, S. P. Schottler, and J. K. Willenbring (2014), Identifying Sediment Sources and Sinks in the Root River, Southeastern Minnesota, *Ann. Assoc. Am. Geogr.*, *104*(March 2015), 20–39, doi:10.1080/00045608.2013.843434.

Strobl, C., A.-L. Boulesteix, A. Zeileis, and T. Hothorn (2007), Bias in random forest variable importance measures: illustrations, sources and a solution., *BMC Bioinformatics*, *8*, 25, doi:10.1186/1471-2105-8-25.

Strobl, C., A.-L. Boulesteix, T. Kneib, T. Augustin, and A. Zeileis (2008), Conditional variable importance for random forests., *BMC Bioinformatics*, *9*(23), 307, doi:10.1186/1471-2105-9-307.

Summerfield, M. A., and N. J. Hulton (1994), Natural controls of fluvial denudation rates in major world drainage basins, *J. Geophys. Res.*, *99*(B7), 13871–13883, doi:10.1029/94JB00715.

Symader, W., M. Schorer, and R. Bierl (1997), Space-time patterns of organic contaminants in river bottom sediments, , (243).

Syvitski, J. P., M. D. Morehead, D. B. Bahr, and T. Mulder (2000), Estimating fluvial sediment transport : The rating parameters parameters, *Water Resour. Res.*, *36*(9), 2747–2760.

Syvitski, J. P. M., J. D. Milliman, S. The, N. January, J. P. M. Syvitski, and J. D. Milliman (2014), Geology , Geography , and Humans Battle for Dominance over the Delivery of Fluvial Sediment to the Coastal Ocean All use subject to JSTOR Terms and Conditions A RT I C L E S Geology , Geography , and Humans Battle for Dominance over the Delivery of Fluvia, , *115*(1), 1–19.

Tamene, L., S. J. Park, R. Dikau, and P. L. G. Vlek (2006), Analysis of factors determining sediment yield variability in the highlands of northern Ethiopia, *Geomorphology*, *76*(1–2), 76–91, doi:10.1016/j.geomorph.2005.10.007.

Tarolli, P., G. Sofia, and G. Dalla Fontana (2012), Geomorphic features extraction from high-resolution topography: Landslide crowns and bank erosion, *Nat. Hazards*, *61*(1), 65–83, doi:10.1007/s11069-010-9695-2.

Thorleifson, L. H. (1996), Review of Lake Agassiz history, in *Sedimentology, Geomorphology and History of the Central Lake Agassiz Basin—Field Trip Guidebook B2*, edited by J. T. Teller, L. H. Thorleifson, G. Matile, and W. C. Brisbin, Geological Association of Canada/Mineralogical Association of Canada, Annual Meeting, May 27–29 1996, Winnipeg, Manitoba.

Trimble, S. W. (1999), Decreased Rates of Alluvial Sediment Storage in the Coon Creek Basin, Wisconsin, 1975-93, *Science (80-.).*, *285*(1999), 1244–1246, doi:10.1126/science.285.5431.1244.

Trimble, S. W. (2009), Fluvial processes, morphology and sediment budgets in the Coon Creek Basin, WI, USA, 1975-1993, *Geomorphology*, *108*(1–2), 8–23, doi:10.1016/j.geomorph.2006.11.015.

Trimble, S. W. (2012), *Historical agriculture and soil erosion in the Upper Mississippi Valley Hill Country*, CRC Press.

Turowski, J. M., D. Rickenmann, and S. J. Dadson (2010), The partitioning of the total sediment

load of a river into suspended load and bedload: A review of empirical data, *Sedimentology*, *57*(4), 1126–1146, doi:10.1111/j.1365-3091.2009.01140.x.

United States Environmental Protection Agency (2000), *The quality of our nation's waters: a summary of the National Water Quality Inventory 1998 Report to Congress.*

Upham, W. (1890), *Report of Exploration of the Glacial Lake Agassiz in Manitoba*.

Upham, W. (1895), *The Glacial Lake Agassiz*.

De Vente, J., J. Poesen, M. Arabkhedri, and G. Verstraeten (2007), The sediment delivery problem revisited, *Prog. Phys. Geogr.*, *31*(2), 155–178, doi:10.1177/0309133307076485.

de Vente, J., R. Verduyn, G. Verstraeten, M. Vanmaercke, and J. Poesen (2011), Factors controlling sediment yield at the catchment scale in NW Mediterranean geoecosystems, *J. Soils Sediments*, *11*(4), 690–707, doi:10.1007/s11368-011-0346-3.

Verhoff, F. H., D. A. Melfi, and S. M. Yaksich (1979), Storm travel distance calculations for total phosphorus and suspended materials in rivers, *Water Resour. Res.*, *15*(6), 1354–1360, doi:10.1029/WR015i006p01354.

Verstraeten, G., and J. Poesen (2002), Regional Scale Variability in Sediment and Nutrient Delivery from Small Agricultural Watersheds, *J. Environ. Qual.*, *31*, 870–879.

Viparelli, E., J. Wesley Lauer, P. Belmont, and G. Parker (2013), A numerical model to develop long-term sediment budgets using isotopic sediment fingerprints, *Comput. Geosci.*, *53*, 114–122, doi:10.1016/j.cageo.2011.10.003.

Walling, D., and B. Webb (1982), Sediment availability and the prediction of storm-period sediment yields, *IAHS Publ.*, (137), 327–337.

Walling, D. E. (1974), Suspended sediment and solute yields from a small catchment prior to urbanization, *Fluv. Process. instrumented watersheds*, *6*, 169–192.

Walling, D. E. (1983), The sediment delivery problem, *J. Hydrol.*, *65*(1–3), 209–237, doi:10.1016/0022-1694(83)90217-2.

Walling, D. E., B. W. Webb, and M. a Russell (1997), Sediment-associated nutrient transport in UK rivers, *Freshw. Contam. (Proceedings Rabat Symp. S4, April. 1997) Int Assoc Hydrol Sci*, *243*(243), 69–81.

Walter, R. C., and D. J. Merritts (2008), Natural streams and the legacy of water-powered mills., *Science*, *319*(5861), 299–304, doi:10.1126/science.1151716.

Warrick, J. a. (2014), Trend analyses with river sediment rating curves, *Hydrol. Process.*, doi:10.1002/hyp.10198.

Wischmeier, W. H., and D. D. Smith (1978), Predicting rainfall erosion losses, *Agric. Handb. no. 537*, (537), 285–291, doi:10.1029/TR039i002p00285.

Wolman, B. M. G., and L. B. Leopold (1957), River Flood Plains : Some Observations On Their Formation, *Geol. Surv. Prof. Pap.*, *282–C*, 87–107.

Wolock, D. (2003), *Flow characteristics at U.S. Geological Survey streamgages in the conterminous United States*.

Wood, P., and P. Armitage (1997), Biological Effects of Fine Sediment in the Lotic Environment, *Environ. Manage.*, *21*(2), 203–17, doi:10.1007/s002679900019.

Yang, G., Z. Chen, F. Yu, Z. Wang, Y. Zhao, and Z. Wang (2007), Sediment rating parameters and their implications: Yangtze River, China, *Geomorphology*, *85*, 166–175, doi:10.1016/j.geomorph.2006.03.016.

APPENDICES

Appendix A. Tables of Values for All Response and Predictor Variables Used in RF Models

Table A.1. Watershed Morphometry Metrics

Gage	Gage Number*	Watershed Relief (m)	Watershed Mean Elevation (m)	Watershed Mean Topographic Slope (Degrees)	Hypsometric Integral (-)	Watershed Area (km^2)
Beaver Creek nr Beaver Falls, CSAH2	25053002 (05316570)	76	329	1.50	0.72	526
Bois de Sioux River near Doran, MN	54018001 (05051300)	101	328	1.23	0.76	4915
Chippewa River nr Cyrus, 140th St	26003001 (05301930)	175	412	3.11	0.35	923
Chippewa River nr Milan, MN40	26057001 (05304500)	233	365	2.34	0.31	4897
Clearwater River at Red Lake Falls, MN	66050001 (05078500)	206	383	1.97	0.45	3517
Cottonwood River nr Lamberton, US14	29062002	199	401	2.02	0.41	1156
Cottonwood River nr New Ulm, MN68	29001001 (05317000)	275	367	1.91	0.45	3386
Credit River at Savage	0.9	139	295	4.09	0.53	200
Hawk Creek nr Granite Falls, CR52	25037001 (05314540)	116	332	1.68	0.46	1318
High Island Creek nr Arlington, CR9	33075001 (05326700)	42	318	1.34	0.49	427
High Island Creek nr Henderson, CSAH6	33091001 (05327000)	116	312	1.65	0.77	621
Kandiyohi CD27 nr Sunburg, CSAH1	26047001	27	381	2.25	0.49	32
Kettle River below Sandstone, MN	35065001 (05336700)	155	364	2.14	0.51	2265
Lac qui Parle River nr Lac qui Parle, CSAH31	24023001 (05300000)	325	419	2.20	0.40	2507

Table A.1. (cont.)

Le Sueur River at St. Clair, CSAH 28	**32079001**	**126**	**348**	**2.26**	**0.45**	**903**
Le Sueur River near Rapidan, MN 66	32077002 (05320500)	181	332	1.88	0.52	2865
Le Sueur River nr Rapidan, CR8	32076001	168	339	2.29	0.53	1155
Leaf River nr Staples, CSAH29	13058001 (05244440)	189	429	1.80	0.26	2219
Middle Fork Whitewater River near St. Charles, MN	40019001 (05376100)	98	357	3.79	0.52	65
North Branch Root River at Chatfield, CSAH2	43079001	148	392	2.82	0.69	503
North Fork Crow River nr Rockford, Farmington Ave	18088001 (05278400)	157	347	2.44	0.46	3487
Otter Tail River at Breckenridge, CSAH16	56105001 (05046502)	321	414	3.16	0.38	4943
Pipestone Creek at Pipestone, MN	82035001 (06482430)	59	537	1.10	0.25	79
Pomme De Terre River at Appleton, MN	23007001 (05294000)	226	363	2.51	0.28	2241
Red Lake River at Fisher, MN	63078001 (05080000)	249	363	1.31	0.46	14646
Red River of the North at Wahpeton, ND	57006001	102	326	1.24	0.75	5201
Redwood River at Russell, CR15	27043001 (05314973)	157	529	2.36	0.49	603
Redwood River nr Redwood Falls, MN	27035001 (05316500)	312	422	2.05	0.40	1619
Root River nr Mound Prairie, CSAH25	43007002 (05386070)	240	359	6.12	0.67	4115
Sand Creek at Jordan	8.2	139	308	3.17	0.59	613
Sand Hill River at Climax, MN	61039001 (05069000)	208	335	1.64	0.40	1195

Table A.1. (cont.)

Seven Mile Creek nr North Star, MN169	**28063001**	**81**	**299**	**1.73**	**0.85**	**94**
Snake River nr Pine City, MN	36076001 (05338500)	152	341	1.97	0.39	2507
South Branch Root River at Lanesboro, Rochelle Ave N	43049001 (05384120)	190	378	4.67	0.68	737
South Branch Root River nr Carimona, CSAH12	43067001 (05384030)	141	400	3.22	0.72	345
South Fork Crow River at Delano, Bridge Ave	19001001 (05279400)	178	325	1.90	0.61	3286
South Fork Crow River nr Cosmos, MN7	19024001 (05278500)	62	345	1.67	0.22	631
South Fork Root River at Amherst, CSAH23	43034001	98	368	4.36	0.54	58
South Fork Whitewater River near Altura, MN	40024001 (05376500)	180	362	4.58	0.72	203
Sucker Creek at County Rd. 290 near Palmers, MN	02031001 (04015339)	301	422	3.82	0.68	90
Vermillion River at Farmington, Ash St	38020001	98	315	3.21	0.41	99
Vermillion River at Farmington, Denmark Ave	38027002	100	313	3.27	0.39	158
Watonwan River nr Garden City, CSAH13	31051001 (05319500)	203	349	1.57	0.36	2194
Yellow Bank River nr Odessa, CSAH40	22012001 (05293000)	340	420	2.53	0.41	1207
Yellow Medicine River nr Granite Falls, MN	25075001 (05313500)	301	404	2.07	0.34	1745

* Gage numbers are the DNR/MPCA cooperative ID numbers. Numbers in parentheses are USGS gage numbers, provided for gages that are also associated with the USGS. Sand Creek and Credit River gages are not part of either network. The ID number provided is the distance of the gage upstream (river miles) from the mouth of the river.

Table A.2. Watershed Land Use/Land Cover Metrics

Gage	Percent Agriculture (%)	Percent Wetland (%)	Percent Forest (%)	Percent Lakes (%)	Waterbody Percent (Lake, Marsh, Reservoir) (%)
Beaver Creek nr Beaver Falls, CSAH2	91.7	2.7	2.1	0.0	0.1
Bois de Sioux River near Doran, MN	88.4	3.9	2.0	2.7	3.6
Chippewa River nr Cyrus, 140th St	76.6	1.4	9.7	8.6	9.1
Chippewa River nr Milan, MN40	82.5	3.0	5.8	5.3	6.5
Clearwater River at Red Lake Falls, MN	60.4	9.9	24.7	2.3	9.3
Cottonwood River nr Lamberton, US14	90.9	2.0	3.8	0.6	0.9
Cottonwood River nr New Ulm, MN68	91.7	1.9	3.2	0.6	0.9
Credit River at Savage	43.6	3.8	16.7	6.6	12.1
Hawk Creek nr Granite Falls, CR52	89.8	1.6	2.3	2.2	2.6
High Island Creek nr Arlington, CR9	92.5	1.7	1.9	2.3	3.1
High Island Creek nr Henderson, CSAH6	90.7	1.6	3.5	2.3	2.9
Kandiyohi CD27 nr Sunburg, CSAH1	94.1	0.6	3.3	0.0	1.0
Kettle River below Sandstone, MN	15.9	37.3	41.1	1.8	22.8
Lac qui Parle River nr Lac qui Parle, CSAH31	78.2	5.2	13.0	1.1	1.8
Le Sueur River at St. Clair, CSAH 28	89.3	1.9	3.9	1.8	2.7
Le Sueur River near Rapidan, MN 66	89.2	2.2	3.6	2.0	3.0

Table A.2. (cont.)

Le Sueur River nr Rapidan, CR8	**87.2**	**2.4**	**4.4**	**2.4**	**3.7**
Leaf River nr Staples, CSAH29	54.0	11.7	29.4	1.5	11.2
Middle Fork Whitewater River near St. Charles, MN	85.6	0.1	12.7	0.0	0.0
North Branch Root River at Chatfield, CSAH2	77.4	0.2	18.8	0.1	0.1
North Fork Crow River nr Rockford, Farmington Ave	78.6	2.1	8.3	6.3	8.3
Otter Tail River at Breckenridge, CSAH16	44.1	3.1	30.6	14.1	17.3
Pipestone Creek at Pipestone, MN	90.6	0.1	4.4	0.0	0.0
Pomme De Terre River at Appleton, MN	76.4	3.4	8.5	7.4	8.0
Red Lake River at Fisher, MN	40.8	32.2	13.0	9.7	33.0
Red River of the North at Wahpeton, ND	88.7	3.7	2.0	2.6	3.4
Redwood River at Russell, CR15	77.1	1.1	14.9	3.0	3.4
Redwood River nr Redwood Falls, MN	85.8	1.8	7.0	1.4	1.7
Root River nr Mound Prairie, CSAH25	66.6	0.2	30.4	0.0	0.0
Sand Creek at Jordan	82.6	1.7	8.2	2.7	5.2
Sand Hill River at Climax, MN	84.5	3.8	6.8	2.2	3.0
Seven Mile Creek nr North Star, MN169	88.9	5.3	3.4	0.7	4.1

Table A.2. (cont.)

Snake River nr Pine City, MN	**32.1**	**21.3**	**42.1**	**1.3**	**15.1**
South Branch Root River at Lanesboro, Rochelle Ave N	73.2	0.2	23.7	0.0	0.0
South Branch Root River nr Carimona, CSAH12	80.4	0.2	17.3	0.1	0.1
South Fork Crow River at Delano, Bridge Ave	87.5	1.2	3.9	3.5	4.6
South Fork Crow River nr Cosmos, MN7	85.4	1.3	2.4	6.3	7.3
South Fork Root River at Amherst, CSAH23	80.4	0.1	17.6	0.0	0.0
South Fork Whitewater River near Altura, MN	72.4	0.1	20.7	0.0	0.0
Sucker Creek at County Rd. 290 near Palmers, MN	1.7	21.7	75.1	0.4	14.1
Vermillion River at Farmington, Ash St	75.9	1.4	14.0	0.7	1.0
Vermillion River at Farmington, Denmark Ave	62.5	1.0	13.0	1.9	2.0
Watonwan River nr Garden City, CSAH13	92.1	1.7	2.2	1.3	1.6
Yellow Bank River nr Odessa, CSAH40	69.0	2.9	24.9	1.3	1.5
Yellow Medicine River nr Granite Falls, MN	88.1	2.7	5.9	0.9	1.2

Table A.3. Watershed Soil and Geology Characteristics

Gage	Rock Free K-factor, All Horizons	Rock Free K-factor, Top Horizon	Whole Soil K-factor, All Horizons	Whole Soil K-factor, Top Horizon	STATSGO K-factor	Surface Geology, Uniaxial Compressive Strength (MPa)	Surface Geology Category at Gage	Dominant Surface Geology Category in Watershed
Beaver Creek nr Beaver Falls, CSAH2	0.35	0.27	0.35	0.27	0.30	1.42	Unconsolidated	Calcareous Till
Bois de Sioux River near Doran, MN	0.37	0.25	0.37	0.25	0.32	1.27	Unconsolidated	Calcareous Till
Chippewa River nr Cyrus, 140th St	0.33	0.24	0.33	0.24	0.30	1.37	Unconsolidated	Calcareous Till
Chippewa River nr Milan, MN40	0.36	0.27	0.36	0.27	0.27	1.40	Unconsolidated	Calcareous Till
Clearwater River at Red Lake Falls, MN	0.32	0.23	0.32	0.23	0.25	1.25	Unconsolidated	Unconsolidated
Cottonwood River nr Lamberton, US14	0.36	0.27	0.36	0.27	0.30	1.38	Unconsolidated	Calcareous Till
Cottonwood River nr New Ulm, MN68	0.34	0.27	0.34	0.27	0.29	1.40	Unconsolidated	Calcareous Till
Credit River at Savage	0.33	0.29	0.33	0.29	0.28	1.40	Unconsolidated	Calcareous Till
Hawk Creek nr Granite Falls, CR52	0.39	0.29	0.39	0.29	0.31	1.41	Unconsolidated	Calcareous Till
High Island Creek nr Arlington, CR9	0.33	0.28	0.33	0.28	0.30	1.40	Calcareous Till	Calcareous Till
High Island Creek nr Henderson, CSAH6	0.33	0.28	0.33	0.28	0.30	1.40	Unconsolidated	Calcareous Till
Kandiyohi CD27 nr Sunburg, CSAH1	0.33	0.27	0.33	0.27	0.29	1.40	Calcareous Till	Calcareous Till
Kettle River below Sandstone, MN	0.37	0.28	0.37	0.28	0.28	1.26	Unconsolidated	Non-Calcareous Till
Lac qui Parle River nr Lac qui Parle, CSAH31	0.36	0.25	0.36	0.25	0.31	1.40	Unconsolidated	Calcareous Till
Le Sueur River at St. Clair, CSAH 28	0.34	0.28	0.34	0.28	0.31	1.40	Calcareous Till	Calcareous Till

Table A.3. (cont.)

Le Sueur River near Rapidan, MN 66	**0.34**	**0.28**	**0.34**	**0.28**	**0.31**	**1.17**	**Unconsolidated**	**Unconsolidated**
Le Sueur River nr Rapidan, CR8	0.34	0.28	0.34	0.28	0.30	1.39	Unconsolidated	Calcareous Till
Leaf River nr Staples, CSAH29	0.27	0.20	0.27	0.20	0.20	1.35	Unconsolidated	Unconsolidated
Middle Fork Whitewater River near St. Charles, MN	0.52	0.34	0.51	0.34	0.36	1.59	Calcareous Till	Calcareous Till
North Branch Root River at Chatfield, CSAH2	0.43	0.30	0.43	0.30	0.31	1.46	Unconsolidated	Calcareous Till
North Fork Crow River nr Rockford, Farmington Ave	0.31	0.25	0.31	0.25	0.24	1.42	Unconsolidated	Calcareous Till
Otter Tail River at Breckenridge, CSAH16	0.30	0.22	0.29	0.22	0.23	1.38	Unconsolidated	Calcareous Till
Pipestone Creek at Pipestone, MN	0.44	0.30	0.44	0.30	0.32	0.77	Calcareous Till	Calcareous Till
Pomme De Terre River at Appleton, MN	0.35	0.24	0.35	0.24	0.29	1.41	Unconsolidated	Unconsolidated
Red Lake River at Fisher, MN	0.33	0.23	0.33	0.23	0.25	1.11	Unconsolidated	Unconsolidated
Red River of the North at Wahpeton, ND	0.37	0.25	0.37	0.25	0.32	1.24	Unconsolidated	Calcareous Till
Redwood River at Russell, CR15	0.39	0.27	0.39	0.27	0.32	1.40	Unconsolidated	Calcareous Till
Redwood River nr Redwood Falls, MN	0.36	0.27	0.36	0.27	0.30	1.38	Unconsolidated	Calcareous Till
Root River nr Mound Prairie, CSAH25	0.47	0.34	0.46	0.34	0.32	1.53	Unconsolidated	Colluvium
Sand Creek at Jordan	0.34	0.28	0.34	0.28	0.30	1.40	Calcareous Till	Calcareous Till
Sand Hill River at Climax, MN	0.37	0.27	0.37	0.27	0.28	1.25	Unconsolidated	Unconsolidated

Table A.3. (cont.)

Seven Mile Creek nr North Star, MN169	**0.34**	**0.28**	**0.34**	**0.28**	**0.30**	**1.40**	**Calcareous Till**	**Calcareous Till**
Snake River nr Pine City, MN	0.47	0.32	0.47	0.32	0.27	1.21	Unconsolidated	Non-Calcareous Till
South Branch Root River at Lanesboro, Rochelle Ave N	0.47	0.34	0.47	0.34	0.32	1.42	Colluvium	Colluvium
South Branch Root River nr Carimona, CSAH12	0.45	0.31	0.45	0.31	0.28	1.40	Colluvium	Colluvium
South Fork Crow River at Delano, Bridge Ave	0.33	0.26	0.33	0.26	0.30	1.41	Unconsolidated	Calcareous Till
South Fork Crow River nr Cosmos, MN7	0.33	0.26	0.33	0.26	0.31	1.40	Unconsolidated	Calcareous Till
South Fork Root River at Amherst, CSAH23	0.50	0.37	0.50	0.37	0.38	1.40	Calcareous Till	Calcareous Till
South Fork Whitewater River near Altura, MN	0.46	0.32	0.45	0.32	0.34	1.50	Colluvium	Colluvium
Sucker Creek at County Rd. 290 near Palmers, MN	0.50	0.34	0.45	0.34	0.30	1.40	Non-Calcareous Till	Non-Calcareous Till
Vermillion River at Farmington, Ash St	0.36	0.28	0.36	0.28	0.27	1.41	Unconsolidated	Unconsolidated
Vermillion River at Farmington, Denmark Ave	0.38	0.27	0.38	0.27	0.27	1.41	Unconsolidated	Unconsolidated
Watonwan River nr Garden City, CSAH13	0.33	0.27	0.33	0.27	0.30	1.36	Unconsolidated	Unconsolidated
Yellow Bank River nr Odessa, CSAH40	0.36	0.24	0.36	0.24	0.30	1.40	Unconsolidated	Calcareous Till
Yellow Medicine River nr Granite Falls, MN	0.36	0.27	0.36	0.27	0.31	1.40	Calcareous Till	Calcareous Till

Table A.4. Watershed Climate and Hydrology Metrics

Gage	Avg. Maximum Temperature (°C)	Mean Annual Precipitation (mm)	5-year Recurrence 10-Minute Duration Precipitation Intensity (mm/hr)	5-year Recurrence 60-Minute Duration Precipitation Intensity (mm/hr)	5-year Recurrence 24-Hour Duration Precipitation Intensity (mm/hr)	Baseflow Index (%)
Beaver Creek nr Beaver Falls, CSAH2	12.5	717.5	120.0	43.9	3.4	45.9
Bois de Sioux River near Doran, MN	12.0	622.7	110.4	40.2	3.3	38.9
Chippewa River nr Cyrus, 140th St	11.1	657.6	116.8	42.1	3.4	56.2
Chippewa River nr Milan, MN40	11.9	674.9	116.1	42.8	3.5	48.3
Clearwater River at Red Lake Falls, MN	10.0	617.8	112.4	40.7	3.2	48.3
Cottonwood River nr Lamberton, US14	12.7	709.7	126.5	44.2	3.6	38.3
Cottonwood River nr New Ulm, MN68	12.8	721.7	126.3	44.6	3.6	43.1
Credit River at Savage	12.9	793.8	120.4	45.5	3.7	52.8
Hawk Creek nr Granite Falls, CR52	12.4	705.9	115.0	43.5	3.5	45.7
High Island Creek nr Arlington, CR9	12.6	752.1	124.6	44.7	3.7	48.9
High Island Creek nr Henderson, CSAH6	12.6	762.4	124.1	44.7	3.7	49.5
Kandiyohi CD27 nr Sunburg, CSAH1	12.2	711.6	117.8	44.0	3.6	47.9
Kettle River below Sandstone, MN	10.8	760.7	114.3	41.9	3.6	48.7
Lac qui Parle River nr Lac qui Parle, CSAH31	12.5	652.9	111.4	42.3	3.4	32.6
Le Sueur River at St. Clair, CSAH 28	12.7	828.1	126.2	46.5	3.9	50.1

Table A.4. (cont.)

Le Sueur River near Rapidan, MN 66	**12.9**	**818.1**	**128.4**	**47.0**	**4.0**	**49.2**
Le Sueur River nr Rapidan, CR8	12.7	821.2	126.2	46.3	3.9	49.7
Leaf River nr Staples, CSAH29	10.5	663.1	114.1	42.1	3.4	67.7
Middle Fork Whitewater River near St. Charles, MN	12.4	858.0	120.4	46.5	4.0	68.0
North Branch Root River at Chatfield, CSAH2	12.2	861.6	121.2	46.7	4.0	61.4
North Fork Crow River nr Rockford, Farmington Ave	12.2	738.7	122.4	44.1	3.6	52.5
Otter Tail River at Breckenridge, CSAH16	10.7	648.7	111.9	41.4	3.3	61.5
Pipestone Creek at Pipestone, MN	12.5	685.9	120.0	44.4	3.6	32.9
Pomme De Terre River at Appleton, MN	11.6	643.3	113.6	41.3	3.4	48.4
Red Lake River at Fisher, MN	9.9	615.4	111.4	40.0	3.3	42.5
Red River of the North at Wahpeton, ND	11.9	621.8	110.2	40.2	3.3	39.1
Redwood River at Russell, CR15	12.2	691.1	119.5	44.0	3.6	33.5
Redwood River nr Redwood Falls, MN	12.5	691.0	119.5	43.8	3.6	36.2
Root River nr Mound Prairie, CSAH25	12.5	873.0	121.2	46.9	4.0	64.9
Sand Creek at Jordan	12.8	784.8	121.4	45.4	3.7	51.1
Sand Hill River at Climax, MN	10.3	617.7	112.7	41.1	3.3	44.0
Seven Mile Creek nr North Star, MN169	12.9	775.3	124.6	44.6	3.8	46.9

Table A.4. (cont.)

Snake River nr Pine City, MN	**11.2**	**765.4**	**120.4**	**43.8**	**3.5**	**52.4**
South Branch Root River at Lanesboro, Rochelle Ave N	12.4	875.0	121.1	47.3	4.0	60.0
South Branch Root River nr Carimona, CSAH12	12.2	870.5	121.0	47.4	4.0	56.5
South Fork Crow River at Delano, Bridge Ave	12.4	746.3	123.6	44.5	3.6	49.9
South Fork Crow River nr Cosmos, MN7	12.3	734.1	122.5	44.9	3.6	49.5
South Fork Root River at Amherst, CSAH23	12.6	879.9	121.9	47.4	4.0	63.2
South Fork Whitewater River near Altura, MN	12.4	859.0	119.6	45.9	3.9	68.8
Sucker Creek at County Rd. 290 near Palmers, MN	9.4	774.1	108.7	37.0	3.4	48.0
Vermillion River at Farmington, Ash St	12.9	796.2	120.2	45.7	3.7	52.1
Vermillion River at Farmington, Denmark Ave	12.9	797.1	120.2	45.7	3.7	52.3
Watonwan River nr Garden City, CSAH13	12.9	749.2	126.1	45.9	3.7	49.3
Yellow Bank River nr Odessa, CSAH40	12.3	623.8	113.4	40.8	3.3	31.5
Yellow Medicine River nr Granite Falls, MN	12.6	675.5	113.2	43.1	3.5	34.9

Table A.5. Cumulative, Distance-Weighted Near-channel Metrics, 10 km Upstream of Gage

Gage	Local Relief (m)	Topographic Slope (Degrees)	Rock-Free K-factor, All Horizons (-)	Rock-Free K-factor, Top Horizon (-)	Whole-Soil K-factor, All Horizons (-)	Whole-Soil K-factor, Top Horizon (-)	Waterbody Area (km^2)	Stream Power (W)	Unit Stream Power (W/m)	Channel Gradient (Degrees)
Beaver Creek nr Beaver Falls, CSAH2	48.4	36.7	1.7	1.5	1.7	1.5	0.00	5512	59	3
Bois de Sioux River near Doran, MN	16.2	17.6	2.5	1.7	2.5	1.7	0.00	10540	79	4
Chippewa River nr Cyrus, 140th St	11.4	10.5	1.9	1.5	1.9	1.5	0.00	1509	21	1
Chippewa River nr Milan, MN40	44.5	24.4	2.7	2.3	2.6	2.2	0.00	41621	228	10
Clearwater River at Red Lake Falls, MN	72.2	56.3	2.3	1.4	2.3	1.4	0.00	44687	207	8
Cottonwood River nr Lamberton, US14	23.5	21.9	3.0	2.2	3.0	2.2	0.00	4960	34	2
Cottonwood River nr New Ulm, MN68	47.4	35.9	1.8	1.5	1.8	1.5	0.00	16395	59	2
Credit River at Savage	51.4	40.8	2.4	1.7	2.4	1.7	0.00	3274	53	4
Hawk Creek nr Granite Falls, CR52	47.3	37.5	1.9	1.6	1.9	1.6	0.00	4775	54	4
High Island Creek nr Arlington, CR9	16.9	16.0	1.9	1.7	1.9	1.7	0.00	2351	35	2
High Island Creek nr Henderson, CSAH6	84.1	65.0	2.7	2.4	2.7	2.4	0.01	6990	94	6
Kandiyohi CD27 nr Sunburg, CSAH1	31.5	31.4	2.5	1.9	2.5	1.9	0.00	712	40	4
Kettle River below Sandstone, MN	100.9	80.1	4.5	3.1	4.4	3.1	0.00	92839	344	17
Lac qui Parle River nr Lac qui Parle, CSAH31	48.2	40.2	3.1	2.0	3.1	2.0	0.00	24598	129	5
Le Sueur River at St. Clair, CSAH 28	50.5	45.3	2.9	2.3	2.9	2.3	0.00	21989	143	6

Table A.5. (cont.)

Le Sueur River near Rapidan, MN 66	**76.9**	**56.2**	**2.4**	**1.7**	**2.4**	**1.7**	**0.00**	**28343**	**119**	**6**
Le Sueur River nr Rapidan, CR8	63.8	51.2	2.2	1.6	2.2	1.6	0.00	12505	80	4
Leaf River nr Staples, CSAH29	17.5	17.8	1.9	1.1	1.9	1.1	0.00	4993	21	1
Middle Fork Whitewater River near St. Charles, MN	124.5	91.4	6.3	4.6	6.3	4.6	0.00	19364	230	13
North Branch Root River at Chatfield, CSAH2	93.8	66.6	4.1	3.2	4.0	3.2	0.00	38425	184	9
North Fork Crow River nr Rockford, Farmington Ave	20.3	16.8	1.4	1.1	1.4	1.1	0.01	5594	31	1
Otter Tail River at Breckenridge, CSAH16	10.9	10.0	2.5	1.7	2.5	1.7	0.00	7836	49	2
Pipestone Creek at Pipestone, MN	23.7	26.1	5.2	3.7	5.2	3.7	0.00	592	27	3
Pomme De Terre River at Appleton, MN	25.5	24.3	2.3	1.8	2.3	1.8	0.12	6367	65	4
Red Lake River at Fisher, MN	10.4	9.9	1.7	1.5	1.7	1.5	0.00	36597	119	4
Red River of the North at Wahpeton, ND	22.4	22.4	3.3	2.1	3.3	2.1	0.00	8793	66	6
Redwood River at Russell, CR15	69.9	66.4	4.3	2.8	4.2	2.8	0.00	4035	59	4
Redwood River nr Redwood Falls, MN	49.0	37.9	2.4	1.6	2.4	1.6	0.00	13728	81	3
Root River nr Mound Prairie, CSAH25	193.8	131.2	5.9	4.3	5.6	4.3	0.00	134718	354	16
Sand Creek at Jordan	44.9	38.1	2.1	1.6	2.1	1.6	0.00	8062	69	3
Sand Hill River at Climax, MN	53.4	52.2	3.3	2.8	3.3	2.8	0.00	13481	117	6

Table A.5. (cont.)

Seven Mile Creek nr North Star, MN169	**175.3**	**128.1**	**3.0**	**2.7**	**3.0**	**2.7**	**0.00**	**6591**	**150**	**12**
Snake River nr Pine City, MN	21.0	16.7	3.6	2.9	3.6	2.9	0.64	16884	44	2
South Branch Root River at Lanesboro, Rochelle Ave N	176.5	125.2	6.0	4.4	5.8	4.4	0.01	48447	261	14
South Branch Root River nr Carimona, CSAH12	150.3	113.5	6.8	5.1	6.7	5.1	0.00	28153	213	14
South Fork Crow River at Delano, Bridge Ave	42.6	38.3	3.8	3.0	3.8	3.0	0.01	11249	74	4
South Fork Crow River nr Cosmos, MN7	19.5	19.9	3.8	2.8	3.8	2.8	0.00	646	15	1
South Fork Root River at Amherst, CSAH23	90.6	67.9	4.9	3.8	4.8	3.8	0.00	18261	218	13
South Fork Whitewater River near Altura, MN	203.6	124.4	4.6	3.1	3.1	2.9	0.00	32515	283	16
Sucker Creek at County Rd. 290 near Palmers, MN	48.9	38.4	3.5	2.5	3.3	2.5	0.00	24516	187	9
Vermillion River at Farmington, Ash St	22.5	20.7	3.2	2.4	3.2	2.4	0.01	1315	25	2
Vermillion River at Farmington, Denmark Ave	28.6	27.9	4.8	3.1	4.8	3.1	0.00	2113	34	2
Watonwan River nr Garden City, CSAH13	47.3	38.2	1.7	1.3	1.7	1.3	0.00	19011	75	3
Yellow Bank River nr Odessa, CSAH40	43.7	36.5	2.5	1.6	2.5	1.6	0.00	14016	113	6
Yellow Medicine River nr Granite Falls, MN	46.0	37.7	3.5	2.5	3.5	2.5	0.00	33269	197	10

Table A.6. Cumulative, Distance-Weighted Near-channel Metrics, 50 km Upstream of Gage

Gage	Local Relief (m)	Topographic Slope (Degrees)	Rock-Free K-factor, All Horizons	Rock-Free K-factor, Top Horizon	Whole-Soil K-factor, All Horizons	Whole-Soil K-factor, Top Horizon	Waterbody Area (km^2)	Stream Power (W)	Unit Stream Power (W/m)	Channel Gradient (Degrees)
Beaver Creek nr Beaver Falls, CSAH2	228	184	13.8	11.3	13.8	11.3	0.0	16328.8	223.2	14.9
Bois de Sioux River near Doran, MN	170	176	28.7	19.6	28.6	19.6	0.1	43294.4	416.1	27.3
Chippewa River nr Cyrus, 140th St	244	196	22.5	16.5	22.4	16.5	0.2	7518.1	197.2	20.6
Chippewa River nr Milan, MN40	335	258	34.5	25.3	34.2	25.1	0.1	179336.8	1042.8	47.0
Clearwater River at Red Lake Falls, MN	348	288	18.8	13.3	18.8	13.3	0.0	126947.8	742.8	37.1
Cottonwood River nr Lamberton, US14	240	208	23.4	18.1	23.3	17.9	0.0	19408.6	217.7	15.9
Cottonwood River nr New Ulm, MN68	391	301	13.2	11.0	13.2	11.0	0.0	97291.9	442.2	23.1
Credit River at Savage	215	176	11.8	9.2	11.8	9.2	0.2	7550.0	150.5	16.5
Hawk Creek nr Granite Falls, CR52	257	208	18.6	13.0	18.5	13.0	0.0	27927.7	311.7	19.2
High Island Creek nr Arlington, CR9	97	96	15.9	12.5	15.9	12.5	0.5	4710.1	82.8	6.0
High Island Creek nr Henderson, CSAH6	467	377	20.8	18.3	20.8	18.3	0.1	28761.1	457.9	30.9
Kandiyohi CD27 nr Sunburg, CSAH1	98	95	10.0	7.9	10.0	7.9	0.0	1208.0	81.3	10.0
Kettle River below Sandstone, MN	435	354	20.7	13.8	20.6	13.8	0.2	196077.7	789.3	42.0
Lac qui Parle River nr Lac qui Parle, CSAH31	274	232	18.6	13.1	18.6	13.1	0.0	96561.4	555.4	25.7
Le Sueur River at St. Clair, CSAH 28	327	296	21.6	17.4	21.6	17.4	0.2	56787.7	434.8	23.4

Table A.6. (cont.)

Le Sueur River near Rapidan, MN 66	**643**	**499**	**21.0**	**16.3**	**21.0**	**16.3**	**0.0**	**131917.0**	**832.7**	**42.9**
Le Sueur River nr Rapidan, CR8	451	367	15.8	12.6	15.8	12.6	0.0	54753.6	459.6	28.0
Leaf River nr Staples, CSAH29	144	142	18.1	12.7	18.1	12.7	0.9	15218.6	116.9	7.4
Middle Fork Whitewater River near St. Charles, MN	535	394	39.6	27.3	39.3	27.3	0.0	39227.1	649.8	45.7
North Branch Root River at Chatfield, CSAH2	844	601	34.3	25.2	32.1	24.9	0.0	198374.2	1246.8	74.5
North Fork Crow River nr Rockford, Farmington Ave	200	174	21.2	16.4	21.1	16.3	0.6	14719.1	165.1	12.8
Otter Tail River at Breckenridge, CSAH16	104	103	15.8	11.3	15.7	11.3	0.1	29960.3	211.3	13.0
Pipestone Creek at Pipestone, MN	124	131	33.0	23.4	33.0	23.4	0.0	2304.9	112.1	12.0
Pomme De Terre River at Appleton, MN	118	112	13.3	9.7	13.3	9.7	0.2	14717.2	160.6	10.5
Red Lake River at Fisher, MN	169	163	21.5	16.3	21.4	16.3	0.0	137765.4	689.2	37.9
Red River of the North at Wahpeton, ND	124	125	24.6	16.2	24.5	16.2	0.0	29299.9	261.4	20.2
Redwood River at Russell, CR15	448	385	31.3	19.6	31.1	19.5	0.1	24349.7	452.3	32.1
Redwood River nr Redwood Falls, MN	200	169	15.2	11.0	15.2	11.0	0.0	44863.5	299.2	14.9
Root River nr Mound Prairie, CSAH25	2437	1696	92.6	69.3	88.0	68.2	0.0	715799.5	3429.6	212.6
Sand Creek at Jordan	469	396	29.9	22.6	29.9	22.5	0.3	31401.6	435.3	30.0
Sand Hill River at Climax, MN	160	164	13.5	10.7	13.5	10.7	0.0	35210.4	319.8	18.1

Table A.6. (cont.)

Seven Mile Creek nr North Star, MN169	**385**	**309**	**15.0**	**12.5**	**15.0**	**12.5**	**0.1**	**12770.5**	**352.1**	**29.9**
Snake River nr Pine City, MN	200	177	34.4	26.3	33.9	26.2	2.6	37892.7	196.7	14.3
South Branch Root River at Lanesboro, Rochelle Ave N	1593	1125	57.6	43.2	56.1	43.1	0.0	168629.1	1545.6	106.2
South Branch Root River nr Carimona, CSAH12	1095	784	45.9	33.4	44.5	33.2	0.0	118561.2	1187.0	78.3
South Fork Crow River at Delano, Bridge Ave	297	264	29.9	21.2	29.9	21.1	0.6	43319.9	355.2	22.9
South Fork Crow River nr Cosmos, MN7	201	213	31.3	23.6	31.2	23.6	0.2	5615.7	149.3	14.3
South Fork Root River at Amherst, CSAH23	356	261	24.2	19.0	24.1	19.0	0.0	29347.0	435.4	29.2
South Fork Whitewater River near Altura, MN	1219	801	36.1	25.3	30.2	24.3	0.0	163522.9	1645.0	101.3
Sucker Creek at County Rd. 290 near Palmers, MN	203	168	18.1	13.0	16.8	13.0	0.2	44389.3	374.6	19.4
Vermillion River at Farmington, Ash St	178	155	22.2	15.6	22.1	15.6	0.1	4903.7	150.4	14.3
Vermillion River at Farmington, Denmark Ave	244	218	32.6	22.1	32.6	22.1	0.0	6645.2	194.9	18.2
Watonwan River nr Garden City, CSAH13	240	198	12.0	9.8	12.0	9.8	0.0	56350.6	263.4	11.3
Yellow Bank River nr Odessa, CSAH40	321	265	22.5	14.6	22.5	14.5	0.1	44642.7	441.2	26.1
Yellow Medicine River nr Granite Falls, MN	231	207	22.6	16.3	22.5	16.3	0.0	72536.8	474.1	26.4

Table A.7. Rating Curve Parameters 1

Gage	Rising Limb Exponent	Rising Limb Coefficient (mg/L)	Rising Limb n	Falling Limb Exponent	Falling Limb Coefficient (mg/L)	Falling Limb n	Combined Exponent	Combined Coefficient (mg/L)	Combined n
Beaver Creek nr Beaver Falls, CSAH2	0.74	29	106	0.63	16	139	0.73	20	245
Bois de Sioux River near Doran, MN	0.17	70	96	0.11	55	157	0.14	61	253
Chippewa River nr Cyrus, 140th St	-2.32	144	29	-2.36	133	55	-2.36	138	84
Chippewa River nr Milan, MN40	0.22	58	58	-0.33	50	84	0.08	47	142
Clearwater River at Red Lake Falls, MN	1.11	14	80	0.81	12	184	0.91	12	264
Cottonwood River nr Lamberton, US14	0.21	99	92	0.15	39	102	0.24	61	194
Cottonwood River nr New Ulm, MN68	0.73	101	130	0.56	59	182	0.66	75	312
Credit River at Savage	1.22	6	71	0.86	4	106	1.04	5	177
Hawk Creek nr Granite Falls, CR52	0.62	40	73	0.65	17	95	0.75	21	168
High Island Creek nr Arlington, CR9	-0.08	35	120	-0.16	24	121	-0.12	29	241
High Island Creek nr Henderson, CSAH6	0.74	154	133	0.65	72	148	0.69	103	281
Kandiyohi CD27 nr Sunburg, CSAH1	0.30	12	23	0.17	7	39	0.35	7	62
Kettle River below Sandstone, MN	0.57	5	77	0.29	3	100	0.43	4	177
Lac qui Parle River nr Lac qui Parle, CSAH31	0.47	41	125	0.37	32	137	0.42	36	262
Le Sueur River at St. Clair, CSAH 28	0.47	94	60	0.34	59	101	0.42	71	161

Table A.7. (cont.)

Le Sueur River near Rapidan, MN 66	**0.67**	**187**	**157**	**0.64**	**79**	**208**	**0.68**	**114**	**365**
Le Sueur River nr Rapidan, CR8	0.61	202	78	0.61	92	128	0.66	124	206
Leaf River nr Staples, CSAH29	-0.25	10	43	-0.52	9	63	-0.41	9	106
Middle Fork Whitewater River near St. Charles, MN	1.03	110	88	0.77	37	70	1.06	69	158
North Branch Root River at Chatfield, CSAH2	1.01	28	27	0.97	16	28	1.07	21	55
North Fork Crow River nr Rockford, Farmington Ave	-1.71	50	35	-2.52	68	41	-2.07	56	76
Otter Tail River at Breckenridge, CSAH16	0.17	37	18	-0.48	40	23	-0.16	38	41
Pipestone Creek at Pipestone, MN	0.66	16	31	0.66	5	42	0.65	8	73
Pomme De Terre River at Appleton, MN	-0.22	68	40	-0.78	75	74	-0.54	71	114
Red Lake River at Fisher, MN	0.94	67	79	0.48	52	114	0.71	57	193
Red River of the North at Wahpeton, ND	0.57	57	59	0.43	44	75	0.49	49	134
Redwood River at Russell, CR15	0.53	27	35	0.45	18	74	0.49	21	109
Redwood River nr Redwood Falls, MN	0.21	95	92	0.37	46	114	0.34	61	206
Root River nr Mound Prairie, CSAH25	1.62	86	59	1.44	55	105	1.58	65	164
Sand Creek at Jordan	0.90	12	38	1.00	5	93	1.01	6	131
Sand Hill River at Climax, MN	0.39	91	70	0.44	74	166	0.43	79	236
Seven Mile Creek nr North Star, MN169	1.05	55	109	1.39	13	90	1.27	26	199

Table A.7. (cont.)

Snake River nr Pine City, MN	**-0.01**	**5**	**122**	**-0.06**	**4**	**132**	**-0.04**	**5**	**254**
South Branch Root River at Lanesboro, Rochelle Ave N	1.40	51	32	1.12	32	30	1.38	42	62
South Branch Root River nr Carimona, CSAH12	0.52	97	63	1.46	17	26	0.93	48	89
South Fork Crow River at Delano, Bridge Ave	-0.64	65	48	-0.84	53	46	-0.68	56	94
South Fork Crow River nr Cosmos, MN7	-0.02	31	15	-0.06	31	48	-0.04	31	63
South Fork Root River at Amherst, CSAH23	0.95	37	23	0.77	27	17	0.90	31	40
South Fork Whitewater River near Altura, MN	1.58	47	31	1.56	20	27	1.69	31	58
Sucker Creek at County Rd. 290 near Palmers, MN	0.87	8	113	0.69	5	102	0.83	6	215
Vermillion River at Farmington, Ash St	0.43	11	72	0.21	6	78	0.40	8	150
Vermillion River at Farmington, Denmark Ave	0.55	14	66	0.26	8	72	0.56	11	138
Watonwan River nr Garden City, CSAH13	0.25	90	142	0.29	55	220	0.32	64	362
Yellow Bank River nr Odessa, CSAH40	0.91	19	71	0.86	12	129	0.92	13	200
Yellow Medicine River nr Granite Falls, MN	0.45	55	49	0.18	40	53	0.33	46	102

Table A.8. Rating Curve Parameters 2

Gage	Shape	Hysteresis	Low Flow (90% Exceedance Q) TSS (mg/L)
Beaver Creek nr Beaver Falls, CSAH2	Threshold	0.32	8.000691
Bois de Sioux River near Doran, MN	Power	0.07	42.64276
Chippewa River nr Cyrus, 140th St	Peaked/Negative	0.06	33.28053
Chippewa River nr Milan, MN40	Peaked/Negative	0.41	31.51656
Clearwater River at Red Lake Falls, MN	Power	0.08	3.219883
Cottonwood River nr Lamberton, US14	Power	0.39	32.869
Cottonwood River nr New Ulm, MN68	Power	0.25	18.25709
Credit River at Savage	Power	0.28	1.104034
Hawk Creek nr Granite Falls, CR52	Threshold	0.34	21.67791
High Island Creek nr Arlington, CR9	Peaked/Negative	0.10	38.90307
High Island Creek nr Henderson, CSAH6	Power	0.30	19.7752
Kandiyohi CD27 nr Sunburg, CSAH1	Threshold	0.34	11.82638
Kettle River below Sandstone, MN	Power	0.22	1.997218
Lac qui Parle River nr Lac qui Parle, CSAH31	Power	0.07	13.19774
Le Sueur River at St. Clair, CSAH 28	Power	0.16	26.75581

Table A.8. (cont.)

Le Sueur River near Rapidan, MN 66	**Power**	**0.37**	**28.09424**
Le Sueur River nr Rapidan, CR8	Power	0.34	28.95912
Leaf River nr Staples, CSAH29	Peaked/Negative	0.21	2.161273
Middle Fork Whitewater River near St. Charles, MN	Power	0.60	20.44843
North Branch Root River at Chatfield, CSAH2	Power	0.27	5.876883
North Fork Crow River nr Rockford, Farmington Ave	Peaked/Negative	0.25	36.59295
Otter Tail River at Breckenridge, CSAH16	Peaked/Negative	0.18	28.23386
Pipestone Creek at Pipestone, MN	Threshold	0.52	17.49607
Pomme De Terre River at Appleton, MN	Peaked/Negative	0.25	30.88971
Red Lake River at Fisher, MN	Power	0.06	24.08384
Red River of the North at Wahpeton, ND	Power	0.09	28.44277
Redwood River at Russell, CR15	Power	0.19	4.840874
Redwood River nr Redwood Falls, MN	Threshold	0.23	27.47547
Root River nr Mound Prairie, CSAH25	Power	0.24	22.82156
Sand Creek at Jordan	Threshold	0.27	3.9383
Sand Hill River at Climax, MN	Power	0.08	42.15183
Seven Mile Creek nr North Star, MN169	Threshold	0.42	3.55528

Table A.8. (cont.)

Snake River nr Pine City, MN	**Peaked/Negative**	**0.04**	**4.963689**
South Branch Root River at Lanesboro, Rochelle Ave N	Power	0.32	10.07131
South Branch Root River nr Carimona, CSAH12	Threshold	0.28	4.238888
South Fork Crow River at Delano, Bridge Ave	Peaked/Negative	0.21	24.24112
South Fork Crow River nr Cosmos, MN7	Peaked/Negative	-0.05	34.29802
South Fork Root River at Amherst, CSAH23	Threshold	0.30	28.06102
South Fork Whitewater River near Altura, MN	Power	0.38	5.116525
Sucker Creek at County Rd. 290 near Palmers, MN	Power	0.23	1.26898
Vermillion River at Farmington, Ash St	Power	0.22	4.298237
Vermillion River at Farmington, Denmark Ave	Power	0.31	5.499473
Watonwan River nr Garden City, CSAH13	Threshold	0.20	18.73141
Yellow Bank River nr Odessa, CSAH40	Threshold	0.23	7.877737
Yellow Medicine River nr Granite Falls, MN	Threshold	0.35	16.94151

Appendix B. Daily Discharge versus Instantaneous Discharge Analysis

Daily mean discharge data are reported by the DNR/MPCA cooperative for the TSS measurements. We also obtained 15-minute interval discharge data from the gaging agencies (MDNR, USGS, or MCES depending on the gage), and associated the high-resolution discharge data with the TSS measurements. The high-resolution data are more representative of the streamflow conditions at the exact time the sediment samples were obtained, especially during rising and falling limbs of flood flows, where the flow may change dramatically over the course of the day. In such cases, the mean flow may not be a very good estimate of the discharge at the instant the sample was taken. However, for most gages, the high-resolution data were only available for the years after 2007, meaning that over half of the study period lacked high-resolution Q data.

We compared Q-TSS rating curves constructed using the available high-resolution data with rating curves constructed using the daily Q data (using only data points which also had corresponding high-resolution Q data). Note that these comparisons were done using SRCs constructed using all Q-TSS data points, not the high-flow (i.e. rising and falling limb) subsets of the data used for our RF models. Figures B.1 and B.2 show the percent difference and absolute difference, respectively, in SRC exponents for SRC constructed using the mean daily discharge and high-resolution discharge. For most gages, with the exception of several small watersheds with flashier discharge regimes, the rating curves constructed with daily and high-resolution data were quite similar. Most gages have less than 10 percent difference between the two exponent values. The few gages that have higher percent differences, notably the Snake River and Kandiyohi County Ditch 27, have very small exponent values, skewing the percent difference calculation high. The absolute differences plot shows that these gages do not have large absolute

differences in the exponent values. Therefore, we decided to use the daily Q data rather than the high-resolution data, making the judgement that using a longer period of record (with slightly less accurate Q measurements) was preferable to using Q data with better accuracy but reduced temporal coverage.

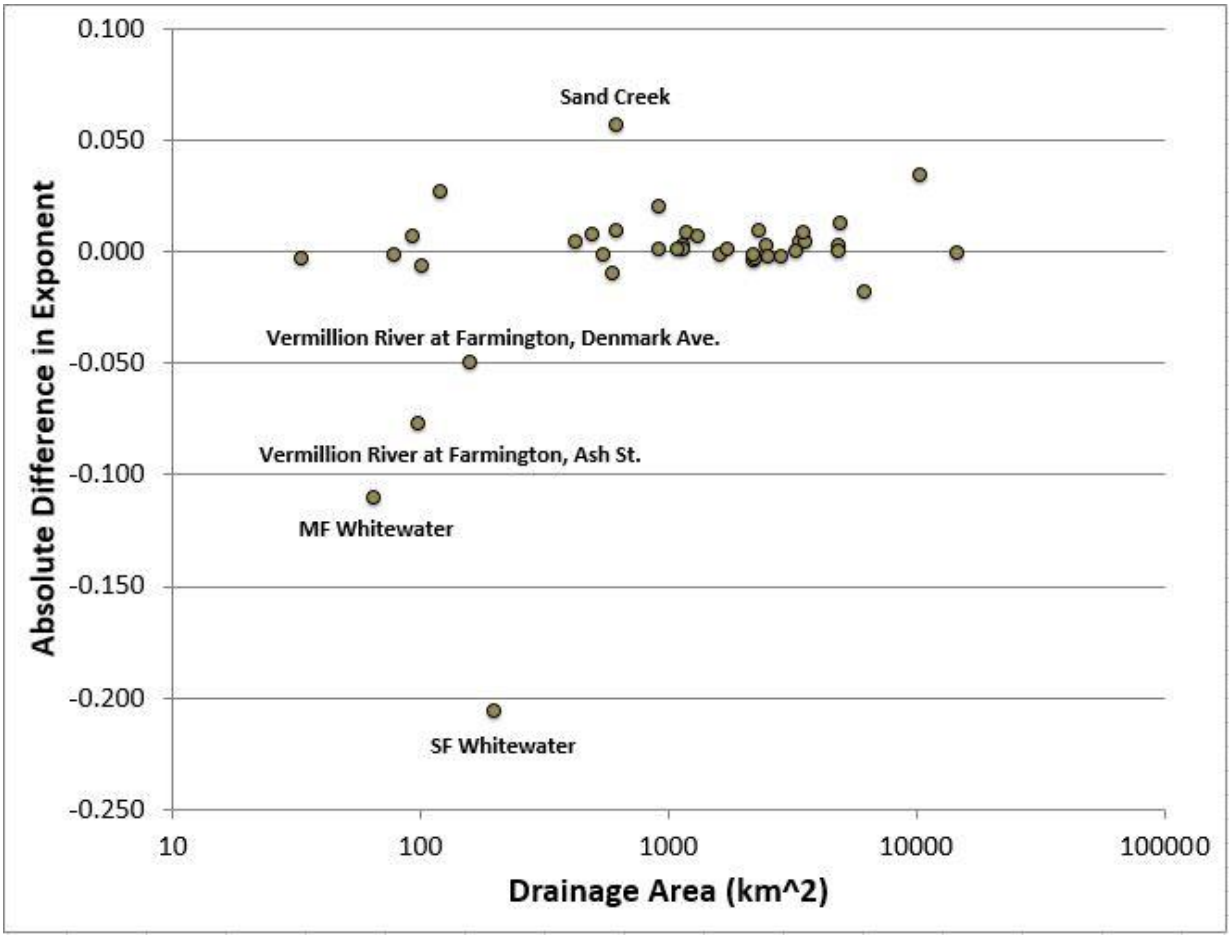

Figure B.1. Absolute difference in rating curve exponents for SRCs created using mean daily and instantaneous flow data.

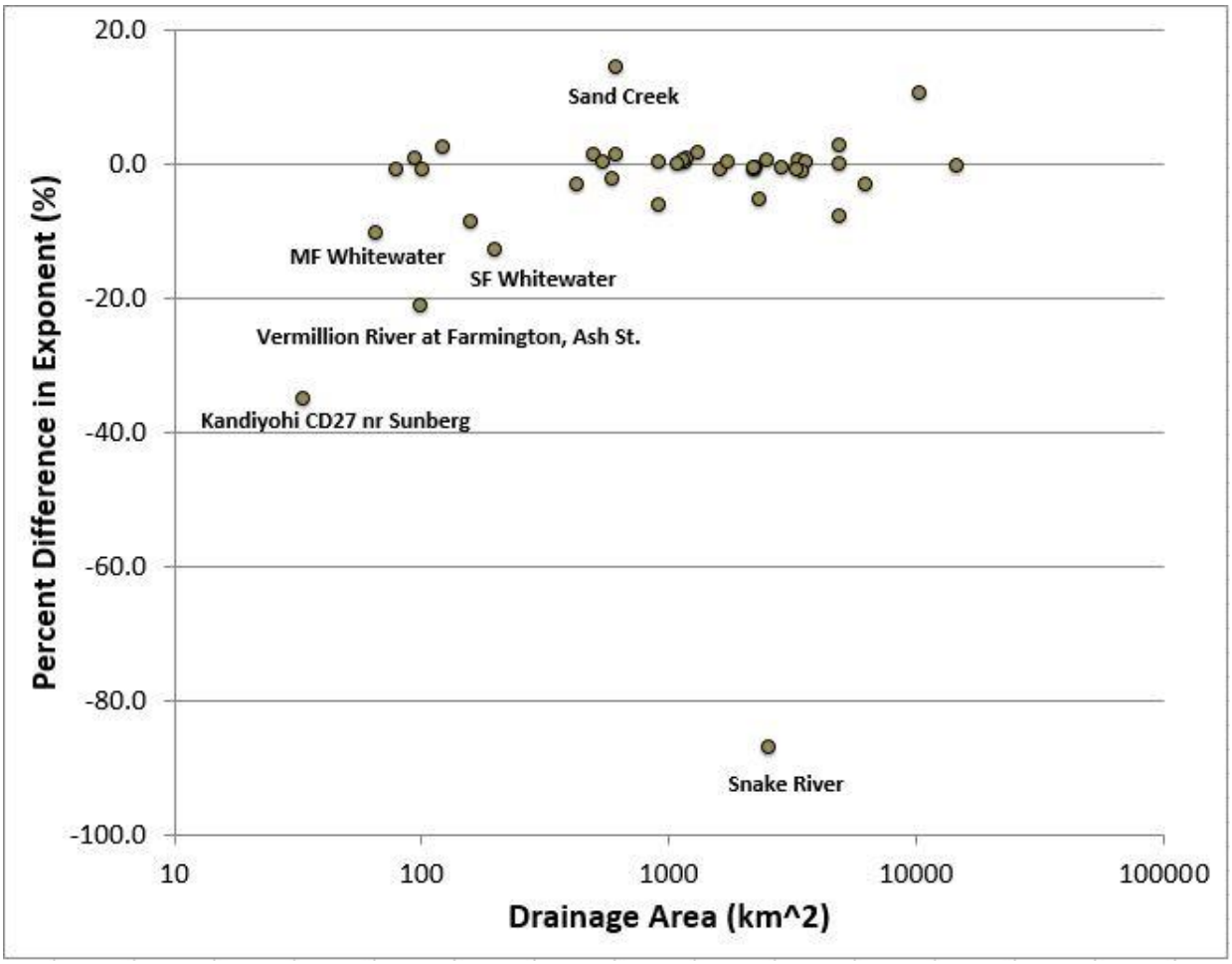

Figure B.2. Percent difference in exponents for SRCs created using mean daily and instantaneous flow data. Note Snake River is an outlier, with large percent difference but very little absolute difference, due to exponent value very near to zero.

Appendix C. Q-TSS Relations for All Study Gages

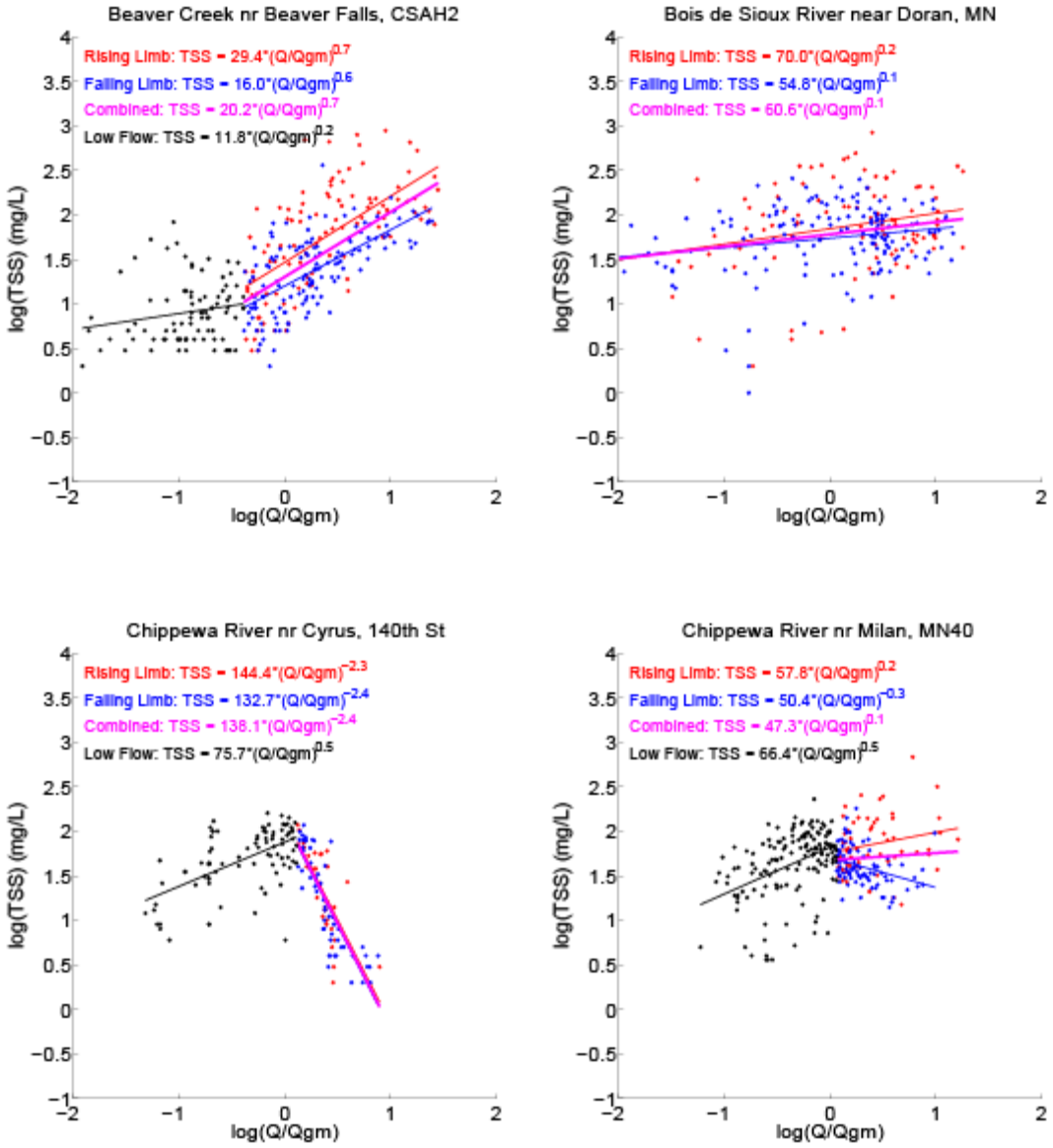

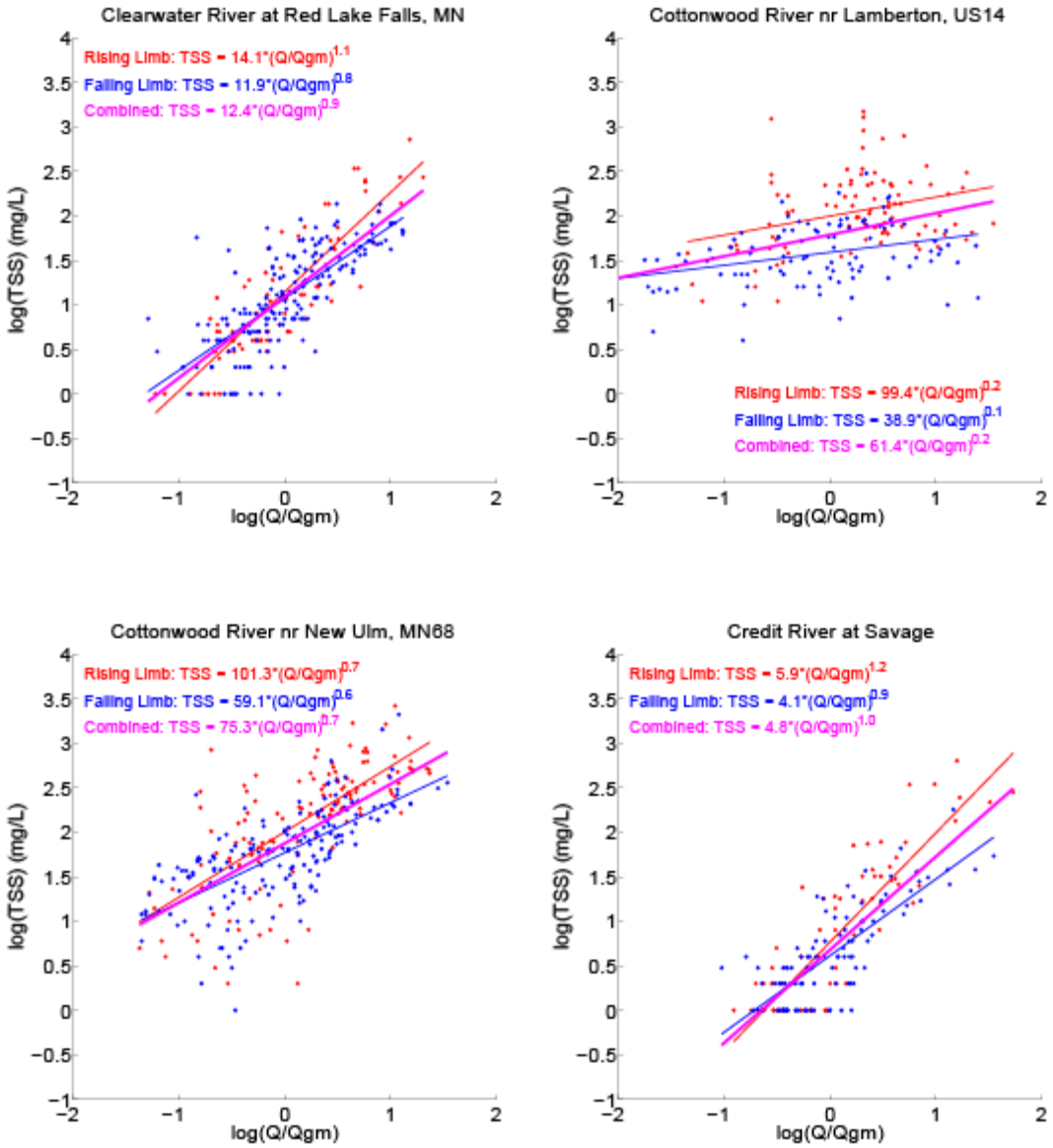
Clearwater River at Red Lake Falls, MN
Rising Limb: TSS = 14.1*(Q/Qgm)^1.1
Falling Limb: TSS = 11.9*(Q/Qgm)^0.8
Combined: TSS = 12.4*(Q/Qgm)^0.9
log(TSS) (mg/L)
log(Q/Qgm)
Cottonwood River nr Lamberton, US14
Rising Limb: TSS = 99.4*(Q/Qgm)^0.2
Falling Limb: TSS = 38.9*(Q/Qgm)^0.1
Combined: TSS = 61.4*(Q/Qgm)^0.2
log(TSS) (mg/L)
log(Q/Qgm)
Cottonwood River nr New Ulm, MN68
Rising Limb: TSS = 101.3*(Q/Qgm)^0.7
Falling Limb: TSS = 59.1*(Q/Qgm)^0.6
Combined: TSS = 75.3*(Q/Qgm)^0.7
log(TSS) (mg/L)
log(Q/Qgm)
Credit River at Savage
Rising Limb: TSS = 5.9*(Q/Qgm)^1.2
Falling Limb: TSS = 4.1*(Q/Qgm)^0.9
Combined: TSS = 4.8*(Q/Qgm)^1.0
log(TSS) (mg/L)
log(Q/Qgm)

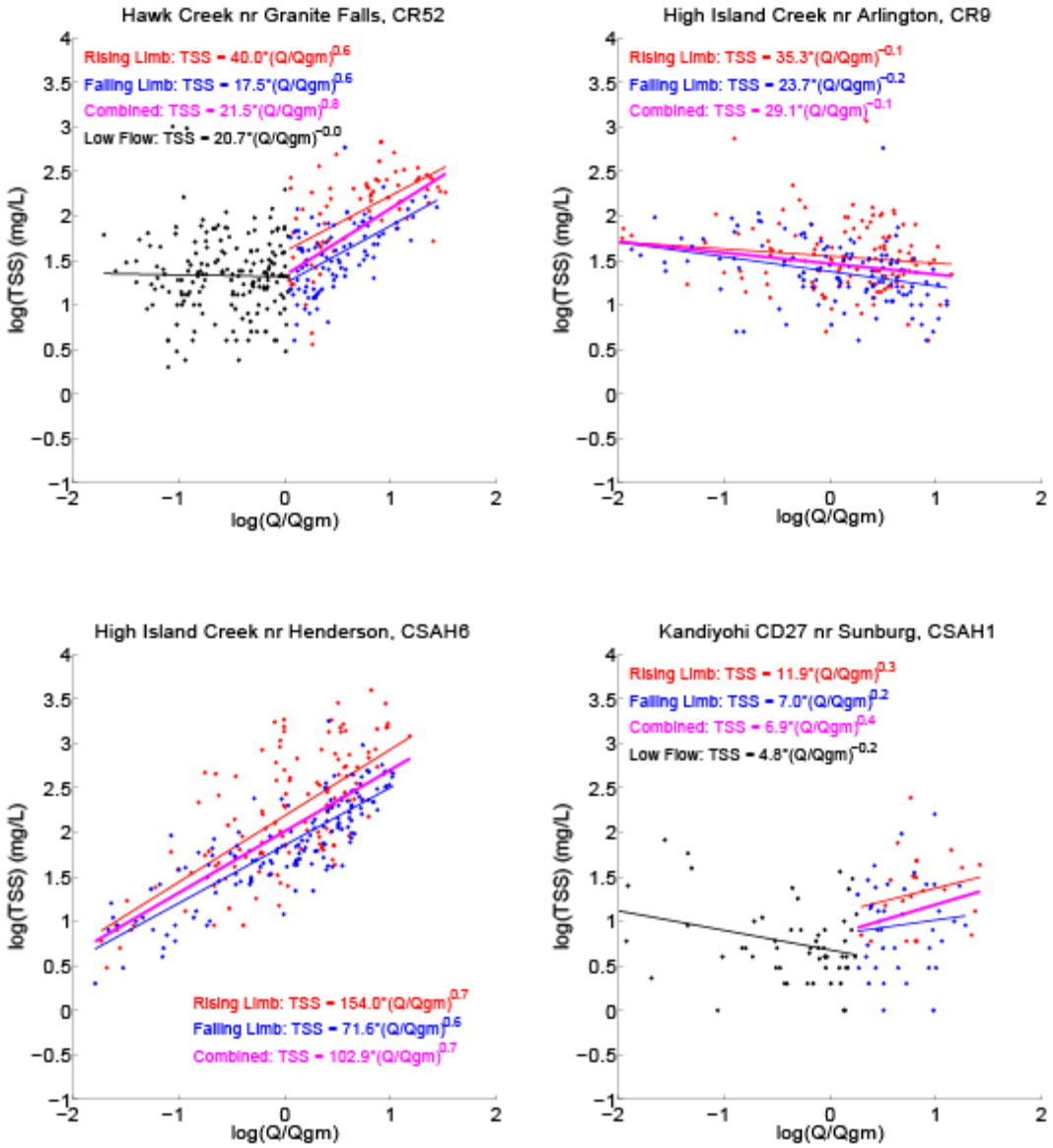
Hawk Creek nr Granite Falls, CR52
Rising Limb: TSS = 40.0*(Q/Qgm)^0.6
Falling Limb: TSS = 17.5*(Q/Qgm)^0.6
Combined: TSS = 21.5*(Q/Qgm)^0.8
Low Flow: TSS = 20.7*(Q/Qgm)^-0.0
High Island Creek nr Arlington, CR9
Rising Limb: TSS = 35.3*(Q/Qgm)^-0.1
Falling Limb: TSS = 23.7*(Q/Qgm)^-0.2
Combined: TSS = 29.1*(Q/Qgm)^-0.1
High Island Creek nr Henderson, CSAH6
Rising Limb: TSS = 154.0*(Q/Qgm)^0.7
Falling Limb: TSS = 71.6*(Q/Qgm)^0.6
Combined: TSS = 102.9*(Q/Qgm)^0.7
Kandiyohi CD27 nr Sunburg, CSAH1
Rising Limb: TSS = 11.9*(Q/Qgm)^0.3
Falling Limb: TSS = 7.0*(Q/Qgm)^0.2
Combined: TSS = 6.9*(Q/Qgm)^0.4
Low Flow: TSS = 4.8*(Q/Qgm)^-0.2
log(TSS) (mg/L)
log(Q/Qgm)

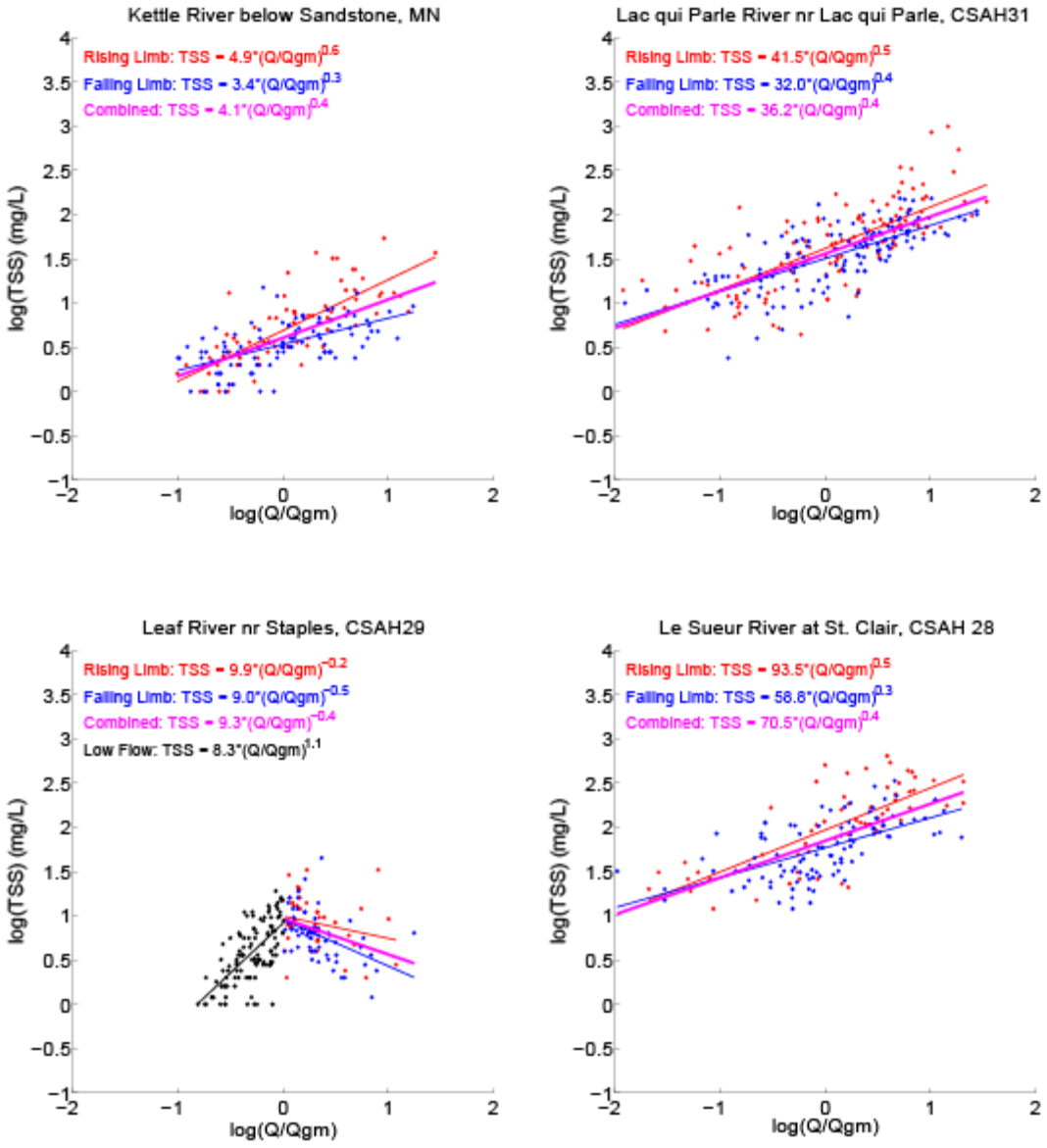
Kettle River below Sandstone, MN
Rising Limb: TSS = 4.9*(Q/Qgm)^0.6
Falling Limb: TSS = 3.4*(Q/Qgm)^0.3
Combined: TSS = 4.1*(Q/Qgm)^0.4
log(TSS) (mg/L)
log(Q/Qgm)
Lac qui Parle River nr Lac qui Parle, CSAH31
Rising Limb: TSS = 41.5*(Q/Qgm)^0.5
Falling Limb: TSS = 32.0*(Q/Qgm)^0.4
Combined: TSS = 36.2*(Q/Qgm)^0.4
log(TSS) (mg/L)
log(Q/Qgm)
Leaf River nr Staples, CSAH29
Rising Limb: TSS = 9.9*(Q/Qgm)^-0.2
Falling Limb: TSS = 9.0*(Q/Qgm)^-0.5
Combined: TSS = 9.3*(Q/Qgm)^-0.4
Low Flow: TSS = 8.3*(Q/Qgm)^1.1
log(TSS) (mg/L)
log(Q/Qgm)
Le Sueur River at St. Clair, CSAH 28
Rising Limb: TSS = 93.5*(Q/Qgm)^0.5
Falling Limb: TSS = 58.8*(Q/Qgm)^0.3
Combined: TSS = 70.5*(Q/Qgm)^0.4
log(TSS) (mg/L)
log(Q/Qgm)

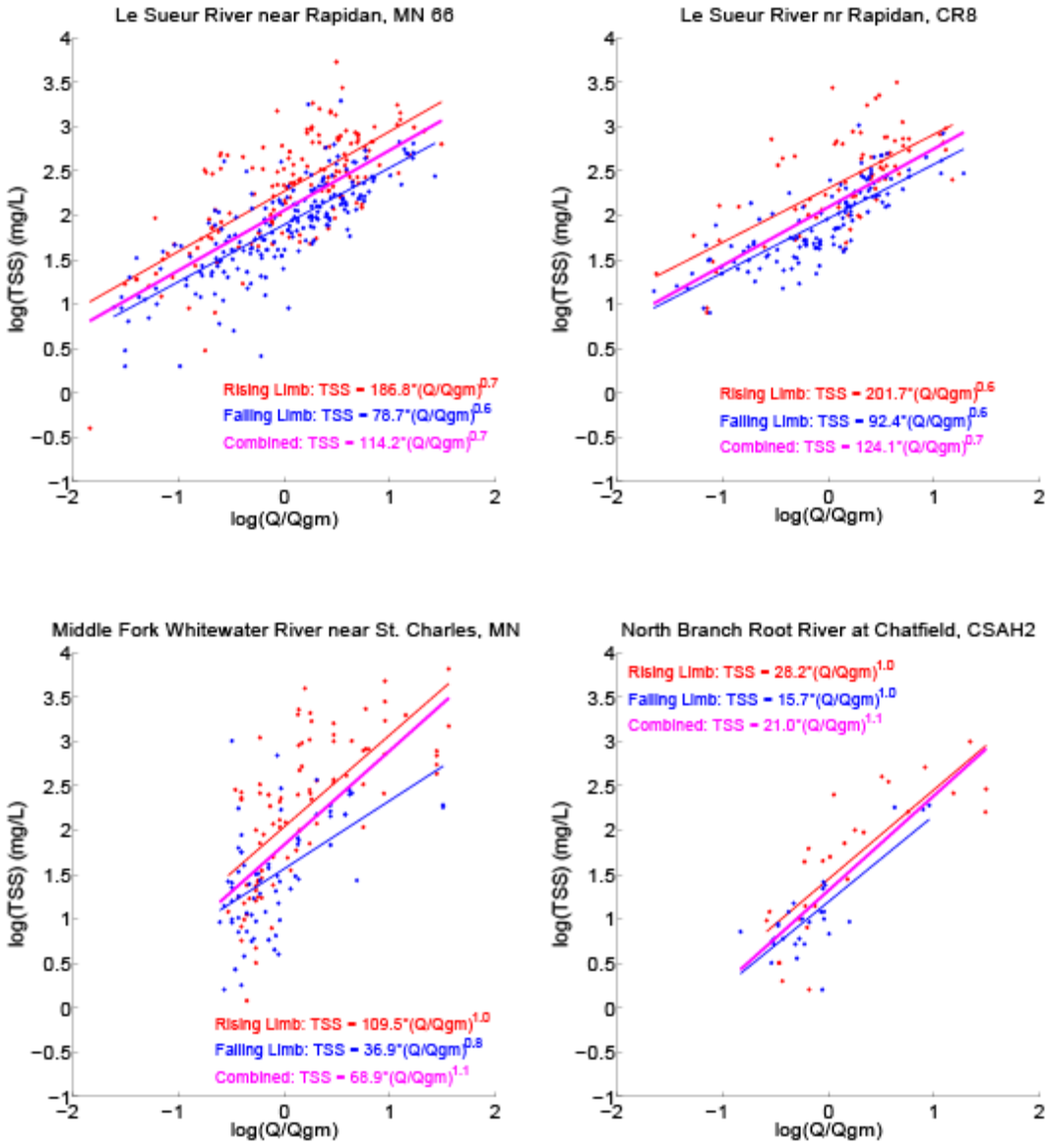
Le Sueur River near Rapidan, MN 66
log(TSS) (mg/L)
log(Q/Qgm)
Rising Limb: TSS = 186.8*(Q/Qgm)^0.7
Falling Limb: TSS = 78.7*(Q/Qgm)^0.6
Combined: TSS = 114.2*(Q/Qgm)^0.7
Le Sueur River nr Rapidan, CR8
log(TSS) (mg/L)
log(Q/Qgm)
Rising Limb: TSS = 201.7*(Q/Qgm)^0.6
Falling Limb: TSS = 92.4*(Q/Qgm)^0.6
Combined: TSS = 124.1*(Q/Qgm)^0.7
Middle Fork Whitewater River near St. Charles, MN
log(TSS) (mg/L)
log(Q/Qgm)
Rising Limb: TSS = 109.5*(Q/Qgm)^1.0
Falling Limb: TSS = 36.9*(Q/Qgm)^0.8
Combined: TSS = 68.9*(Q/Qgm)^1.1
North Branch Root River at Chatfield, CSAH2
log(TSS) (mg/L)
log(Q/Qgm)
Rising Limb: TSS = 28.2*(Q/Qgm)^1.0
Falling Limb: TSS = 15.7*(Q/Qgm)^1.0
Combined: TSS = 21.0*(Q/Qgm)^1.1

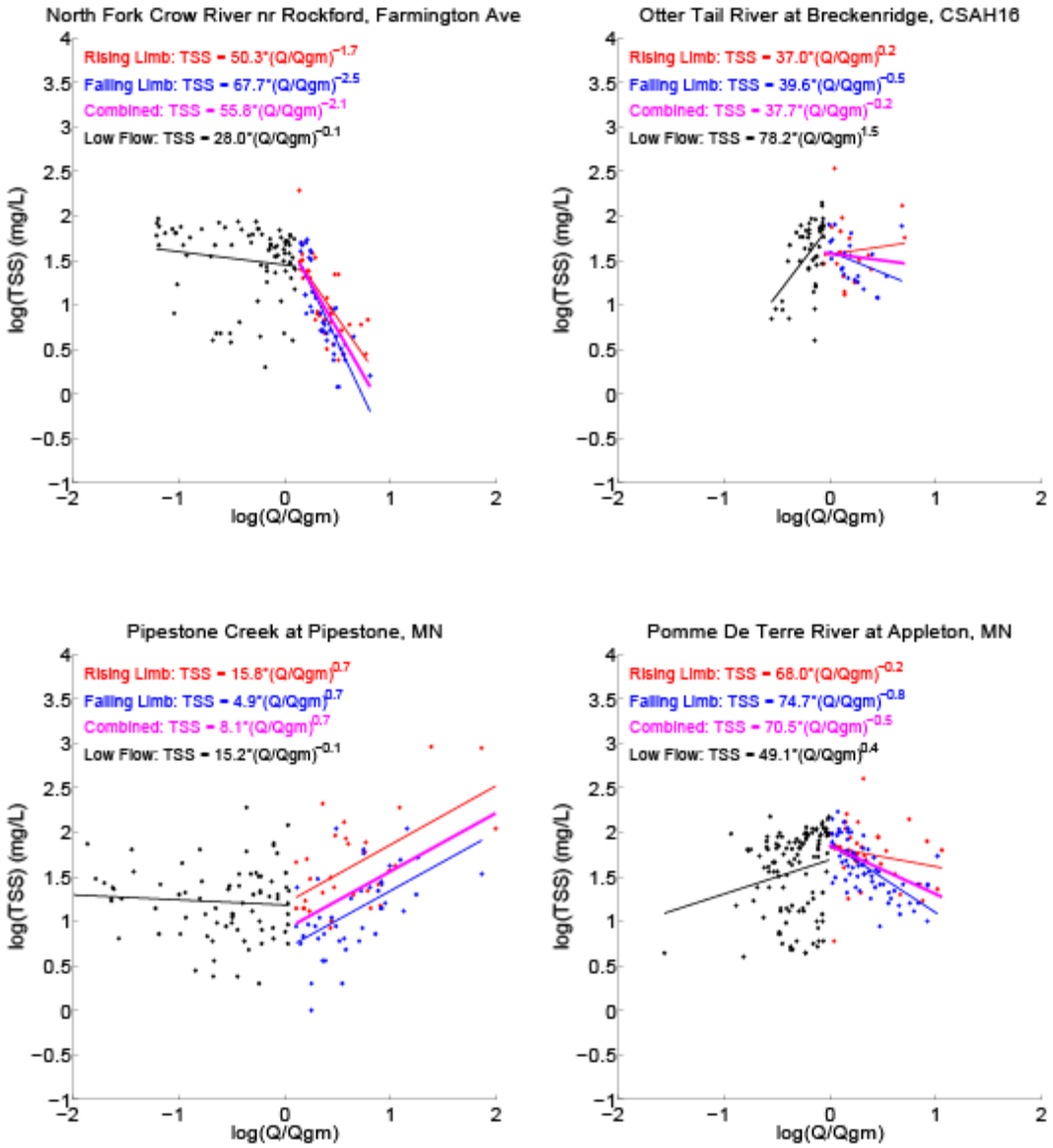
North Fork Crow River nr Rockford, Farmington Ave
Rising Limb: TSS = 50.3*(Q/Qgm)^-1.7
Falling Limb: TSS = 67.7*(Q/Qgm)^-2.5
Combined: TSS = 55.8*(Q/Qgm)^-2.1
Low Flow: TSS = 28.0*(Q/Qgm)^-0.1
log(TSS) (mg/L)
log(Q/Qgm)
Otter Tail River at Breckenridge, CSAH16
Rising Limb: TSS = 37.0*(Q/Qgm)^0.2
Falling Limb: TSS = 39.6*(Q/Qgm)^-0.5
Combined: TSS = 37.7*(Q/Qgm)^-0.2
Low Flow: TSS = 78.2*(Q/Qgm)^1.5
log(TSS) (mg/L)
log(Q/Qgm)
Pipestone Creek at Pipestone, MN
Rising Limb: TSS = 15.8*(Q/Qgm)^0.7
Falling Limb: TSS = 4.9*(Q/Qgm)^0.7
Combined: TSS = 8.1*(Q/Qgm)^0.7
Low Flow: TSS = 15.2*(Q/Qgm)^-0.1
log(TSS) (mg/L)
log(Q/Qgm)
Pomme De Terre River at Appleton, MN
Rising Limb: TSS = 68.0*(Q/Qgm)^-0.2
Falling Limb: TSS = 74.7*(Q/Qgm)^-0.8
Combined: TSS = 70.5*(Q/Qgm)^-0.5
Low Flow: TSS = 49.1*(Q/Qgm)^0.4
log(TSS) (mg/L)
log(Q/Qgm)

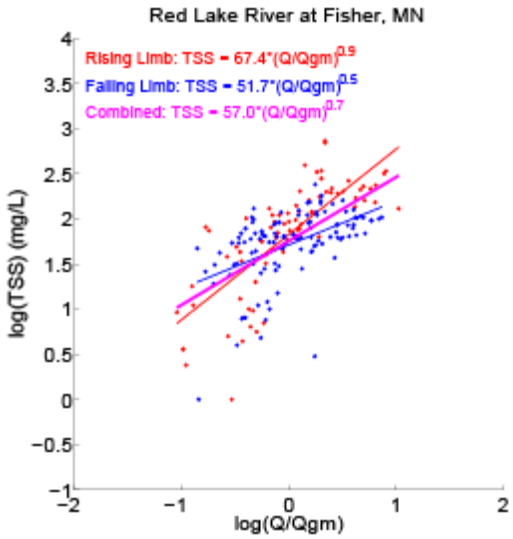
Red Lake River at Fisher, MN
Rising Limb: TSS = 67.4*(Q/Qgm)^0.9
Falling Limb: TSS = 51.7*(Q/Qgm)^0.5
Combined: TSS = 57.0*(Q/Qgm)^0.7
log(TSS) (mg/L)
log(Q/Qgm)

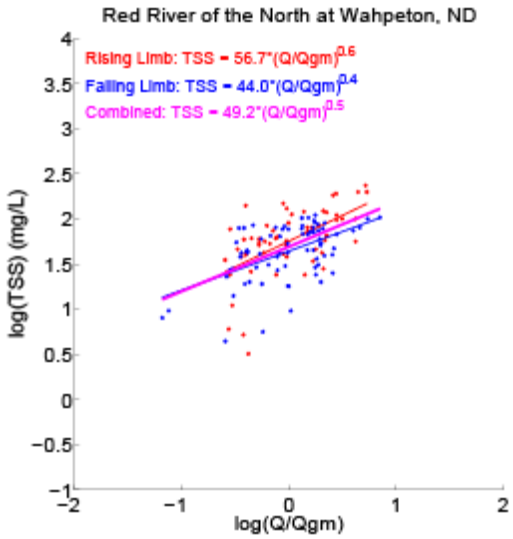
Red River of the North at Wahpeton, ND
Rising Limb: TSS = 56.7*(Q/Qgm)^0.6
Falling Limb: TSS = 44.0*(Q/Qgm)^0.4
Combined: TSS = 49.2*(Q/Qgm)^0.5
log(TSS) (mg/L)
log(Q/Qgm)

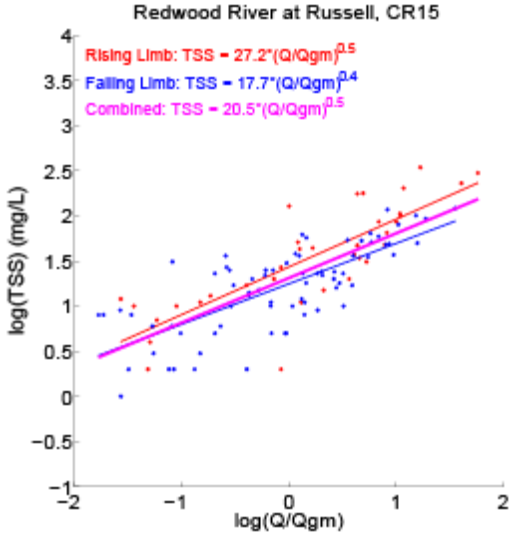
Redwood River at Russell, CR15
Rising Limb: TSS = 27.2*(Q/Qgm)^0.5
Falling Limb: TSS = 17.7*(Q/Qgm)^0.4
Combined: TSS = 20.5*(Q/Qgm)^0.5
log(TSS) (mg/L)
log(Q/Qgm)

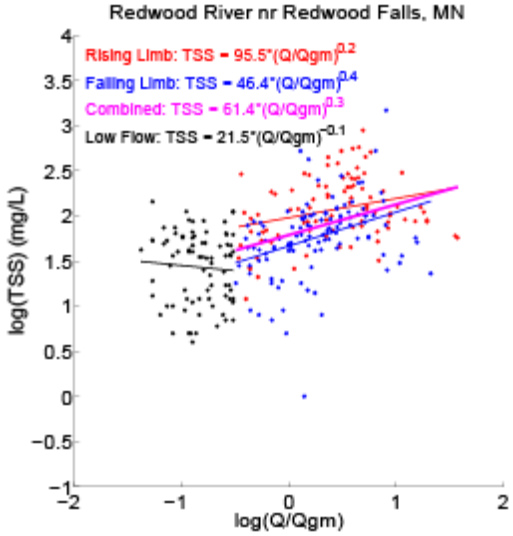
Redwood River nr Redwood Falls, MN
Rising Limb: TSS = 95.5*(Q/Qgm)^0.2
Falling Limb: TSS = 46.4*(Q/Qgm)^0.4
Combined: TSS = 61.4*(Q/Qgm)^0.3
Low Flow: TSS = 21.5*(Q/Qgm)^-0.1
log(TSS) (mg/L)
log(Q/Qgm)

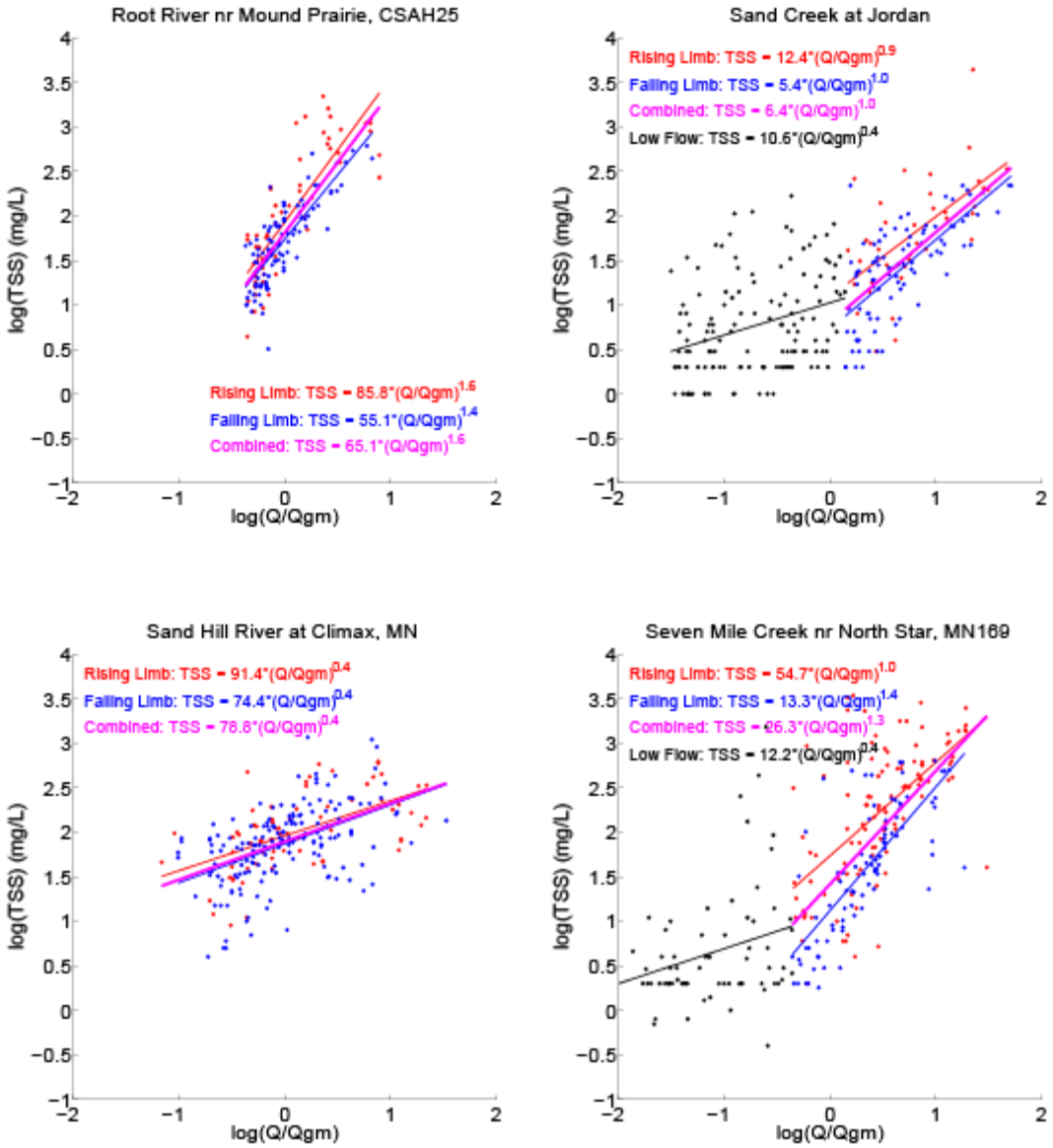
Root River nr Mound Prairie, CSAH25
Rising Limb: TSS = 85.8*(Q/Qgm)^1.6
Falling Limb: TSS = 55.1*(Q/Qgm)^1.4
Combined: TSS = 65.1*(Q/Qgm)^1.6
Sand Creek at Jordan
Rising Limb: TSS = 12.4*(Q/Qgm)^0.9
Falling Limb: TSS = 5.4*(Q/Qgm)^1.0
Combined: TSS = 6.4*(Q/Qgm)^1.0
Low Flow: TSS = 10.6*(Q/Qgm)^0.4
Sand Hill River at Climax, MN
Rising Limb: TSS = 91.4*(Q/Qgm)^0.4
Falling Limb: TSS = 74.4*(Q/Qgm)^0.4
Combined: TSS = 78.8*(Q/Qgm)^0.4
Seven Mile Creek nr North Star, MN169
Rising Limb: TSS = 54.7*(Q/Qgm)^1.0
Falling Limb: TSS = 13.3*(Q/Qgm)^1.4
Combined: TSS = 26.3*(Q/Qgm)^1.3
Low Flow: TSS = 12.2*(Q/Qgm)^0.4
log(TSS) (mg/L)
log(Q/Qgm)

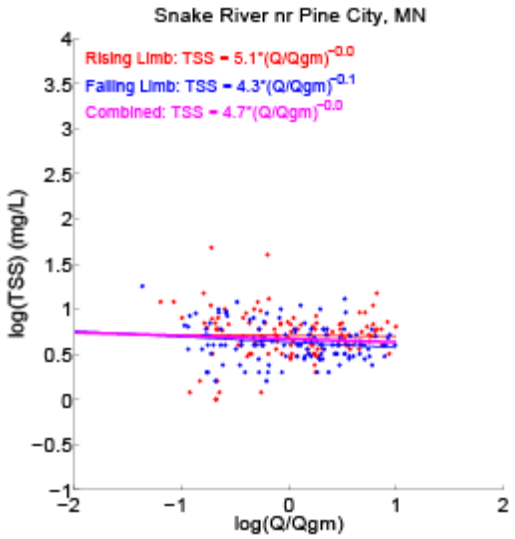
Snake River nr Pine City, MN
Rising Limb: TSS = 5.1*(Q/Qgm)^-0.0
Falling Limb: TSS = 4.3*(Q/Qgm)^-0.1
Combined: TSS = 4.7*(Q/Qgm)^-0.0
log(TSS) (mg/L)
log(Q/Qgm)

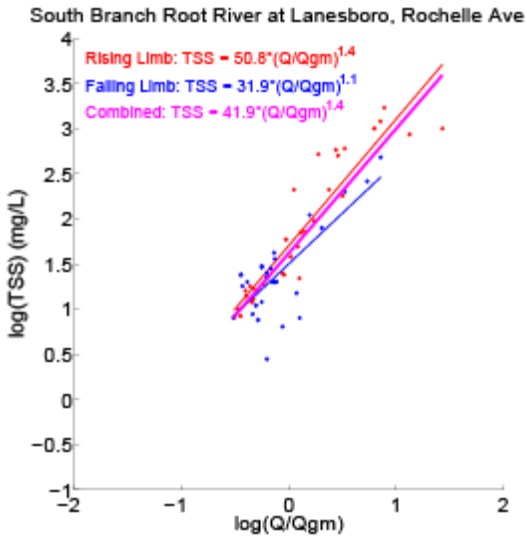
South Branch Root River at Lanesboro, Rochelle Ave N
Rising Limb: TSS = 50.6*(Q/Qgm)^1.4
Falling Limb: TSS = 31.9*(Q/Qgm)^1.1
Combined: TSS = 41.9*(Q/Qgm)^1.4
log(TSS) (mg/L)
log(Q/Qgm)

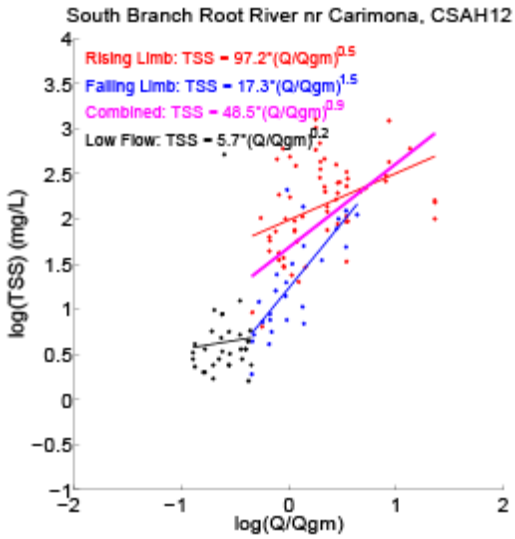
South Branch Root River nr Carimona, CSAH12
Rising Limb: TSS = 97.2*(Q/Qgm)^0.5
Falling Limb: TSS = 17.3*(Q/Qgm)^1.5
Combined: TSS = 48.5*(Q/Qgm)^0.9
Low Flow: TSS = 5.7*(Q/Qgm)^0.2
log(TSS) (mg/L)
log(Q/Qgm)

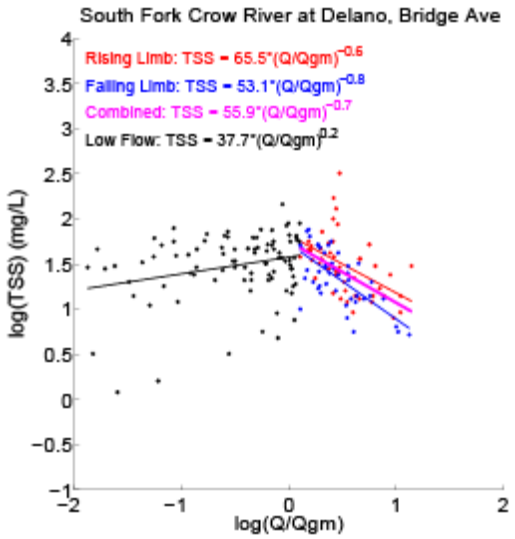
South Fork Crow River at Delano, Bridge Ave
Rising Limb: TSS = 65.5*(Q/Qgm)^-0.6
Falling Limb: TSS = 53.1*(Q/Qgm)^-0.8
Combined: TSS = 55.9*(Q/Qgm)^-0.7
Low Flow: TSS = 37.7*(Q/Qgm)^0.2
log(TSS) (mg/L)
log(Q/Qgm)

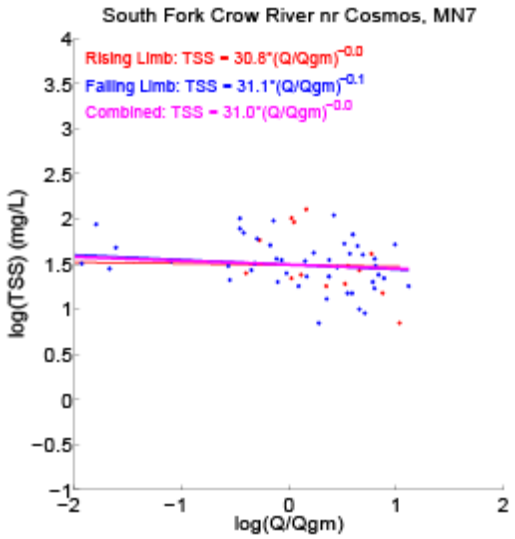
South Fork Crow River nr Cosmos, MN7
Rising Limb: TSS = 30.8*(Q/Qgm)^-0.0
Falling Limb: TSS = 31.1*(Q/Qgm)^-0.1
Combined: TSS = 31.0*(Q/Qgm)^-0.0
log(TSS) (mg/L)
log(Q/Qgm)

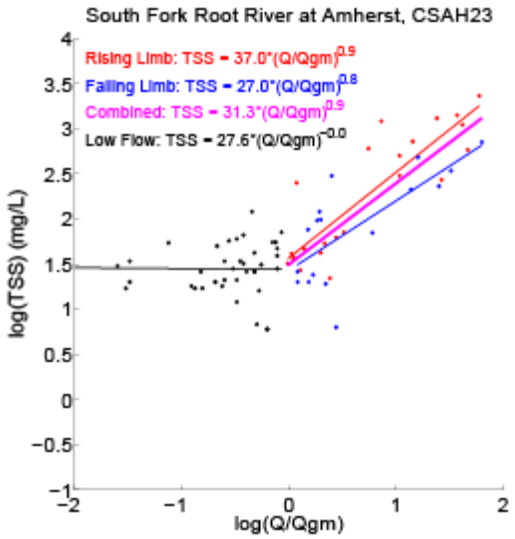
South Fork Root River at Amherst, CSAH23
Rising Limb: TSS = 37.0*(Q/Qgm)^0.9
Falling Limb: TSS = 27.0*(Q/Qgm)^0.8
Combined: TSS = 31.3*(Q/Qgm)^0.9
Low Flow: TSS = 27.6*(Q/Qgm)^-0.0
log(TSS) (mg/L)
log(Q/Qgm)

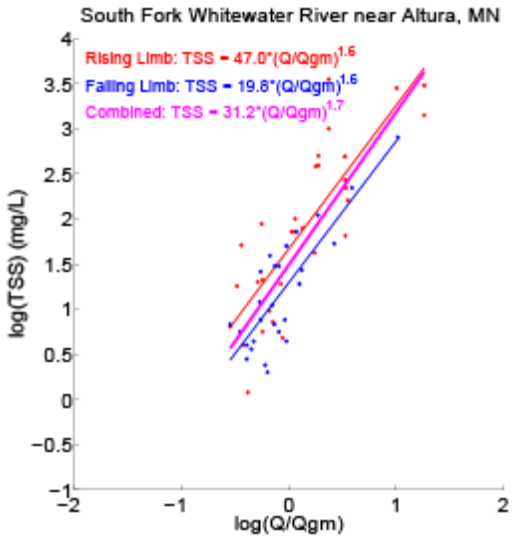
South Fork Whitewater River near Altura, MN
Rising Limb: TSS = 47.0*(Q/Qgm)^1.6
Falling Limb: TSS = 19.8*(Q/Qgm)^1.6
Combined: TSS = 31.2*(Q/Qgm)^1.7
log(TSS) (mg/L)
log(Q/Qgm)

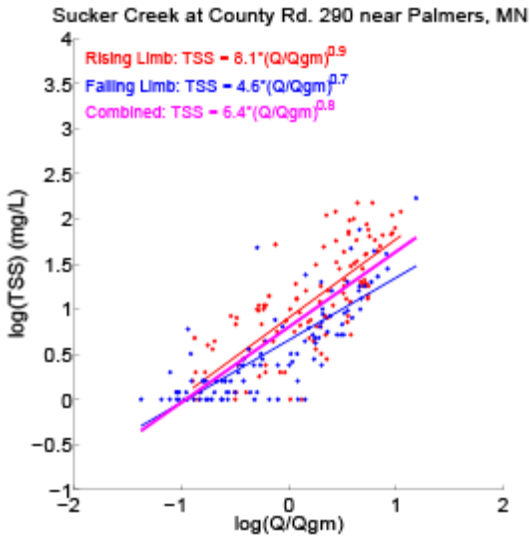
Sucker Creek at County Rd. 290 near Palmers, MN
Rising Limb: TSS = 8.1*(Q/Qgm)^0.9
Falling Limb: TSS = 4.6*(Q/Qgm)^0.7
Combined: TSS = 6.4*(Q/Qgm)^0.8
log(TSS) (mg/L)
log(Q/Qgm)

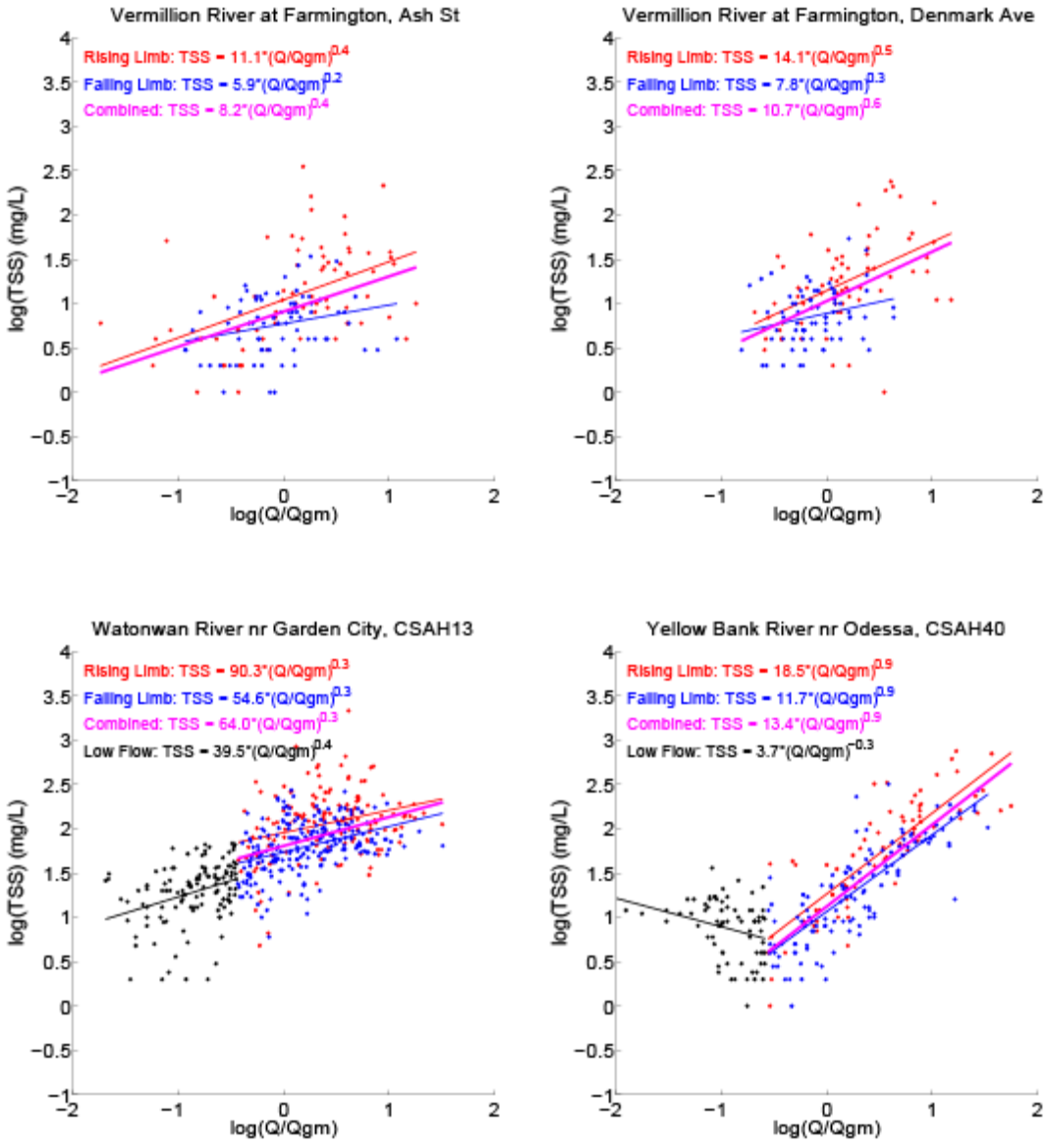
Vermillion River at Farmington, Ash St
Rising Limb: TSS = 11.1*(Q/Qgm)^0.4
Falling Limb: TSS = 5.9*(Q/Qgm)^0.2
Combined: TSS = 8.2*(Q/Qgm)^0.4
log(TSS) (mg/L)
log(Q/Qgm)
Vermillion River at Farmington, Denmark Ave
Rising Limb: TSS = 14.1*(Q/Qgm)^0.5
Falling Limb: TSS = 7.8*(Q/Qgm)^0.3
Combined: TSS = 10.7*(Q/Qgm)^0.5
log(TSS) (mg/L)
log(Q/Qgm)
Watonwan River nr Garden City, CSAH13
Rising Limb: TSS = 90.3*(Q/Qgm)^0.3
Falling Limb: TSS = 54.6*(Q/Qgm)^0.3
Combined: TSS = 64.0*(Q/Qgm)^0.3
Low Flow: TSS = 39.5*(Q/Qgm)^0.4
log(TSS) (mg/L)
log(Q/Qgm)
Yellow Bank River nr Odessa, CSAH40
Rising Limb: TSS = 16.5*(Q/Qgm)^0.9
Falling Limb: TSS = 11.7*(Q/Qgm)^0.9
Combined: TSS = 13.4*(Q/Qgm)^0.9
Low Flow: TSS = 3.7*(Q/Qgm)^-0.3
log(TSS) (mg/L)
log(Q/Qgm)

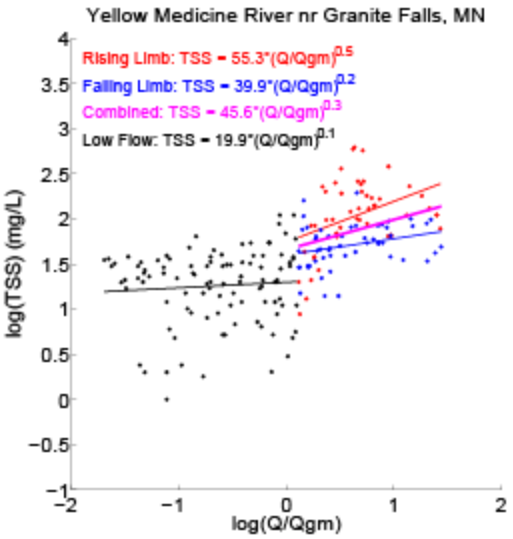
Yellow Medicine River nr Granite Falls, MN
Rising Limb: TSS = 55.3*(Q/Qgm)^0.5
Falling Limb: TSS = 39.9*(Q/Qgm)^0.2
Combined: TSS = 45.6*(Q/Qgm)^0.3
Low Flow: TSS = 19.9*(Q/Qgm)^0.1
log(TSS) (mg/L)
log(Q/Qgm)
4
3.5
3
2.5
2
1.5
1
0.5
0
−0.5
−1
−2
−1
0
1
2